DTIC FILE COPY

(2)

WRDC-TR-89-3125

Volume II

MINIMUM FLYING QUALITIES

Volume II: Pilot Modeling for Flying Qualities Applications

AD-A218 561

Duane T. McRuer
Warren F. Clement
Peter M. Thompson
Raymond E. Magdaleno

Systems Technology, Inc.
13766 South Hawthorne Blvd
Hawthorne, CA 90250-7083

January 1990

Final Report for Period October 1985 - July 1989

DTIC
ELECTE
MAR 0 1 1990
S B D

Approved for Public Release; Distribution Unlimited

FLIGHT DYNAMICS LABORATORY
WRIGHT RESEARCH AND DEVELOPMENT CENTER
AIR FORCE SYSTEMS COMMAND
WRIGHT-PATTERSON AIR FORCE BASE, OHIO 45433-6553

90 02 28 026

NOTICE

When Government drawings, specifications, or other data are used for any purpose other than in connection with a definitely Government-related procurement, the United States Government incurs no responsibility or any obligation whatsoever. The fact that the government may have formulated or in any way supplied the said drawings, specifications, or other data, is not to be regarded by implication, or otherwise in any manner construed, as licensing the holder, or any other person or corporation; or as conveying any rights or permission to manufacture, use, or sell any patented invention that may in any way be related thereto.

This report is releasable to the National Technical Information Service (NTIS). At NTIS, it will be available to the general public, including foreign nations.

This technical report has been reviewed and is approved for publication.

CAPT MARK J. DETROIT, USAF
Control Dynamics Branch
Flight Control Division

DAVID K. BOWSER, Chief
Controls Dynamics Branch
Flight Control Division

FOR THE COMMANDER

H. MAX DAVIS, Assistant for
Research and Technology
Flight Control Division
Flight Dynamics Laboratory

If your address has changed, if you wish to be removed from our mailing list, or if the addressee is no longer employed by your organization please notify AFWAL/FIGCB, WPAFB, OH 45433-6553 to help us maintain a current mailing list.

Copies of this report should not be returned unless return is required by security considerations, contractual obligations, or notice on a specific document.

Unclassified
SECURITY CLASSIFICATION OF THIS PAGE

REPORT DOCUMENTATION PAGE

Form Approved
OMB No. 0704-0188

1a. REPORT SECURITY CLASSIFICATION Unclassified	1b. RESTRICTIVE MARKINGS
2a. SECURITY CLASSIFICATION AUTHORITY	3. DISTRIBUTION/AVAILABILITY OF REPORT Approved for public release; distribution unlimited
2b. DECLASSIFICATION/DOWNGRADING SCHEDULE	
4. PERFORMING ORGANIZATION REPORT NUMBER(S) STI-TR-1235-1-II	5. MONITORING ORGANIZATION REPORT NUMBER(S) WRDC-TR-89-3125, Volume II
6a. NAME OF PERFORMING ORGANIZATION Systems Technology, Inc. 6b. OFFICE SYMBOL (If applicable)	7a. NAME OF MONITORING ORGANIZATION Flight Dynamics Laboratory (WRDC/FIGCB) Wright Research and Development Center
6c. ADDRESS (City, State, and ZIP Code) 13766 South Hawthorne Boulevard Hawthorne, California 90250-7083	7b. ADDRESS (City, State, and ZIP Code) Wright-Patterson Air Force Base, Oh 45433-6553
8a. NAME OF FUNDING/SPONSORING ORGANIZATION Flight Dynamics Laboratory Wright Research and Development Center 8b. OFFICE SYMBOL (If applicable) WRDC/FIGCB	9. PROCUREMENT INSTRUMENT IDENTIFICATION NUMBER F33615-85-C-3610
8c. ADDRESS (City, State, and ZIP Code) Wright-Patterson AFB OH 45433-6553	10. SOURCE OF FUNDING NUMBERS PROGRAM ELEMENT NO: 62201F PROJECT NO: 2403 TASK NO: 05 WORK UNIT ACCESSION NO: 64

11. TITLE (Include Security Classification)
Minimum Flying Qualities
Volume II: Pilot Modeling for Flying Qualities Applications

12. PERSONAL AUTHOR(S)
Duane T. McRuer, Warren F. Clement, Peter M. Thompson, Raymond E. Magdaleno

13a. TYPE OF REPORT	13b. TIME COVERED	14. DATE OF REPORT (Year, Month, Day)	15. PAGE COUNT
Final	FROM Oct. '85 TO Jul. '89	1990 January	132

16. SUPPLEMENTARY NOTATION

17. COSATI CODES

FIELD	GROUP	SUB-GROUP
01	03	
17	07	

18. SUBJECT TERMS (Continue on reverse if necessary and identify by block number)
Flying Qualities
Minimum Flying Qualities
Multi-Axis Flying Qualities
Pilot Modeling
Optimal Control Pilot Modeling
Piloted Simulation

19. ABSTRACT (Continue on reverse if necessary and identify by block number)

The project was initiated to explore the modern nature of minimum flying qualities in the presence of modern aircraft and multi-redundant flight control system technology. It had several phases, including: 1) an intensive effort to develop and/or elaborate existing pilot modeling analysis techniques to apply to situations associated with minimum flying qualities, divided attention pilot operations, and multi-axis control tasks; 2) preliminary analyses and associated fixed base simulations to expand the meager multi-axis data base and to serve as pilot studies for more extensive simulations on the Air Force's Large Amplitude Multimode Aerospace Research Simulator. 3) an extensive simulation program on LAMARS to investigate minimum flying qualities and related situations; and 4) analysis and interpretation of both the early and LAMARS simulation efforts in the context of the pilot modeling advances. The project documentation appears in three volumes. Volume I reports on the results of 2) through 4) above. Volume II is a stand-alone monograph on pilot modeling, including procedures for estimating pilot workload as "measured" by pilot ratings. Volume III is a stand-alone monograph which presents a detailed implementation of a much expanded version of the human optimal control model on Program CC.

20. DISTRIBUTION/AVAILABILITY OF ABSTRACT ☒ UNCLASSIFIED/UNLIMITED ☐ SAME AS RPT ☐ DTIC USERS	21. ABSTRACT SECURITY CLASSIFICATION Unclassified
22a. NAME OF RESPONSIBLE INDIVIDUAL Capt Mark J. Detroit	22b. TELEPHONE (Include Area Code) (513) 255-8499 22c. OFFICE SYMBOL WRDC/FIGC

DD Form 1473, JUN 86 Previous editions are obsolete

SECURITY CLASSIFICATION OF THIS PAGE
Unclassified

TABLE OF CONTENTS

Page

I. INTRODUCTION 1

A. General Background 1
B. The Several Natures of Man Machine Control -- A Catalog of Behavioral Complexities 4

II. COMPENSATORY OPERATION AND THE CROSSOVER MODEL 9

A. Compensatory Models in General 9
B. The Crossover Model Describing Function 12
C. Remnant 19

III. THE STRUCTURAL ISOMORPHIC HUMAN OPERATOR MODEL 22

A. Background 22
B. The Full Attention Model 22
C. Equalization Selection and Adjustment 28
D. Divided Attention Pilot-Vehicle-Task Model 36

IV. ALGORITHMIC HUMAN PILOT MODEL 55

A. Overview of the Model 55
B. Details of the Human OCM 60
C. Implementation 68
D. An Example for $Y_c = K_c/s$ 72
E. Concluding Remarks 75

V. ESTIMATION OF PILOT RATINGS 78

A. Pilot Rating Functionals 80
B. Workload, Attentional Demands and the Product Rule for Multi-Axis Ratings 87
C. The Clinical Approach to Rating Estimation 91

REFERENCES 104

APPENDIX A. PILOT-VEHICLE ANALYSIS OF MULTI-AXIS TASKS 111

Accession For
NTIS GRA&I ☑
DTIC TAB ☐
Unannounced ☐
Justification
By
Distribution/
Availability Codes
Dist | Avail and/or Special
A-1

LIST OF FIGURES

		Page
1.	Major Human Pilot Pathways in a Pilot-Vehicle System	5
2.	A Generalized Man-Machine System Structure	10
3.	Simple Compensatory System and Operator Responses	13
4.	Data and Crossover Models for a Simple Rate-Control-Like Controlled Element	15
5.	Variation of Crossover Model Dynamic Stimulus-Response Latency with Degree of Operator Lead Equalization	15
6.	Characteristics of the Crossover Model	17
7.	Normalized Remnant Spectra	20
8.	Structural Isomorphic Model of Man-Machine System	25
9.	Mean-Squared Error Based on Crossover Model	35
10.	Pilot-Vehicle System for Divided Attention Control Task	39
11.	Features of Finite Dwell Sampling	44
12.	Consequences of Divided Attention	44
13a.	Effect of Divided Attention Remnant on System Performance as a Function of Normalized Crossover Frequency	46
13b.	Effect of Divided Attention Remnant on System Performance as a Function of Phase Margin	47
14.	Effect of Divided Attention on Phase Margins for Minimum Mean-Squared Error	49
15a.	$\bar{\underline{A}}^{-1}(\phi_M, \tau_e/T_d)$ as a Function of Normalized Crossover Frequency	51
15b.	$\bar{\underline{A}}^{-1}(\phi_M, \tau_e/T_d)$ as a Function of Phase Margin	52
16.	Algorithmic (Linear Optimal Control) Model of Man-Machine System	56
17.	The Human Optimal Control Model	64
18.	Iterative Algorithm for Solving the OCM	69
19.	Cooper-Harper Handling Qualities Rating Scale	79

LIST OF FIGURES

Page

20. The Elements of the "Paper Pilot" for the Hover Task (Ref. 64) 82

21. "Paper Pilot" Rating Functionals 83

22. Comparison of Actual Pilot Ratings with Ratings Computed Using Modified Hover "Paper Pilot" Rating Functional (Ref. 68) 83

23. Pilot Rating vs. Value of Model Index of Performance (Ref. 72) 85

24. Pilot Rating vs. Performance Index for Dander Single and Multi-Axis Tasks (See Appendix) 87

25. Single-Loop Primary Task with Secondary Cross-Coupled Loading Task 88

26. Calibration of Pilot Rating with Attentional Workload and Excess Control Capacity 92

27. Correlations Obtained with Product Method 93

28. Pilot Rating Decrements as Functions of Lead Equalization and Gain Tracking with Full Attention, Single Axis 96

LIST OF TABLES

Page

1. Experimental Procedures to Evoke Human Operator Behavioral Changes 23

2. Typical Pilot Equalization Characteristics 30

3. Time Delay Adjustment 31

4. Basic Divided Attention Relationships 50

5. Procedures for Adjustment of the Algorithmic Model 77

6. Pilot-Vehicle System Factors in Pilot Rating 98

7. Desirable Closed Loop Dynamic Features 101

8. Typical Pilot Centered Path Regulation Problems 103

FOREWORD

The work reported herein was performed during the period from October 1985 to May 1989 under Contract F33615-85-C-3610 from the Air Force Wright Research and Development Center (formerly Air Force Wright Aeronautical Laboratories), Air Force Systems Command. Mr. Thomas Gentry of WRDC was the original Contract Technical Monitor; this duty was later transferred to Captain Mark Detroit (USAF). Mr. Duane McRuer was the STI Technical Director. The STI Project Engineers were Messrs. Roger H. Hoh and David G. Mitchell.

The project was initiated to explore the modern nature of minimum flying qualities in the presence of modern aircraft and multi-redundant flight control system technology. It had several phases including: 1) an intensive effort to develop and/or elaborate existing pilot modeling analysis techniques to apply to situations associated with minimum flying qualities, divided attention pilot operations, and multi-axis control tasks; 2) preliminary analyses and associated fixed base simulations to expand the meager multi-axis data base and to serve as pilot studies for more extensive simulations on the LAMARS; 3) an extensive simulation program on LAMARS to investigate minimum flying qualities and related situations; and 4) analysis and interpretation of both the early and LAMARS simulation efforts in the context of the pilot modeling advances. The project documentation appears in three volumes. Volumes II and III present the results of 1) above while Volume I covers 2) through 4) above. This Volume (II) is a stand-alone monograph on pilot modeling, including procedures for estimating pilot workload as "measured" by pilot ratings. Volume III is a stand-alone monograph which presents a detailed implementation of a much expanded version of the human optimal control model on Program CC. This permits detailed analyses using algorithmic pilot models on personal computers with commercially available controls analysis software. It is expected to make pilot-vehicle analyses by flying qualities engineers possible on a more routine basis.

The authors wish to acknowledge the significant contributions of Professor David Schmidt, now at Arizona State University, and Professor Ronald A. Hess of University of California at Davis for assistance with

the optimal control module. Dr. Schmidt accomplished an important breakthrough in pilot rating assessment using the OCM which is summarized in the appendix to this report. Dr. Hess was of great help in increasing our understanding of the OCM to the point where the new implementation of Volume III could be undertaken. The authors are also grateful to the STI publications staff, Ms. Bess Shields, Ms. Dorie Taylor, Ms. Laura Sherard, and Mr. Charles Reaber for their careful work in preparing the report for publication.

SECTION I

INTRODUCTION

A. GENERAL BACKGROUND

The human operator in a man-machine system is the archetype hierarchical, adaptive, optimalizing, decision-making controller. In accomplishing these functions the human exhibits a bewildering variety of behavior which defy quantitative description when considered in the large. Nonetheless, since World War II scientists and engineers have attempted to describe specific elements within this functional list in terms of quantitative models. Because we are speaking of human activities in a control context, the field of control theory has been a major source of paradigms for quantitative descriptions. Because control theories can also be classified using similar adjectives, it is not surprising that almost every new advance in control theory has led to attempts to better understand additional aspects of human behavior in the perspective of this advance. When these attempts have been fruitful a control theory paradigm has emerged which is useful in quantifying the human's operations. Just as theory has been used to "explain" experiment, so unexplained experimental results beget new theory. The results of this widespread synergistic activity have been documented in hundreds of research papers and in a series of sum mary surveys which have appeared aperiodically. (A chronological listing of surveys is given at the end of this report, succeeding the reference list). As a consequence, much of the successful art is now mature. Furthermore, it has become a fundamental mode of thinking on the part of technical practitioners in the fields of operator/vehicle control system integration, vehicle handling qualities and, indeed, all aspects of interactive man-machine systems.

Besides the technological aspects of manual control, interdisciplinary activities between control engineers, physiologists, and experimental psychologists have led to control theory descriptions of human subsystem behavior and to the interpretation of the human's psychophysiological outputs in control engineering terms. These interdisciplinary areas have been especially productive in building psychophysiological models of those

human subsystems involved in the human controller, in understanding biodynamics as affected by environmental variables, in establishing connections between behavior and subjective workload indices, and in interpreting objectively the effects of alcohol, drugs, fatigue, etc., as operator impairments.

From this rich variety of man-machine control aspects that have been addressed, the emphasis here will be confined to models particularly pertinent to ordinary and minimum flying qualities situations. Although this will not be an exhaustive cross-section of the field, the models treated will be quite comprehensive (as encapsulations of experimental data) and representative of useful theory (in that both classical and modern control viewpoints are presented).

Flying qualities in general can be divided into "unattended" (and trim), large amplitude maneuvering, and "closed-loop" operations. All three categories have some degree of pilot interaction. The differences in pilot behavior exhibited in this wide range of operations are "explained" in the most general control-oriented pictures of pilot-vehicle systems by signal "pathways" internal to the human. We shall end this introductory section with an explanation of this general paradigm for human control behavior as the underlying basis for the simpler models (which are components of the general paradigm) commonly used for flying qualities analysis. The general paradigm also serves to introduce some of the mysterious complexities which face researchers who wish to describe human dynamics in general.

From this starting point the scope will be contracted to manageable proportions by reducing the types of behavior which are to be characterized by pilot models. The man-machine systems most relevant for the exposure of critical flying qualities involve operations in which the pilot controls the effective aircraft dynamics in a closed-loop fashion. "Closed-loop" in this sense means operations wherein at least part of the pilot's control actions are conditioned by the differences between the aircraft's desired and actual outputs. The kinds of piloting covered include precision control, regulation, and stabilization tasks; the types of flying qualities tests represented include "flying qualities while

tracking". For these cases the man-machine system, and the associated human pilot behavior, are referred to as "compensatory". Fortunately, compensatory operations are the most definitive in disclosing critical flying qualities deficiencies and the associated pilot models are the most extensive and advanced.

There are currently three predominant types of human operator models used to describe compensatory behavior. By far the simplest model the human pilot-vehicle system dynamics in the crossover frequency region. (The crossover frequency occurs where the open-loop amplitude ratio of the pilot-vehicle system is unity.) It is often sufficient for flying qualities analyses intended to elicit the governing vehicle parameters, key variations, and basic relationships. Section II will treat this fundamental model.

The most elaborate description of human dynamic properties as a controller is the structural-isomorphic model. This is an expansion of the crossover model which attempts to account for many of the subsystem aspects of the human controller as well as the total input-output behavior. It is covered in Section III. The fourth section brings a quite different perspective to dynamic pilot modeling in reviewing an algorithmic model, also called the optimal control model (OCM). The primary purpose of this model is to mimic the human operator's total response by appropriate specialization of modern control computational procedures. Because the "Crossover Model" is the most broadly applicable and best understood of human dynamic descriptions, the behavior predicted by either the structural-isomorphic or the algorithmic models must "reduce" to this form in the crossover frequency region. Thus the more elaborate models must inevitably return to the crossover model as a necessary limiting case "consequence".

In order to exercise the algorithmic model a new formulation of the computational steps involved in the optimal control model has been developed in the context of a commercially available control system analysis program (Program CC). Besides the PC compatible format this new formulation includes additional sequences which allow the analyst to determine the actual estimated pilot characteristics from the optimal controller

solution. These steps should improve the understanding and interpretation of algorithmic model-based estimates, and should broaden the use of the OCM by making it available as a PC compatible routine. The new formulation is documented in Volume III.

In modern high performance aircraft the pilot is no longer primarily a controller. Instead communications, monitoring and management of automated equipment, planning, re-adjusting to adapt to changing circumstances, etc. place increasingly arduous demands on the pilot. Thus flying qualities for stressful, high workload mission phases requires the pilot to divide his attention between control and managerial tasks. The dynamic models for the pilot must take these divided attention operations into account. This is done for both classical and algorithmic models in the later parts of their respective sections.

The first four sections of the report focus on the dynamics of pilots in flying qualities tasks for both full and divided attention conditions. The fifth, and last, section and two appendices address the workload associated with generating these dynamics and accomplishing the control task. This is measured by subjective impressions delivered as pilot ratings. Ideally we would like to predict the workload (pilot ratings) along with the prediction of the underlying pilot dynamics. To some extent this can be done, although much is left for the future. Thus Section V presents only a status current at the start of the present program. New results, based on the new experimental data obtained as part of this project, are presented in Volume I.

B. THE SEVERAL NATURES OF MAN MACHINE CONTROL -- A CATALOG OF BEHAVIORAL COMPLEXITIES

The human pilot is complicated to describe quantitatively because of his enormous versatility as an information processing device. Figure 1 shows the general pathways required to describe human behavior in an interactive man-machine system wherein the human operates on visually sensed inputs and communicates with the machine via a manipulative output. This control system block diagram indicates the minimum number of the major functional signal pathways internal to the human operator which must

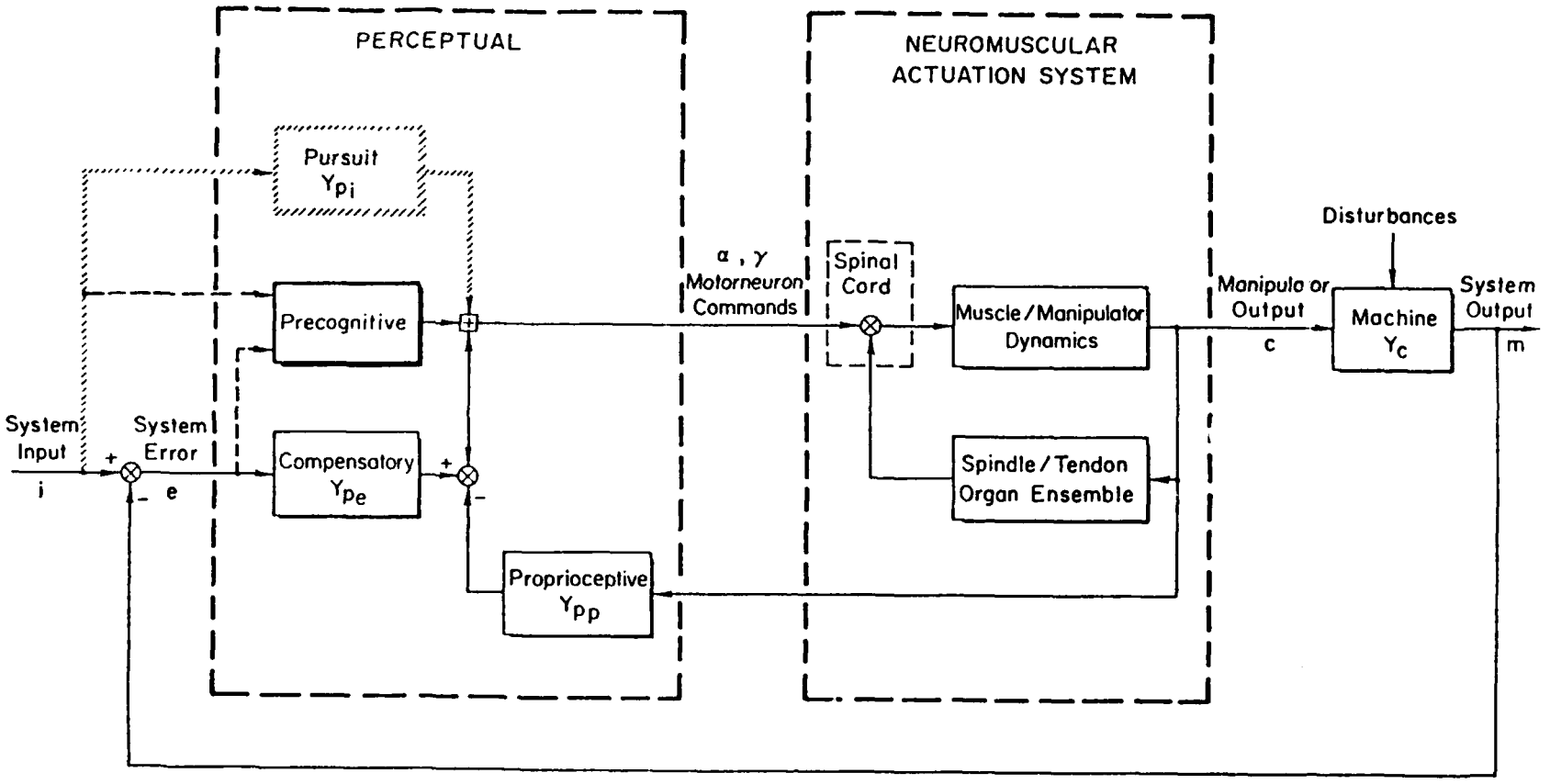

Figure 1. Major Human Pilot Pathways in a Pilot-Vehicle System

be present functionally in order to characterize different behavioral features of the human controller. The constituent sensing, data processing, computing, and actuating elements are connected as internal signal processing pathways which can be reconfigured as the situation changes. Functional operations on internal signals within a given pathway may also be modified. Thus, we have adaptation both of the pathways involved and of the functions performed. The specific internal signal organizational possibilities shown have been discovered by manipulating experimental situations (e.g., by changing system inputs and machine dynamics) to isolate different combinations of the specific blocks shown.

To describe the components of the figure start at the far right with the controlled element; this is the machine being controlled by the human. To its left is the actual interface between the human and the machine -- the neuromuscular actuation system, which is the human's output mechanism. This in itself is a complicated feedback control system capable of operating as an open-loop or combined open-loop/closed-loop system, although that level of complication is not explicit in the simple feedback control system shown here. The neuromuscular system comprises limb, muscle, and manipulator dynamics in the forward loop and muscle spindle and tendon organ ensembles as feedback elements. All these elements operate within the human at the level from the spinal cord to the periphery.

There are other sensor sources, such as joint receptors and peripheral vision, which indicate limb output position. These operate through higher centers and are subsumed in the proprioceptive feedback loop incorporating a block at the perceptual level further to the left in the diagram. If motion cues are present these too can be associated in similar proprioceptive blocks with feedbacks from the controlled element output.

The three other pathways shown at the perceptual level correspond to three different types of control operations on the visually presented system inputs. Depending on which pathway is effectively present, the control structure of the man-machine system can appear to be open-loop, or combination open-loop closed-loop, or totally closed-loop with respect to visual stimuli.

When the compensatory block is appropriate at the perceptual level, the human controller acts in response to errors or controlled element output quantities only. With this pathway operational, continuous closed-loop control is exerted on the machine so as to minimize system errors in the presence of commands and disturbances. Compensatory behavior will be present when the commands and disturbances are random-appearing and when the only information displayed to the human controller consists of system errors or machine outputs.

When the command inputs can be distinguished from the system outputs by virtue of the display (e.g., i and m are shown or are detectable as separate entities relative to a reference) or preview (e.g., as in following a curved pathway), the pursuit pathway joins the compensatory. This new pathway provides an open-loop control in conjunction with the compensatory closed-loop error-correcting action. The quality of the overall control can, in principle, be much superior to that where compensatory acts alone.

An even higher level of control is possible. When complete familiarity with the controlled element dynamics and the entire perceptual field is achieved, the operator can generate neuromuscular commands which are deft, discrete, properly timed, scaled, and sequenced so as to result in machine outputs which are exactly as desired. These neuromuscular commands are selected from a repertoire of previously learned control movements. They are conditioned responses which may be triggered by the situation and the command and control quantities, but they are not continuously dependent on these quantities. This pure open-loop programmed-control-like behavior is called precognitive. Like the pursuit pathway, it often appears in company with the compensatory operations as a dual-mode control -- a form where the control exerted is initiated and largely accomplished by the precognitive action and then may be completed with compensatory error-reduction operations.

The above description of pathways available for human control activities has emphasized the visual modality. Similar behavior patterns are present in the other modalities as well. Thus, man's interactions with

machines can be even more extraordinarily varied than described here, and can range completely over the spectrum from open-loop to closed-loop in character in one or more modalities. Just what pathways of the overall system are present at a particular time depends on the detailed nature of the specific task at hand and the corresponding perceptual situation. All of the fundamental pathways are involved in various piloted-aircraft maneuvers. Thus all these features are potentially significant in vehicle flying qualities. In the sequel we shall, however, consider only the simplest form of closed-loop behavior -- compensatory operations.

SECTION II

COMPENSATORY OPERATION AND THE CROSSOVER MODEL

A. COMPENSATORY MODELS IN GENERAL

The compensatory pathways in the visual modality have been by far the most extensively studied in man-machine systems. Thousands of experiments have been performed, and most of the adaptive features of the human operator associated with these kinds of operations are well understood. Both classical control and optimal control theoretical formulations are available to predict steady-state and dynamic performance.

Figure 2 illustrates in vector block diagram form a general system configuration appropriate to closed-loop man-machine control. The diagram shows the human operating on a number of perceived quantities, $\mathbf{y}(t)$, and exerting control over an aircraft ("controlled element") by actuating a number of controls, $\mathbf{u}_n(t)$. The response of the controlled element to actuation of the controls and to disturbances is presented on a "display." As used here, display includes dynamic geometrical perspectives of the visual field, other visual stimuli present on physical display elements either on the aircraft or in the surround, and proprioceptive, tactile, aural, and other information impinging on the pilot. From the display the human separates the information needed for monitoring from that required for control purposes. Only the latter directly affects the human's operations as a controller, although both present attentional demands and thereby affect workload.

After receiving the displayed information the pilot internally selects and equalizes appropriate signals and sends the results on to the neuromuscular actuation subsystem for control action. The equalization and neuromuscular properties depend on the task variables (effective aircraft dynamics, display, and inputs); they constitute the pilot's adaptive features whereby he attempts to offset any dynamic deficiencies of the remaining system elements. In the process of accomplishing control the human introduces observation, scanning, divided attention, equalization, and motor noises which, joined together are referred to as "remnant".

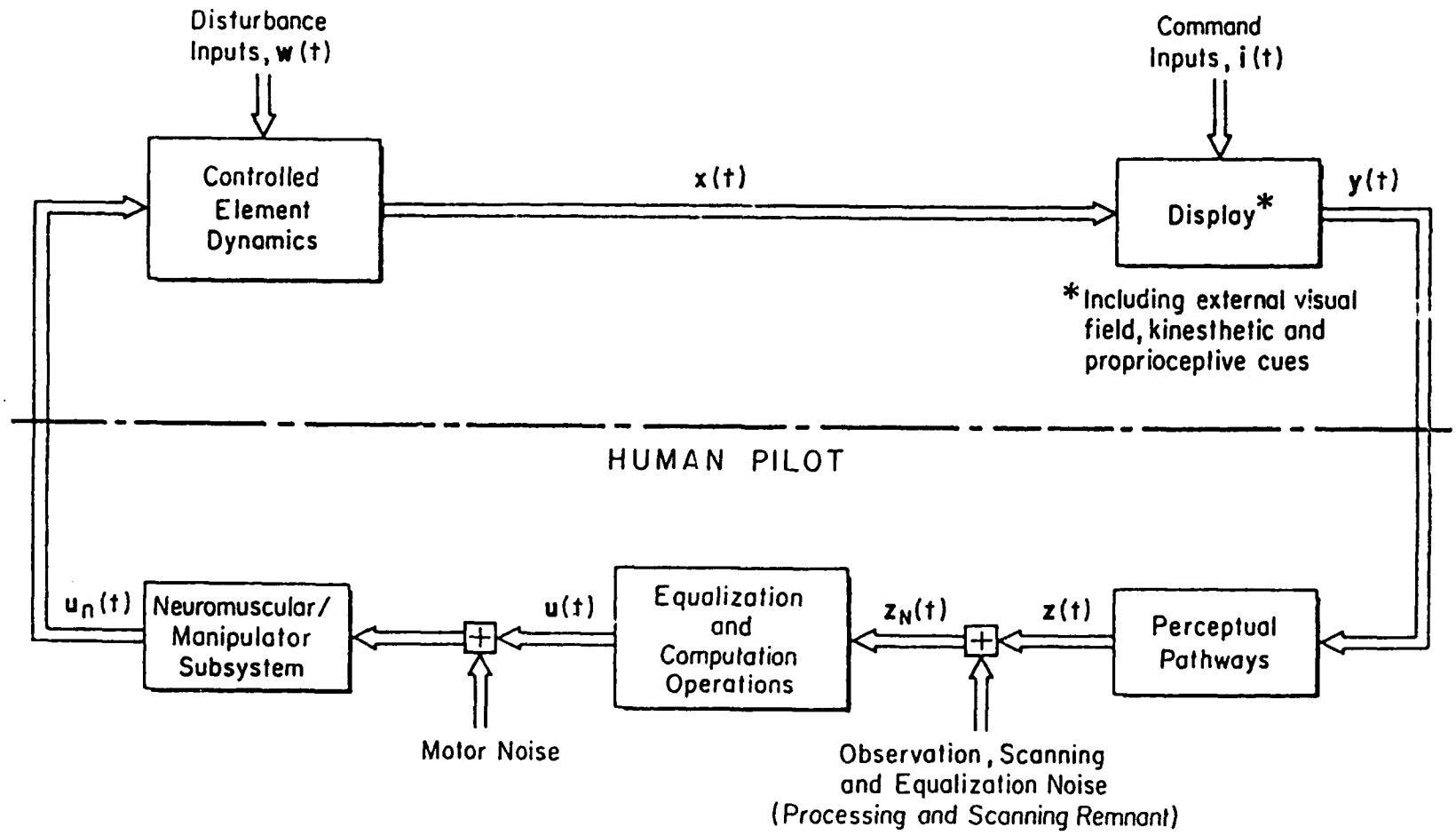

Figure 2. A Generalized Man-Machine System Structure

These unwanted components of the operator's signals are functions of the task and the qualities of the display.

As noted in the Introduction, two types of human operator models are available to handle the details in Fig. 2. The first is a multiloop, multi-modality model, based on describing functions, which is structurally isomorphic in that its component dynamics are intended to parallel the dynamics of more or less identifiable human operator subsystems. The emphasis is on cause and effect relationships having similarity in form and structural connections with those of the human operator. The second type of model is algorithmic. It uses linear-quadratic-guassian optimal control theory, modified to permit a pure time delay and operator-induced noises to be given quantities along with the machine characteristics.

Both types of models represent the man-machine system as quasilinear in the sense that the response to a given input is divided into two parts -- a component which corresponds to the responses of equivalent linear elements driven by that input and a "remnant" or noise component which represents the difference between the response of the actual system and an equivalent system based on the linear element. Verbal-analytical instructions which express the adaptation of the human population to the task variables are an important formal feature of the structural isomorphic model and have counter parts, such as the specification of the performance index, in the algorithmic model form. For limited situations, both representations can be used to predict human operator dynamic behavior (in some sense), operator-induced noise (remnant), workload indices, visual scanning effects, and overall system performance such as mean-squared system errors and control activities.

The major fundamental differences between the models are their conceptual bases, i.e., causal and structural isomorphic as contrasted to algorithmic and (potentially) teleologic; the computational techniques associated with the exercise of the model; and the nature of model identification processes. At the present time there are other differences between the structural isomorphic and algorithmic models relating to their regimes of application and their validated capabilities for prediction. These latter differences are not, however, fundamental; instead, they reflect the relative maturity and extent of application.

B. THE CROSSOVER MODEL DESCRIBING FUNCTION

Both the structural isomorphic and the algorithmic model approaches will be described below. As a preliminary let us first examine some of the general characteristics of human pilot dynamic response in compensatory man-machine systems by considering an elementary example. Figure 3a shows a display and functional block diagram of a simple single-loop man-machine system. The controlled element dynamics are given by:

$$Y_c = \frac{K_c}{s(Ts + 1)} \tag{1}$$

This could represent, for example, the idealized roll angle to aileron transfer function. The compensatory display presents the pilot with a visual stimulus which shows only the difference between the system forcing function and the system output. (Historically this is the definition of <u>compensatory</u>; modern usage applies the word compensatory to the <u>situations</u> wherein the human operates on errors regardless of the display details.) The pilot's task is to minimize the presented error signal by attempting to keep it superimposed on a stationary point or line on the display. This is accomplished by the manipulative control action c(t) which affects the controlled element, and gives rise to the system output m(t) being controlled. The usual purpose of a system of this nature is to make the system output closely resemble the system forcing function or, in other words, to make the output follow the input. The quality of the following is indicated by the system error, which is, of course, the operator's visual stimulus.

Figure 3b (Ref. 1) presents typical time histories in this system when a random-appearing forcing function is applied. The first thing to notice about the time histories is that the system output, m, does indeed follow the forcing function, i, very closely. Only a slight time lag keeps the output from being a nearly identical duplicate of the forcing function, although there are some small, random wiggles here and there on the output. On the other hand, the operator's output does not correspond at all well with the system error, even if the error is delayed. However, the operator output lagged by (s + 1/T) is approximately proportional to

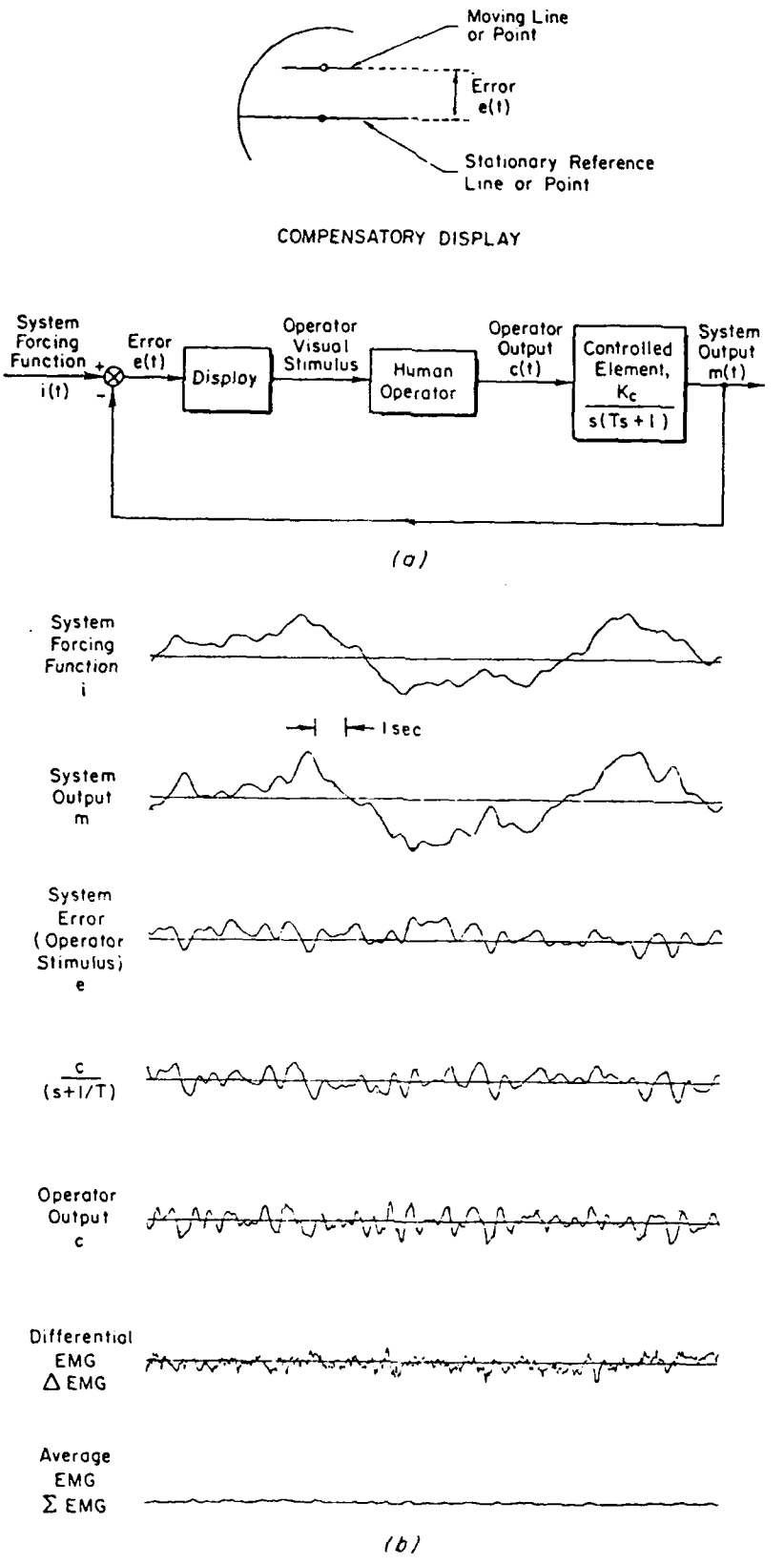

Figure 3. Simple Compensatory System and Operator Responses

the error signal delayed by 0.16 sec. Thus, as an approximation, the operator's transfer characteristic can be inferred to be:

$$Y_p \doteq K_p(Ts + 1)e^{-\tau s} \tag{2}$$

This result states that the operator develops a lead which is approximately equal to the first-order lag component of the controlled element dynamics and that the operator's response lags his stimulus by τ sec. The open-loop man-machine transfer characteristic appears as:

$$G = Y_pY_c \doteq \frac{[K_p(Ts + 1e^{-\tau s}]K_c}{s(Ts + 1)} \tag{3}$$

$$= \frac{K_pK_ce^{-\tau s}}{s}$$

or

$$G = Y_pY_c = \frac{\omega_c{}^{-\tau s}}{s} \tag{4}$$

The data of Fig. 4 illustrate how well Eq. 4 is obeyed for a particular Y_c and a variety of subjects. The agreement with the amplitude ratio is excellent over a broad range of frequencies. The phase agreement is good in the region of the crossover frequency, ω_c, but departs somewhat at lower frequencies.

If now a large variety of controlled element forms are used and similar measurements are taken, the human transfer characteristics will be different for each controlled element. But, for a very wide range of controlled element dynamics, the <u>form</u> of the total open-loop transfer characteristic about the crossover frequency will remain substantially invariant. In other words, experiment shows that Eq. 4 has some pretension to general applicability. The effective time delay, τ, which is of course only a low-frequency approximation to all manner of high-frequency leads and lags, is not a constant. It depends primarily on the amount of lead equalization required of the operator, as shown in Fig. 5 (Ref. 1). This indicates that pilot equalization to offset controlled element dynamic deficiencies has an associated computational time penalty. With this proviso on τ, the Eq. 4 relationship becomes the well-known

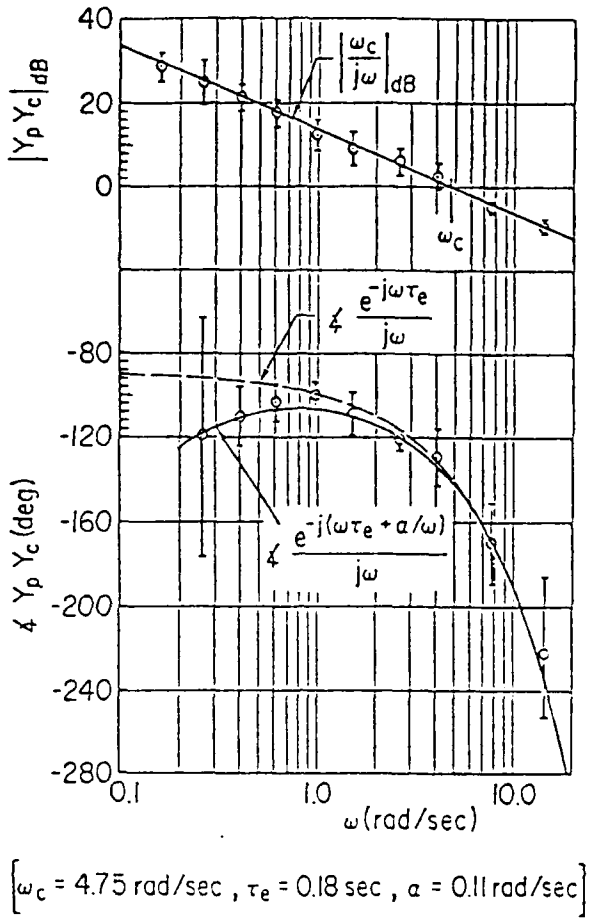

Figure 4. Data and Crossover Models for a Simple Rate-Control-Like Controlled Element

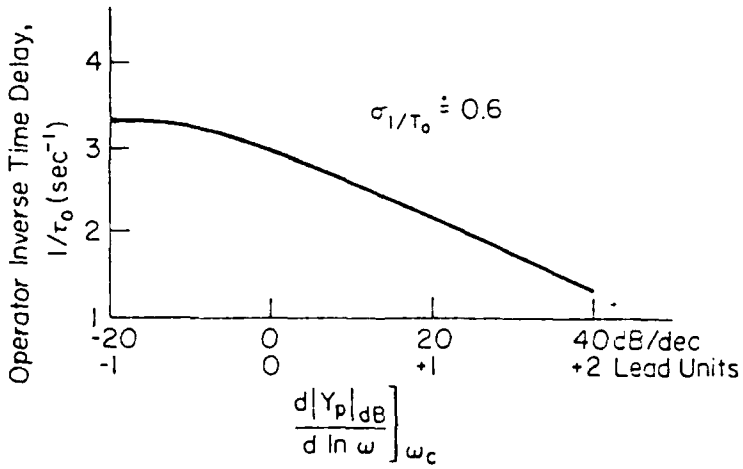

Figure 5. Variation of Crossover Model Dynamic Stimulus-Response Latency with Degree of Operator Lead Equalization

simplified <u>crossover model</u> of compensatory manual control theory. For the vast majority of flying qualities applications the pilot lead equalization ranges from none to first order. Thus, in order to estimate the effective time delay, τ_e, we need only to approximate that portion of Fig. 5 in the interval

$$0 < \left.\frac{d(|Y_p|_{dB})}{d(\log \omega)}\right|_{\omega_c} < 20 \text{ dB/decade}$$

This is given by

$$\frac{1}{\tau_o}\left(\frac{1}{\text{sec}}\right) \doteq 3 - \frac{0.833}{20}\left.\frac{d(|Y_p|_{dB})}{d(\log \omega)}\right|_{\omega_c}$$

The human operator's adaptation to controlled element dynamics is implicit in the relationship, i.e., for a particular set of controlled element dynamics defined by Y_c the human will adopt a crossover region transfer characteristic $Y_p \doteq \omega_c e^{-j\omega\tau}/j\omega\ Y_c$. The general form of the human's response would thus be determined by the specifics of Y_c, and changes in this task variable evoke changes in Y_p, such that the crossover model open-loop transfer characteristic form is preserved. An extremely important consequence is that a <u>duality principle</u> is established for those cases where the crossover model is valid. That is, since Y_c and Y_p are related by Eq. 4, properties of <u>either</u> can be used as "coordinates" in describing results of experiments. In particular one can use <u>open-loop</u> effective aircraft dynamics to specify what is needed to achieve "good" pilot dynamics (and subjective ratings) in <u>closed-loop</u> operations.

The crossover model also applies when the machine dynamics are smoothly time varying (Ref. 2). The crossover frequency tends to be constant for a given set of task variables. It increases slightly as forcing function bandwidth is increased and is reduced for very small input amplitudes. This is a consequence of the operator's indifference threshold, which is the most important nonlinearity to be considered in connection with crossover model transfer characteristics.

Most of the interesting open and closed loop dynamic characteristics of the crossover model are summarized in Fig. 6 (adapted from Ref. 1).

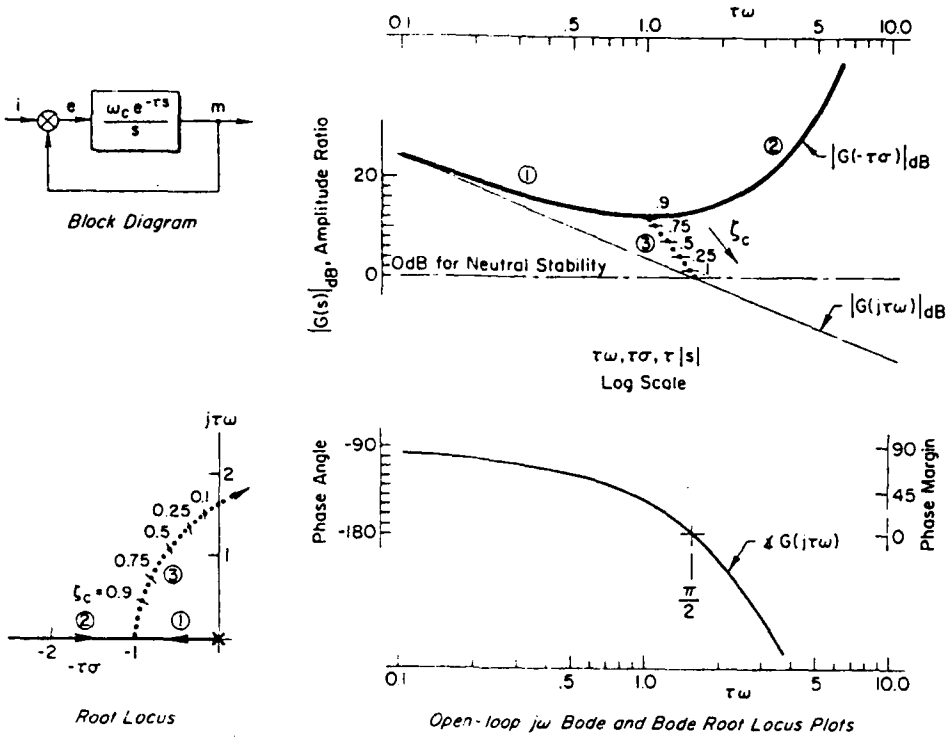

a) System Survey for Crossover Model

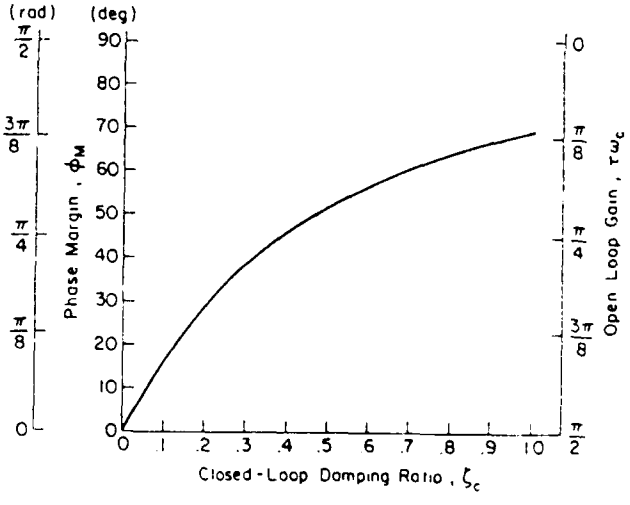

b) Phase Margin as a Function of Closed-Loop Damping Ratio

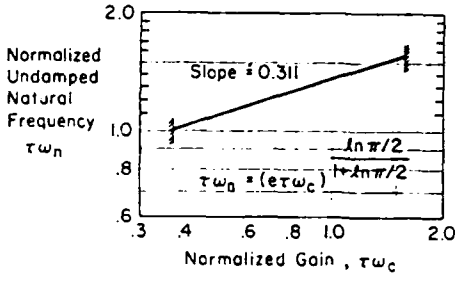

c) Closed-Loop Undamped Natural Frequency as a Function of Crossover Frequency

d) Various Relationships

$$\frac{M(s)}{I(s)} = \frac{\omega_c e^{-\tau s}}{s + \omega_c e^{-\tau s}} \quad ; \quad \frac{E(s)}{I(s)} = \frac{s}{s + \omega_c e^{-\tau s}}$$

$$\phi_M = \frac{\pi}{2} - \tau\omega_c \quad ; \quad |G_M|_{dB} = \left| \left[1 - \frac{2\phi_M}{\pi} \right]^{-1} \right|_{dB}$$

$$\tau\omega_n = \tau\omega_c e^{\tau\omega_n \zeta} = \frac{\cos^{-1}\zeta}{\sqrt{1-\zeta^2}} \quad ; \quad \tau\omega_n = (e\tau\omega_c)\frac{\ln \pi/2}{1 + \ln \pi/2}$$

Figure 6. Characteristics of the Crossover Model

Because only two parameters are present many features can be presented as functions of non-dimensional quantities, such as the normalized crossover frequency, $\omega_c \tau$, which is also the normalized open-loop gain. The system survey summarizes the key open and closed loop features. For instance, the most significant property of feedback systems is that which prevails when the open-loop transfer characteristic is much larger than 1, for then the system output is almost exactly equal to the system input and the system error is very small. From examination of the $G(j\omega)$ Bode plot it can be seen that this occurs at low frequencies and is, of course, the reason that the system output and system forcing function were similar in the example of Fig. 4. At high frequencies $|G(j\omega| \ll 1$, so the closed-loop relationship between $M(j\omega)$ and $I(j\omega)$ is substantially the same as the open-loop, i.e., the feedback loop is effectively open. For the crossover model, the frequency which divides these two regimes of near-ideal following of the forcing function and little or no feedback action is the crossover frequency, ω_c. In Fig. 6a this is the intersection of the 0 dB line established for a particular gain with the $G(j\omega)$ Bode plot. The name "crossover frequency" comes from this crossover intersection of the 0 dB line by the open-loop frequency response characteristic. For stable operation of the system the normalized crossover frequency, $\tau\omega_c$, can range from 0 to $\pi/2$.

When $\tau\omega_c$ is relatively small compared to $\pi/2$, then $\tau\omega_c$ is also tantamount to the closed-loop system "bandwidth" (the frequency at which the output amplitude is 3 dB less than the amplitude of an input sinusoid). For higher crossover frequencies this direct equivalence between $\tau\omega_c$ and system bandwidth degrades because of a peaking in the closed-loop frequency response near the crossover frequency, but even for this kind of a system $\tau\omega_c$ is always equal to or less than the bandwidth and thus provides a lower bound.

The root locus plots emphasize the closed-loop system roots. The root locus plots shown in Fig. 6a indicate that the root which starts at the origin for open-loop (zero gain) conditions progresses further into the left half plane as the gain $\tau\omega_c$ is increased. At the point $\tau\sigma = -1$ (for which $\tau\omega_c = 1/e$), this branch of the locus meets with the first of an

infinity of branches present because of the $e^{-\tau s}$ term (the other branches are not shown). The quadratic formed by the two branches then increases in undamped natural frequency and decreases in damping as gain is increased until neutral stability occurs at the gain $\tau\omega_c = \pi/2$.

Some connections between the dominant closed-loop mode characteristics, i.e. ζ and ω_n, and the open-loop characteristics, ω_c and τ, are illustrated in Fig. 6b. Other relationships, such as the phase margin, Φ_M, and gain margin, G_M, are recapitulated in Fig. 6d.

An "extended crossover model" form is sometimes used to improve the low frequency phase fit. It is,

$$G = Y_p Y_c = \frac{\omega_c \, e^{-\left(j\omega + \frac{j\alpha}{\omega}\right)}}{j\omega}, \quad \omega_1 < \omega \approx \omega_c < \omega_2 \tag{5}$$

Figure 4 illustrates how well the additional term, $e^{-j\alpha/\omega}$, describes those phase contributions in the crossover region which arise from leads and lags (in the pilot and/or the rest of the system) which are present well below the crossover frequency band. The phase contribution represented by $e^{-j\alpha/\omega}$ in Eq. 5, is not intended to extend to extremely low frequencies.

C. REMNANT

The second component of the operator's response is operator-induced noise or remnant. This can, in principle, result from several sources, but in single-loop systems with linear manipulators the basic cause appears to be random time-varying behavior within the operator primarily associated with fluctuations in the effective time delay. This can be interpreted as a random change in phase, akin to a random frequency modulation, or to variations of internal sampling rate in a sampled data interpretation of the operator (Refs. 1, 3-6). In any event, the remnant is a continuous, relatively broadband, power spectral density which, as shown in Fig. 7, scales approximately with the mean-squared error (Refs. 4, 5).

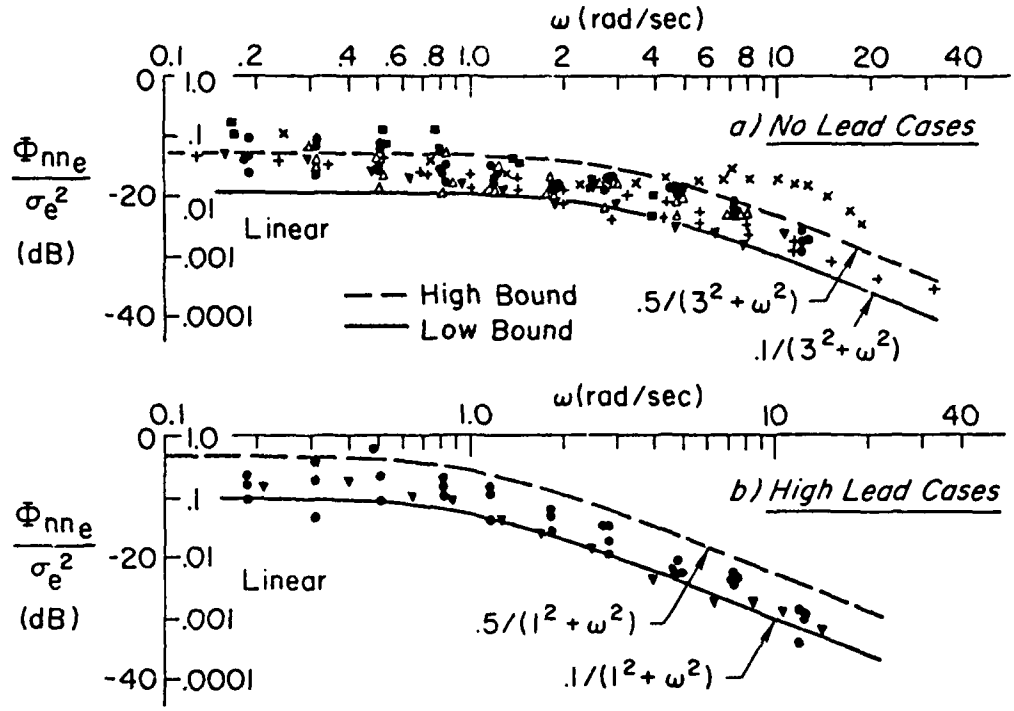

Figure 7. Normalized Remnant Spectra

Task variables other than the machine dynamics, as well as environmental and operator-centered variables, can change open-loop gain, effective time delay, and remnant. Accordingly, ω_c and τ variations become a quantification of changes or differences in the task, environmental, and operator-centered variables expressed directly in terms of the operator's control actions. In measuring the effects of training for instance, ω_c increases with trials until stable conditions are obtained for that particular subject and set of constant task and environmental variables. Similarly, the remnant may also change as a function of the control situations. For instance, comparison of Figs. 7a and 7b shows the change in remnant bandwidth and level associated with the lead equalization required to offset controlled element lags. As another example Ref. 7 shows that operator gain is decreased and remnant is increased as a consequence of ingested alcohol.

To generalize these remarks, the total pilot actions can be thought of as that of an adaptive plastic sensory-motor link -- adaptive in that the pilot is task-adjusted to offset controlled element dynamic deficiencies and to respond to forcing function commands or regulate against disturbances; plastic in that the adaptive characteristics are further shaped by the external and internal (pilot-centered) environments. These behavioral features must be accounted for in either the structural isomorphic or algorithmic models. A general description of these models and some of their characteristics follows.

SECTION III

THE STRUCTURAL ISOMORPHIC HUMAN OPERATOR MODEL

A. BACKGROUND

The extensive analytical and experimental studies of closed-loop man-machine systems conducted since World War II have had as a principal goal the mathematical quantification of human dynamic behavior and the development of laws which permit this behavior to be predicted. In general, emphasis has been on the human operator as a complete entity rather than as a summation of functional subsystems.

In recent years, the precision and dynamic range of measurements taken with the total human operator have increased greatly -- to the point that certain of the measurements made over certain frequency ranges can be associated with the human subsystem dynamics. Thus, the study of the human operator as a whole has now arrived at the stage where not only must subsystem models sum up to be compatible with the total human dynamic model, but subsystem and total system studies can be directly related. Accordingly, control engineering descriptions of the overall human (see, e.g., the list of surveys), dynamical descriptions of the human motor coordination system, studies of predictive control conducted for physiological understanding, and studies of neuromuscular actuation systems, which were originally separated disciplines, now become united.

As described in Ref. 8, the adaptive and plastic properties of the operator permit the experimenter to set the stage and write a script calling for a particular form of action. Table 1 illustrates some of the experimental procedures which can be used to evoke various types of behavior.

B. THE FULL ATTENTION MODEL

By properly selecting combinations of these procedures and techniques, particular channels of human dynamic operations can be isolated, examined, and measured. Appropriate models which "explain" each of these varieties of behavior and which are also compatible with what is known

TABLE 1. EXPERIMENTAL PROCEDURES TO EVOKE HUMAN OPERATOR BEHAVIORAL CHANGES

PROCEDURE (EFFECTS)	BEHAVIORAL MODIFICATIONS (EXAMPLES)
Controlled Element Adjustment	Equalization changes and associated time delay increments
Manipulator Modification	Scaling of joint movement and force ranges; Activation of proprioceptive pathways
System Forcing Function Changes	
Bandwidth	Fine tune task-induced stress;
	Adjust average neuromuscular tension and associated time delay increments;
Amplitudes	Operator gain (for amplitudes near indifference threshold)
Additional Visual Inputs	Scanning, operator gains as affected by parafoveal and foveal viewing
Excitation of Additional Modalities	Activation of additional internal pathways (e.g., vestibular, kinesthetic) and consequent equalization changes
External Environmental Modification	Change task-induced stress;
	Differentially change some internal subsystem dynamics
Drugs	Modify operator-centered variables; Differentially affect various internal signal pathways

from other views of experimental psychology and physiology can then be constructed to form a current version of the structural isomorphic model. One such construction, which is somewhat simplified, is given in Fig. 8. Here the controlled element and display blocks constitute the machine, whereas all the remaining detail reflects the man.

Starting at the far right is the neuromuscular actuation system. Because the man-machine system depicted here is operating on random-appearing signals which have essentially stationary statistics, the neuromuscular system is fluctuating about an operating point which in general corresponds to some steady-state or average tension. This is graphically illustrated by examination of the average and differential EMG signals shown in Fig. 3b. Consequently, the dynamic operations of muscles, which can act only in contraction, can be treated as positive or negative fluctuations of many agonist/antagonist pairs about a steady tension bias value. This permits a great simplification in depicting the dynamic essentials in terms of a block diagram. The forward path of the neuromuscular system shown includes ensembles of muscles operating on coupled skeletal and manipulator dynamics. The feedback path sensors operating at the spinal level are primarily spindle and Golgi tendon organs. Because the individual actions of specific sensors are difficult to separate in the intact human the system shown has a feedback element labeled as spindle/tendon organ ensembles. The spindle characteristics may very well be predominant for the small motions and relatively light forces involved in most of the measurements thus far accomplished. The effective dynamics of the closed-loop neuromuscular system from the alpha motor neuron command signals to manipulator force can be approximated over a wide frequency range by the third-order transfer function shown. This form is also compatible with small perturbation dynamics based on experimentally verified analytical models of muscle and manipulator characteristics (Refs. 9, 10). The parameter values are strongly dependent on the steady-state neuromuscular tension, γ_o, due to the gamma motor system. The gamma commands also affect the dynamics of the spindle ensembles and, in fact, provide another pathway (not shown) capable of actuating the neuromuscular system via the spindle ensembles. These features are pictured by the arrows indicating variation in the Z_{sp} and P_{sp} factors in the neuromuscular system feedback block and in the γ_b and γ_o inputs.

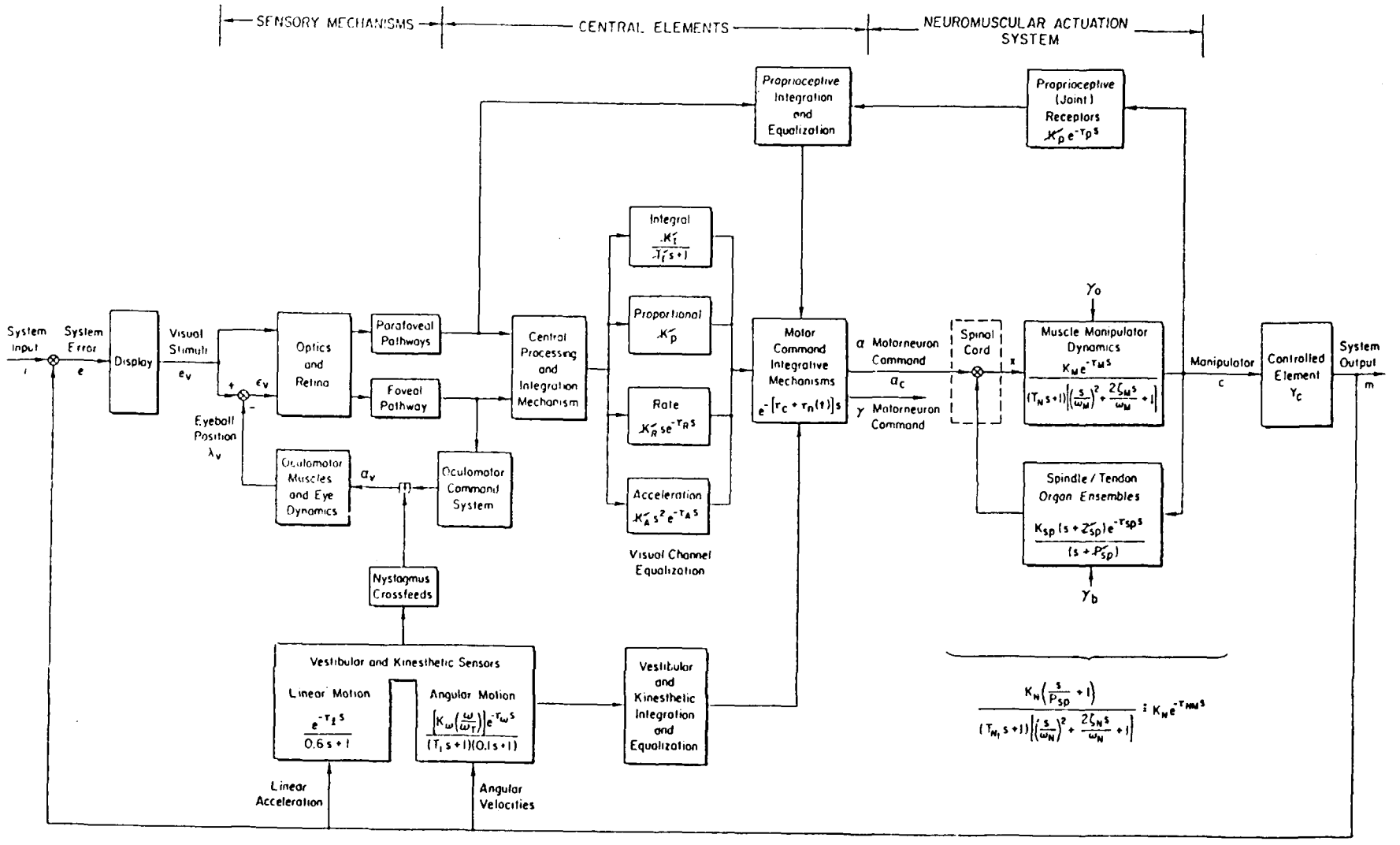

Figure 8. Structural Isomorphic Model of Man-Machine System

This rudimentary level of neuromuscular actuation system description is a minimum to have value even in gross physiological descriptions. It is an essential feature in the study of human pilot characteristics in vibratory environments (Ref. 11) and is also often needed for the study of limb/manipulator system dynamics in aircraft control (e.g., Refs. 12, 13). For many other man-machine system applications, however, the neuromuscular actuation dynamics are so high in frequency as to be relatively unimportant in their details. In these cases, a pure time delay, τ_{nm}, or a first-order lag can be used as a low-frequency approximation.

The neuromuscular actuation system described thus far is appropriate when the manipulator is restrained by a stiff spring and the control actions involve very little joint movement. When significant joint movements are present, proprioceptive pathway elements enter into the neuromuscular actuation system dynamics. These derive from several sources, the most important being peripheral vision and joint receptors in the limb. These feedbacks act through higher centers and thereby exhibit larger response time delays. When they are present, the neuromuscular actuation system bandwidth may be reduced significantly.

Proceed now to the sensory mechanisms at the far left of the human operator. A good deal of the detail in the visual pathway is intended to emphasize the parallel operations of parafoveal and foveal vision and the control of eye movements. An important feature of the visual pathways is that essentially continuous signals from a particular display element can be available to the operator, by virtue of the parallel foveal and parafoveal pathways, even when the eye is scanning. The essence of past work in man-machine systems involving many displays (Refs. 1, 14-18) shows that:

1. A fairly stationary scanning strategy evolves for a given task and display array.

2. The operator's output control motions are much more continuous than a discrete sampling of input signals coincident with foveal eye fixations would imply.

3. The first-order effects of scanning are to reduce gain and increase remnant in the scanned channels.

The degree of gain reduction depends on parafoveal viewing angle and relative parafoveal to foveal dwell times.

The other sensory elements are vestibular and kinesthetic (Refs. 19-23), which are present when the pilot is moving, as in a maneuvering airplane or a moving base simulator. The pilot contains neurological elements capable of sensing rotary and linear accelerations. These are primarily in the vestibular apparatus, although other sensors and pathways can also be involved. The rotary motion feedbacks usually associated with the semicircular canals act like signals from a highly overdamped angular accelerometer. Over the frequency range from about 0.2 to 10 rad/sec the output signal is proportional to angular rate, so the sensor can function as a rate gyro. For prolonged steady turning the sensor washes out; thus, spurious sensations occur in steady rotations or when the turning motion stops. This pathway has a threshold on the order of 1-2 deg/sec. Because the rotary motion sensing apparatus gives rise to an angular-rate-like cue directly, any need for generating angular rate information by means of a lead equalized visual cue may be reduced. This feedback can also be thought of as an inner loop which tends to reduce the effective operator time delay. That is, in terms of crossover model characteristics measured as if visual pathways only were active, the presence of rotary motion can reduce the effective time delay by as much as 0.1 sec.

The other functional operation of the vestibular and kinesthetic pathways is the provision of the "nystagmus crossfeeds" to the oculomotor system. These produce involuntary eye motions as a function of the excitation of the vestibular apparatus. These eye movements can be helpful in properly directing the gaze, although many of their most interesting properties involve their effects in disorientation and illusions. The motion effects which conflict with the visual modality can seriously distort the operator's perception of the state of affairs and can be so severe as to affect the human's control capacity.

Turn now to the central elements. As shown there, the operator can develop a neuromuscular system input command which is the summation of a lag, proportional, lead, and double-lead function of the system error.

The lag and proportional channels have a basic time delay, τ_C, associated with them. The higher derivative channels have additional incremental delays. These incremental time delays constitute the dynamic cost of lead generation. They are about 1/5 sec for rate, τ_R, and greater than 1/2 sec for the acceleration channel, τ_A. The proportional, rate, and acceleration equalizations are shown as separate parallel channels primarily because of their respective latency differences. This independence of these channels is oversimplified, for common neurological apparatus is undoubtedly present for each function. These common elements are modeled here by the central processing and integration block preceding the visual channel and the motor command integrative mechanisms succeeding it. Besides the different time delays, the other evidence for parallel channels is the difference in response quality as a function of the low-frequency equalization supplied by the operator. For example, when very-low-frequency leads are present, as if operations were through the rate or acceleration channels, the operator's output tends to be more discrete and pulselike than when little or no lead is required.

The channel gains and the lag time constant T_I are all shown as variable quantities. These, in conjunction with the neuromuscular system variations with γ_O, constitute the principal adaptive changes in the operator characteristics as display, controlled element, and environmental conditions change. For a given controlled element, these are adjusted such that the crossover model applies over its frequency range of validity. Thus, the extremely complicated structural isomorphic model reduces to the visual and/or vestibular equalization actually present and with neuromuscular dynamics as pertinent to the task. When a higher degree of exactitude is required, the structural isomorphic model is adjusted via a series of analytical/verbal rules which take into account the details of the task variables. A version of these rules is summarized below.

C. EQUALIZATION SELECTION AND ADJUSTMENT

For essentially all flying qualities while tracking aircraft applications the form,

$$\frac{K(T_L j\ \omega + 1)}{(T_I j\ \omega + 1)} \tag{6}$$

is used in lieu of the multi channel parallel equalization elements. This form doesn't reflect the acceleration channel, which is seldom used in aircraft control. For a specific problem a particular equalization is selected from the general form such that the following properties obtain:

(a) The system can be stabilized by proper selection of gain, preferably over a very broad region.

(b) Over a considerable frequency range in the unit gain crossover region (that frequency band centered on the crossover frequency, ω_c), the open-loop describing function $|Y_pY_c(j\omega)1|_{dB}$ has approximately a -20 dB/decade slope.

(c) $|Y_pY_c(j\omega)| >> 1$ at low frequencies to provide good low-frequency closed-loop response to system forcing functions (commands).

Examples of form selection and basic adjustment are provided in Table 2.

1. Time Delay Adjustment

Examples of time delay adjustment appropriate for aircraft are listed in Table 3. (This detailed breakdown replaces the Fig. 5 data for the lead-lag equalization form of Eq. 6.) The visual lag and proportional channels have a basic (minimum) time delay, τ_V, of 0.1 sec associated with either or both of them when all other effects (e.g., motion sensing, full limb/manipulator neuromuscular system, and display computational lags) are represented separately; τ_V should be increased to 0.2 sec, if fixed-base operations are being considered with visual lag and/or proportional equalization, full neuromuscular system and separate display effects. If the problem emphasis is on low frequency phenomena, the neuromuscular system can be approximated by a pure delay; then T_{NM} is added to τ_V, where examples of values for T_{NM} are given in Table 3. Lead equalization developed on visual inputs gives rise to an additional incremental delay, $\Delta\tau_V$. This incremental time delay constitutes the <u>dynamic cost</u> of pilot <u>lead generation in the visual modality</u>.

2. Crossover Frequency with Full Attention

The factors involved in estimating crossover frequency, ω_c, with full attention to control activity consist of the following:

TABLE 2. TYPICAL PILOT EQUALIZATION CHARACTERISTICS

EXAMPLE OF CONTROLLED ELEMENT	CONTROLLED ELEMENT APPROXIMATE TRANSFER FUNCTION IN CROSSOVER REGION	PILOT EQUALIZER FORM	EQUALIZER ADJUSTMENT		
			LOW-FREQUENCY ($\omega \ll \omega_c$)	MID-FREQUENCY (ω_c REGION)	HIGH FREQUENCY ($\omega > \omega_c$)
Perfect ACAH	K_c	Lag-Lead	$1/T_I$	--	T_L to partially offset $\tau + T_{NM}$
Rate Command	$K_c/j\omega$	High-Frequency Lead	--	--	T_L to partially offset $\tau + T_{NM}$ ($T_L \omega_c < 1$)
Lateral Course Displacement	$K_c/(j\omega)^2$	Low-Frequency Lead	$1/T_L$	--	T_L not available to offset $\tau + T_{NM}$
Roll Control	$K_c/j\omega(Tj\omega + 1)$	Mid-Frequency Lead	--	$T_L \doteq T$	--
		High-Frequency Lead	--	--	T_L to partially offset $\tau + T_{NM} + T$
Practical ACAH	$\dfrac{K_c}{\left(\frac{j\omega}{\omega_n}\right)^2 + \frac{2\zeta}{\omega_n} j\omega + 1}$	Low-Frequency Lead $\omega_n \ll 1/\tau$	$1/T_L$	--	--
		Lag-Lead $\omega_n \gg 1/\tau$	$1/T_I$	--	T_L to partially offset $\tau + T_{NM}$

TABLE 3. TIME DELAY ADJUSTMENT

Effective Visual Delay, τ_v	Qualifications
$\tau_{v_{minimum}} = 0.1$ sec	Other effects (e.g., motion sensing, limb-manipulator-neuromuscular system, display computations) are represented by their separate dynamics in Fig. 5
Add T_{NM} to τ_v	If neuromuscular system dynamics are not represented -- where $T_{NM} = 0.1$ sec, if manipulator is stiff (isometric) or $T_{NM} = 0.2$ sec, if manipulator is freely moving (isotonic)
Add 0.1 sec to τ_v	If fixed base operations are being considered
Add another increment to τ_v as a function of the lead equalization, T_L	Refer to figure below for first-order and add $\Delta\tau_v = \frac{1}{2.5 + 0.206/T_L} - 0.25$ sec

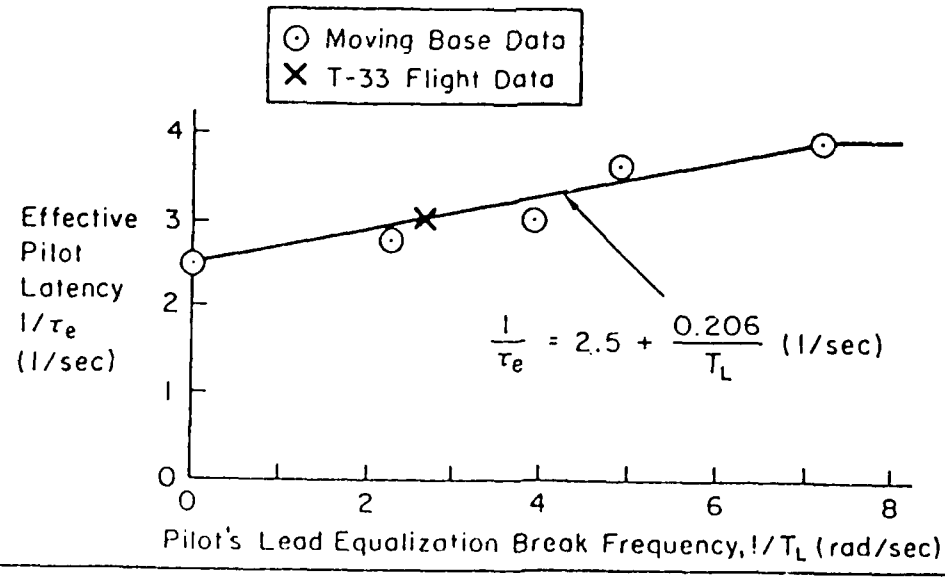

(a) **ω_c estimates for rectangular and quasi-rectangular forcing function spectra** (discrete power-spectral densities that are essentially rectangular and low-pass continuous spectra with a high-frequency cutoff equivalent to a third-or higher-order lag filter). For these forcing functions an effective forcing function bandwidth, ω_{i_e}, can be defined as,

$$\omega_{i_e} \triangleq \frac{\left[\int_0^\infty \Phi_{ii}(\omega)d\omega\right]^2}{\int_0^\infty \left[\Phi_{ii}(\omega)\right]^2 d\omega} \tag{7}$$

(1) **Basic crossover frequency, ω_{c_o}.** The basic crossover frequency for quasi-rectangular forcing function spectra is found by adding the phase angle, $-\omega\tau_o$, due to the human's base effective time delay, to the phase angles of the controlled element and the previously estimated Y_p equalizer characteristics. The net effect of controlled element high-frequency (well past crossover) leads and lags is approximated by an effective time delay, τ_c. Estimates for ω_{c_o} and the associated pilot gain are then made from the conditions for neutral stability,

$$\omega_{c_o} = \frac{\pi}{2(\tau_o + \tau_c)} \tag{8}$$

(2) **Phase margin, ϕ_M.** The phase margin for this forcing function category corresponds to an incremental time delay, $\Delta\tau_e(\omega_{i_e})$.

$$\phi_M \doteq (0.08\ \omega_{i_e})\ \omega_{c_o} \tag{9}$$

(b) **ω_c Estimates for low-pass with a roll-off of less than third-order and augmented (shelf-type) continuous input spectra.** For these types of forcing functions the crossover frequency is adjusted to minimize the mean-square error in the presence of remnant.

(1) **Continuous attention remnant.** Approximations to the forms of injected remnant, Φ_{nn_e}, when reflected to the pilot's input signal under conditions of continuous attention were shown in Fig. 7.

$$\frac{\Phi_{nn_e}}{\sigma_e^2} = \begin{cases} \dfrac{(0.1 \text{ to } 0.5)}{(\omega^2 + 3^2)} & \text{where integral and/or proportional equalization are used} \\[2ex] \dfrac{(0.1 \text{ to } 0.5)}{(\omega^2 + 1)} & \text{where lead equalization is used} \end{cases} \tag{10}$$

$$\text{where } \sigma_e^2 = \int_0^\infty \Phi_{ee}(\omega)d\omega$$

(2) **Nominal crossover frequency, ω_c.** With equalization and effective time delay, τ_e, selected as above, the nominal crossover frequency, ω_c, and associated pilot gain is estimated from the condition to provide minimum mean-squared error in the presence of the appropriate form of continuous attention remnant in Item (b)(1) above. The nominal cases (continuous remnant magnitude set to the geometric mean of the values cited above) are:

	ω_c/ω_u
No Pilot Lead:	0.783
Low-Frequency Pilot Lead:	0.662

where ω_u is the maximum full attention crossover frequency at the maximum full attention crossover frequency at the dynamic stability limit corresponding to zero phase margin ($\phi_M = 0$). Thus $\omega_u = \pi/2\tau_e$.

(c) **Nominal crossover frequency regression.** When ω_{i_e} nears or becomes greater than 0.8 ω_{c_o} for the quasi-rectangular forcing function case or when ω_{i_e}/ω_c is greater than 1 for the low-pass and augmented low-pass spectra, then the cross-over frequency regresses to values much lower than ω_{c_o} and ω_c, respectively.

(d) **Nominal crossover frequency invariance properties.**

(1) $\omega_c - K_c$ independence. After initial adjustment, changes in controlled element gain, K_c, are offset by changes in pilot gain, K_p, i.e., nominal crossover frequency, ω_c, is invariant with K_c.

(2) $\omega_c - \omega_{i_e}$ independence. Nominal crossover frequency increases only slightly with forcing function bandwidth until crossover frequency regression occurs. (Phase margin, of course, increases per Eq. 9.)

(e) **Threshold properties.** With very low stimulus amplitudes, a threshold characteristic should be included in series with the pilot's describing function. Also, when full-attention, nearly continuous control actions are not required, an indifference threshold is likely to be present. Both of these lower ω_c from what would be estimated using the above adjustment rules.

The ω_c regression phenomenon mentioned in the adjustment rules refers to a reduction of pilot gain and, hence, of crossover frequency when the forcing function bandwidth becomes too large. The reason for this is best described by referring to the relative mean-squared error plotted in Fig. 9 for the crossover model subjected to a rectangular forcing function spectrum with bandwidth ω_i. If the ratio ω_i/ω_c is less than about 0.8, an increase in normalized gain ($\tau_e\omega_c$) will result in a decrease in normalized mean-squared error. When this approximate inequality is reversed, the normalized mean-squared error can become greater than 1 as gain is increased. The trend, therefore, for high forcing function bandwidths is to reduce gain. This regression effect has practical consequences whenever the pilot is required to track broadband signals.

The adjustment rules given above are generally adequate for the pilot's lower-frequency dynamics in tasks with spring-restrained manipulators. The higher-frequency properties due primarily to the neuromuscular actuation system are included only to the extent that T_{NM} is a component of τ_e.

The neuromuscular system dynamics will change markedly as the manipulator load dynamics are modified. One of the most important of these possible modifications is reduction in stiffness of the spring restraints. This is a common feature of aileron controls, as opposed to elevator and rudder controls. When the spring forces are light, the manipulator approaches the free-moving (isotonic) extreme. In these cases, the pilot must supply proprioceptive feedbacks that introduce into the neuromuscular system dynamics additional delays that are not present with the isometric situation. Available data from Refs. 10, 24, 25 indicate that the effect of this proprioceptive feedback required of the pilot when the manipulator is free-moving is to increase the effective time delay by approximately 0.1 sec. This can be added directly to the previously discussed time delay, τ_o. It amounts to an additional time delay cost incurred by forcing the pilot to close a positional loop about the manipulator.

For some configurations of manipulator and effective vehicle dynamics, the higher frequency characteristics of the neuromuscular system can be important. In particular, the peaking tendency associated with the

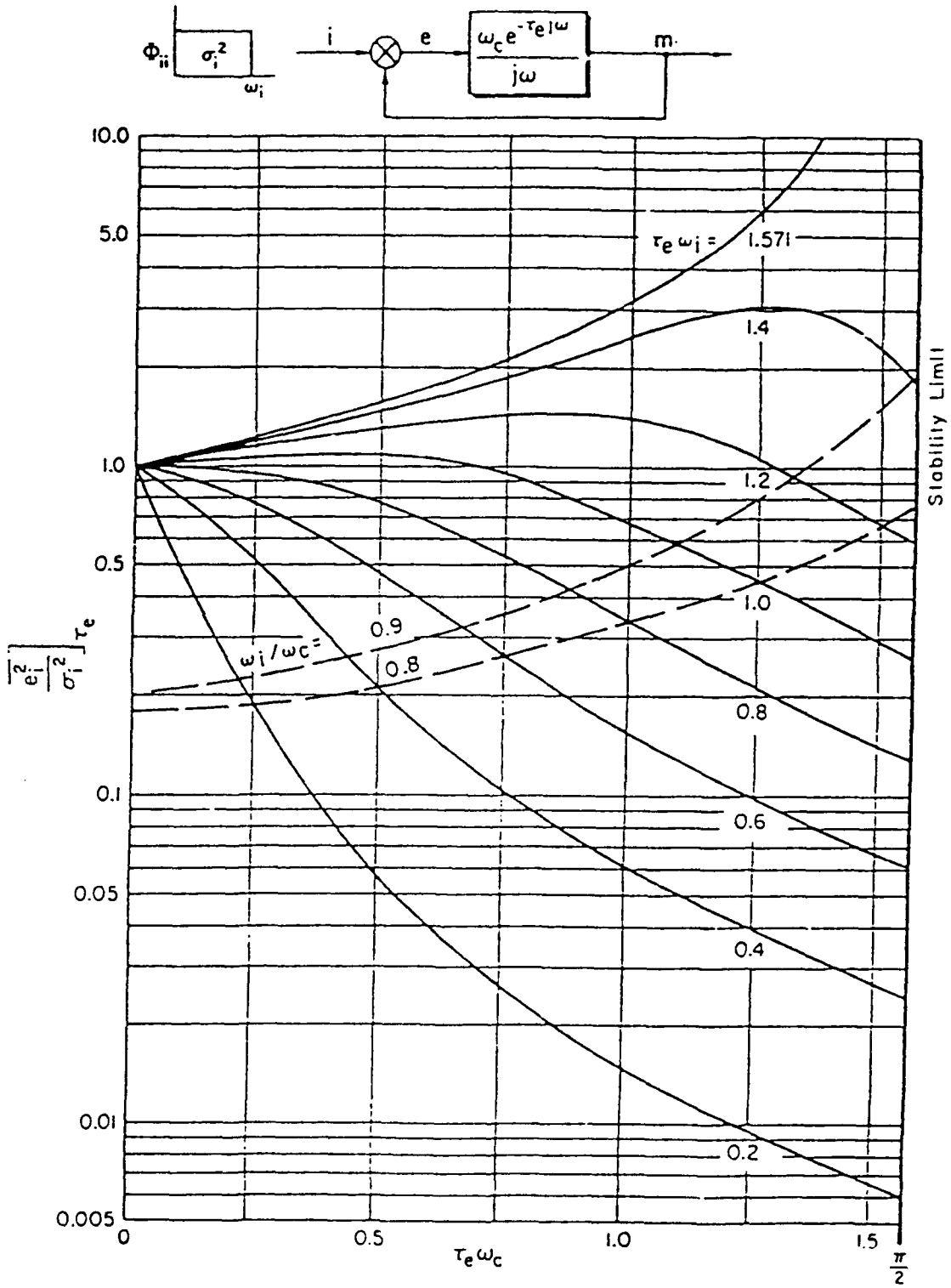

Figure 9. Mean-Squared Error Based on Crossover Model

second-order mode in the limb/manipulator block of Fig. 7 can be sufficiently large to make a higher frequency gain margin (in the frequency range from 2 to 3 Hz) negligible or even negative. Whether this will lead to an instability will depend on the accompanying phase. Such very high frequency pilot-effective vehicle oscillations as "roll ratchet" can be caused by this coupling. The detailed nature of the peaking tendency is a very strong function of the manipulator and the rest of the controlled element dynamics. The peak can be "tuned" to a maximum or minimum by the presence of just the right amount of controlled element lag. Thus, for example, a pure $Y_c = K/s$ will have little if any peaking while a $Y_c = K/s(Ts + 1)$, with T about 0.1 sec, will have a great deal. The known connections are all empirical; therefore, the reader is referred to Refs. 12 and 13, which present all of the available data.

Another "structural model" of the human pilot has been fruitfully applied to flying qualities problems (Refs. 26-29). This model makes most of the adjustments of the pilot equalization via feedback pathways instead of in the forward loop, and the "isomorphic" features and the incremental time delays associated with rate and acceleration equalization are not modeled. A good deal of effort has been spent on validation with the existing data base, and with developing connections with pilot ratings via the theory of Ref. 29.

Having completed this review of the structural-isomorphic and crossover pilot models for full attention situations, we will next examine relationships affecting pilot dynamics in divided attention situations involving control operations.

D. DIVIDED ATTENTION PILOT-VEHICLE-TASK MODEL

The pilot is, in general, involved in two types of operations -- control tasks and a diverse combination of monitoring/supervising/communicating/data-gathering/decision-making activities referred to as "managerial" tasks. While the pilot's attention is "divided" between the "control" and "managerial" tasks, these are often performed nearly simultaneously as parallel processing operations. Neither type of task is necessarily primary or secondary.

In the most complex or demanding mission phases, the two task categories may require all of the pilot's available attention. These high workload mission phases have a major impact in design, because, as tasks that are critical for either control, decision making, or human error potential, they provide the context in which system roles are established and human and equipment resources are allocated.

The managerial tasks often result in discrete action sequences. For many of these, the skilled and experienced pilot has developed a nearly routine, highly rehearsed, response repertoire to meet normal and many unusual demands. These types of nearly automatic action sequences are subject to "slips" of intention or execution, also referred to as "absent-minded errors." A commonly-cited example of a slip is the pilot's failure to lower the landing gear or flaps due to distractions like voice communications and in-cockpit warning alarms. Current studies of cognitive behavior, associated with human error (e.g., Ref. 30), emphasize that slips are most likely to occur under divided attention conditions.

For a given situation, the minimum divided attention level will be established by the control tasks. Consequently, we need a divided attention model for control operations. The model should provide such results as:

- The nature of control task performance degradation due to divided attention
- An indication of the attentional demands required for various levels of control activity and the excess capacity left for managerial tasks.

An elementary model suitable for such purposes is summarized below. It places heavy emphasis on both the attentional demands for control tasks and the excess capacity left for managerial tasks. These are quantitative indices. The attentional demand, η, for control is equal to the average "control dwell fraction" ($0 < \eta \leq 1$), while the "excess capacity" left over for other operations is the average "control interrupt fraction" ($1-\eta$). The control interrupt fraction is therefore also termed the "managerial dwell fraction."

The theory of divided attention operations can be considered as an extension to the well-established theory of display scanning and signal sampling/reconstruction (Refs. 1, 15, and 31). In the control task, the human pilot's behavior can again be characterized in mathematical terms by describing functions that depend on the effective dynamics of the aircraft being controlled, the dynamics of the pilot-vehicle interfaces (displays and controllers), and a "remnant." These two components are depicted in the block diagram of Fig. 10, wherein the dynamics of the effective pilot-vehicle system are characterized by the crossover model described previously. Far more elaborate models of the pilot can be used, but the crossover model is quite adequate to characterize matters at the level needed here.

Recall that, when the pilot's full attention is focused on the control task, the crossover frequency, ω_c, of the pilot-vehicle system is maximized consistent with near minimum mean-squared error. The closed-loop performance issue is handled by a minimization process that arises from a compromise in following the command input while reducing the relative influence of the remnant. The remnant in full attention operations is a broadband random process that can be considered as a pilot-induced noise.

When managerial tasks are also considered, both the describing function and the remnant characterizing the pilot's control behavior will be affected by the divided attention nature of the pilot's total operations. The describing function and remnant will be modified to account for the additional signal processing or supplementary parallel sensing needed to continue control operations while the pilot is attending to the managerial tasks. Depending on the specific details, these modifications may reduce the effective pilot gain, add to the effective time delay, and/or increase the injected noise. Thus the system crossover frequency will be reduced simultaneously with an increased contribution of noise to the uncorrelated system error. Both effects will cause the precision of control task performance to be reduced from a full attention baseline. Similar modifications to the pilot-vehicle dynamics are made even with full-attention control operations when the visual cues are modified to call for divided

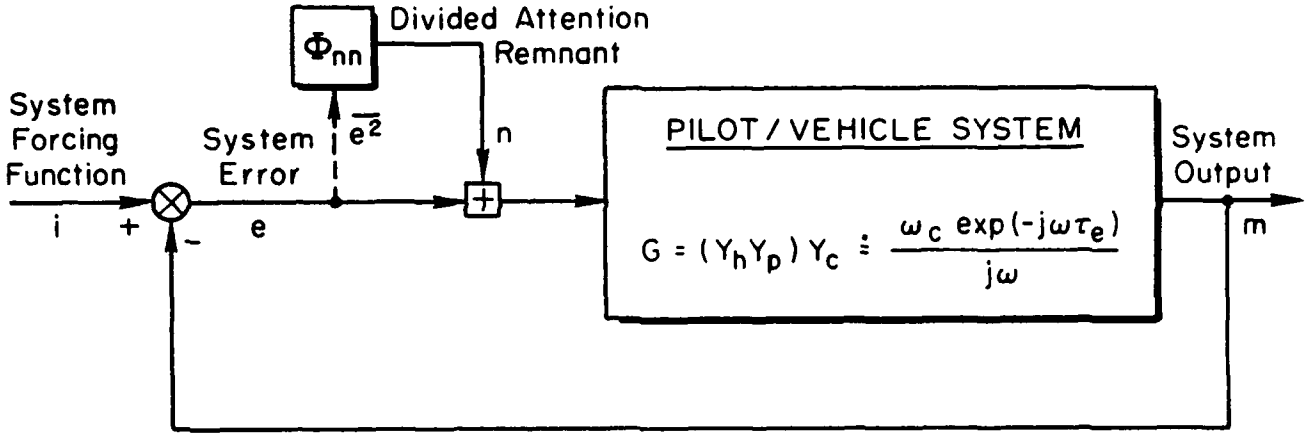

Y_c = Effective dynamics of vehicle (e.g., aircraft plus stability augmentation plus displays)

Y_p = Full attention pilot describing function

Y_h = Perceptual describing function to account for divided attention

ω_c = System crossover frequency

τ_e = Overall pilot-vehicle system effective latency

ϕ_M = System phase margin ($\pi/2 - \tau_e \omega_c$)

Φ_{nn} = Processing remnant spectrum ($\overline{n^2} \sim \overline{e^2}$)

$\overline{e^2}$ = Mean squared system error

Note: e(t) is "error" and subscript "e" in τ_e is "effective"

Figure 10. Pilot-Vehicle System for Divided Attention Control Task

visual attention, for example, in changing from head-up visual meteorological conditions (VMC) to the head-down instrument panel scanning needed for manual approach in IMC operations.

In the divided attention situations of primary interest, it is assumed that the pilot has been well trained in the control and managerial tasks involved. His attention is allocated among control and managerial tasks in which information is simultaneously gathered from several "perceptual fields." These fields may include:

Visual "Segments"

- Foveal
- Parafoveal
- Peripheral

} Parallel Pathways

Proprioceptive "Segments"

- Vestibular
- Joint receptors
- Stretch receptors
- Pressure receptors
- Etc.

} Parallel Pathways

Aural "Segments"

Tactile "Segments"

and others. The word "segment" is intended to convey the properties of extent, thresholds, input/output dynamics, etc., that characterize the particular sensory modalities involved as they are integrated into useful perceptual signal sources. The easiest to describe are the visual perceptual field segments, which can be divided on a physiological basis into foveal, parafoveal, and peripheral pathways. Besides the differing spatial (geometric) extent of these segments there are also differences in threshold, dynamic properties, contrast background, etc. — all the bewildering complexities associated with vision in its myriad details. For our purposes here, the key point to understand is that a visual "display" can be attended to not only with the foveal segment but also with the parafoveal. Thus a control task not requiring the high acuity property of foveal vision could involve sharing between the foveal and parafoveal pathways for control, with attentional adjustments of the foveal pathways between the control operations and elsewhere (e.g., reading information,

conducting visual search, etc.). The "perceptual scanning" process in this case is the "switching" of the input signals for the pilot's control task from the foveal plus parafoveal to the parafoveal alone pathways.

"Perceptual scanning" is, of course, more general than the simple shifts between foveal and parafoveal visual pathways serving to provide continuous information to the pilot from a visual display. All of the other perceptual fields for each input modality are also operating more or less continuously to provide signals that impinge on the pilot's sensorium. Although all of these data inputs are present, they are not necessarily acted upon simultaneously. However, in the highly trained, unimpaired pilot, the inputs delivered from several perceptual fields may be, in some sense, "operated on" in parallel all of the time. One feature of "impairment" is a reduction in this capacity of parallel or nearly simultaneous operations in different input channels.

For example, alcohol-induced impairment significantly reduces divided attention capability. The operator tends to focus on only one aspect of a task at a time, becoming a single channel device. Physical fatigue and task-induced stress can have similar effects, although these are more difficult to quantify in precise terms than alcohol effects.

A related concept needed here is that of "attention," adding to the ability to sense and perceive stimuli a <u>readiness</u> to <u>respond</u> to <u>selected stimuli</u>. By analogy with visual perception, we can conceive of an <u>attentional field</u> having a principal focus and borders. Attentional fields have both spatial and intensive aspects. Thus inattention or impaired attention can result in a narrowing of the spatial borders, an increase in the minimum stimulus needed to cause an operator output, or both. A common example is "tunneling" of vision ("gunsight vision") wherein, under highly stressful conditions, the visual perceptual field is narrowed. As far as active pilot control processes are concerned, the perceptual scanning and attentional field features are joined; that is, all kinds of perceptual inputs are impinging on the pilot at any one time, but the attentional foci serve to activate selected perceptual fields as sources of control or managerial task "signals."

The pilot's primary attention may be shifted from one signal source to another in the course of conducting a particular mission phase. Yet, when a control task is involved, it must be attended to from time to time. So, too, for the managerial tasks. In the course of operational training, the pilot learns to switch primary attention from one task element and/or perceptual segment to another, and then another, and back to the first, etc. This is conveniently thought of as a perceptual scanning process. When the pilot finally becomes skilled in the operational scenario, the scanning behavior over the task duration exhibits certain stable properties in a statistical sense. For instance, the proportion of the time spent on a particular input-gathering chore, the dwell times on certain instruments, and the total time before prominent features of the scanning process are repeated tend to develop stable probabilities. This is not to say that the scanning is either periodic or uniformly sequential (i.e., from "A" to "B" to "C" and back every time) but rather that cyclical activity is present in the perceptual scanning process.

Control tasks conducted under divided attention conditions both in flight and laboratory research have shown that the coverage of elements (e.g., instruments or perceptual fields) in a given array of input sources has a definite average frequency and corresponding mean sampling interval, T_s, albeit with appreciable variance. The mean "control dwell time," T_d is the time spent on information sources needed for control purposes. Its duration depends on what information has to be extracted. The ratio of these two times gives the "control dwell fraction," $\eta = T_d/T_s$, which indicates, on the average, the proportion of the total control plus managerial task scanning time interval required by the control task.

The information transfer characteristics of the divided attention attributes of the human controller may be modeled as a quasi-linear, random-input "perceptual describing function," Y_h. This multiplies the full-attention (continuous control) human describing function(s), Y_p, to provide the describing function(s) for the human pilot's control activities.

The simplest way to develop an internal signal from a finite duration sampled input is to act proportionally to the sampled signal. Then,

during the fixation period, T_d, the pilot's output would be proportional to the perceptual input being sampled, while outside the fixation period, it will be zero (see Fig. 11 lines a and b). The describing function is based on the best linear fit of the output, in the mean-squared sense. For this simple finite dwell time sampling, the perceptual describing function is just the dwell fraction itself, $Y_h = \eta$. The "remnant" accounts for all of the pilot's higher frequency power not linearly connected with the input. The describing function and remnant are shown on line c of Fig. 11, (Ref. 15). [It is important to emphasize that the signals shown in Fig. 11 are highly idealized for clarity. Everything is really much more random: the signals themselves, the dwell times (T_d), and the sampling intervals (T_s).]

From Fig. 11 it is easy to see, as the divided attention level is changed to reduce the control dwell fraction, η, that

- The describing function, Y_h, is reduced
- The remnant is increased

The crossover model in Fig. 11 shows that a reduction in Y_h will cause a concomitant reduction in the pilot-vehicle system crossover frequency, ω_c. For the crossover model, ω_c is also the pilot-vehicle system loop gain. Because this is directly related to the system phase margin, ϕ_M, by

$$\phi_M = \frac{\pi}{2} - \tau_e \omega_c \tag{11}$$

where τ_e is the overall pilot-vehicle system latency, then the reduction in ω_c will be reflected in increased phase margin.

As can readily be appreciated from the above discussion, the effects of divided attention can have profound consequences on the pilot-vehicle system performance in control activities. These can be conveniently summarized by the illustrative case sketched in Fig. 12. As already noted, divided attention results in lower crossover frequency and associated increased phase margin. As far as the pilot-vehicle system dynamics are concerned, a major consequence is a significantly increased error in control activities. As shown in Fig. 12, divided attention penalizes the error performance in two ways:

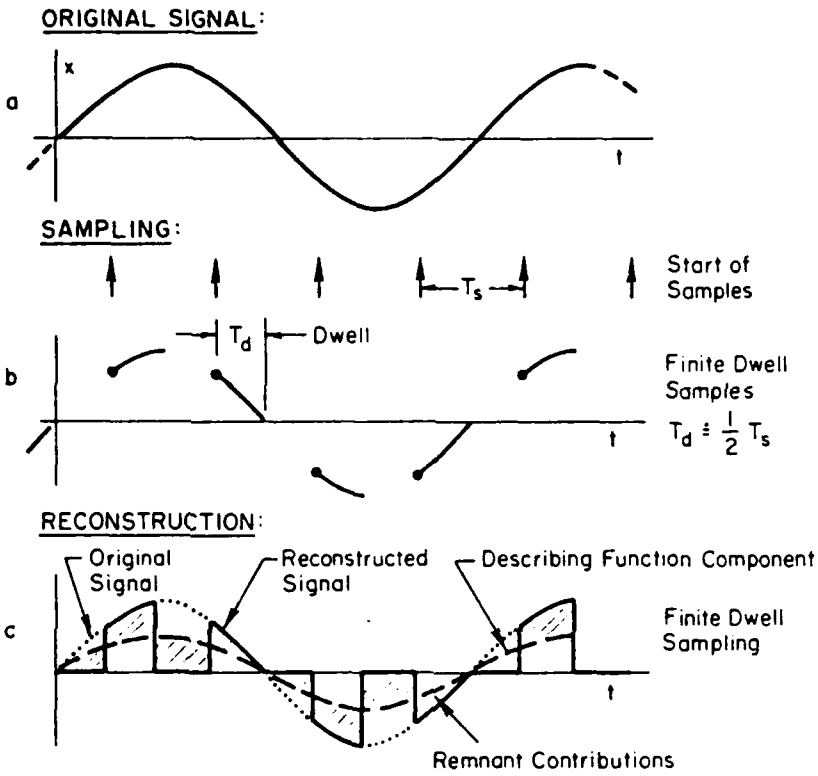

Figure 11. Features of Finite Dwell Sampling

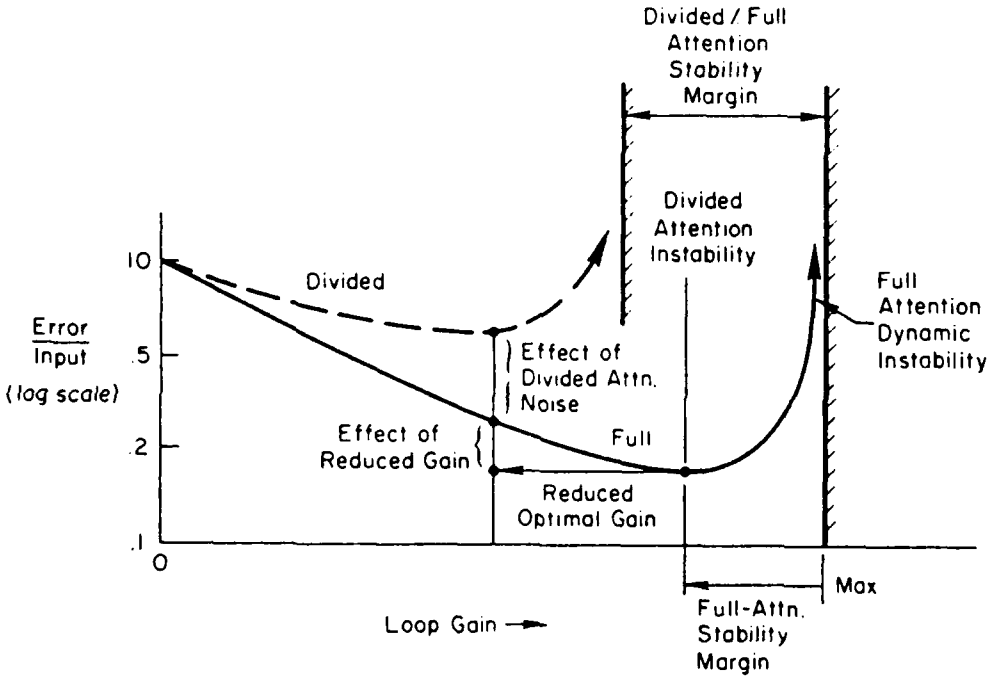

Figure 12. Consequences of Divided Attention

- By reduction of the permissible crossover gain, and
- By a major increase in the remnant due to the divided attention (i.e., lack of attention to the control tasks).

Figure 12 shows that the full attention pilot-vehicle system error begins to increase only as the dynamic stability limit is approached; at lower gains, error is reduced as gain increases. While a similar trend is shown for divided attention, the error may still increase without bound for circumstances where there is still a large dynamic stability margin. This is because the closed-loop effect of divided attention remnant, the power level of which scales with mean-squared error as in Weber-law noise, causes error signal instability in the mean-squared sense (Refs. 15 and 32). From the analyst's point of view, this property of control tasks with divided attention requires a larger phase margin (even more stable operation of the control task than with full attention) as the control dwell fraction is decreased.

A Weber-law model of divided attention remnant has been applied to the error signal in the "crossover model" shown in Fig. 10 (Refs. 15, 33 through 36). The model of divided attention remnant includes factors representing average attentional dwell time fraction (on the control task) and variability thereabout. A quantitative example of the effects of divided attention on performance is presented in Fig. 13. In Fig. 13a, the abscissa is normalized crossover frequency (analogous to Fig. 12), while Fig. 13b provides the same data plotted with phase margin as the abscissa. The forcing function is white noise passed through a third-order Butterworth filter with normalized breakpoint, $\omega_i \tau_e = 0.25$. The full attention condition is the lowest curve in both portions of Fig. 13. The divided attention conditions that govern the remnant are shown as families with control task dwell fraction, η, as the parameter. In this example, the normalized control dwell interval is set at $T_d/\tau_e = 1.5$, and the normalized lower bound on the scanning interval, $\delta = 0.5$.

Figures 12 and 13 show the profound effects of divided attention on control system performance particularly emphasizing the two "stability limits." The first is the full attention limit given by $\omega_u = \pi/2\tau_e$, which is approached by the full attention, $\eta = 1$, curve. The second is the

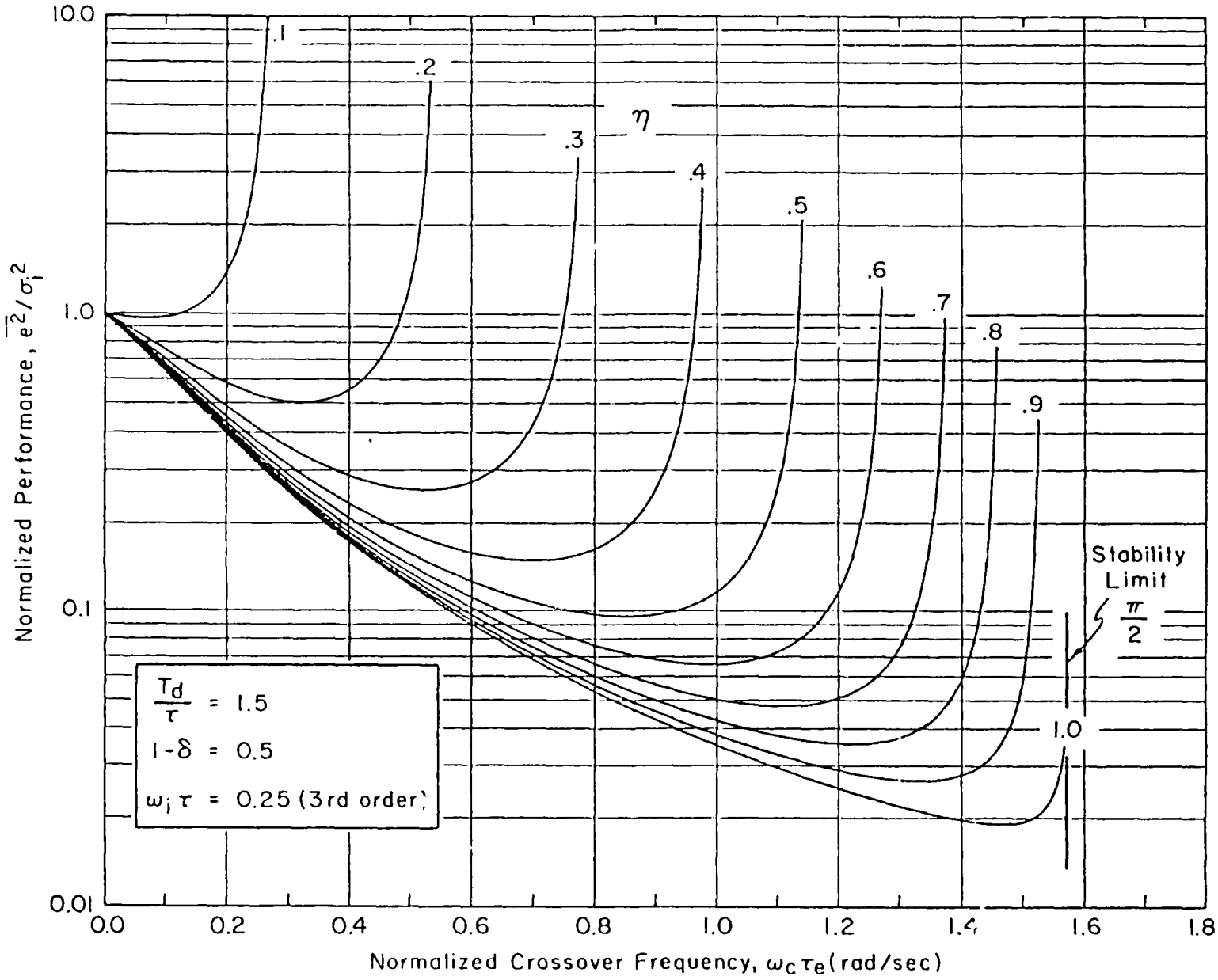

Figure 13a. Effect of Divided Attention Remnant on System Performance as a Function of Normalized Crossover Frequency

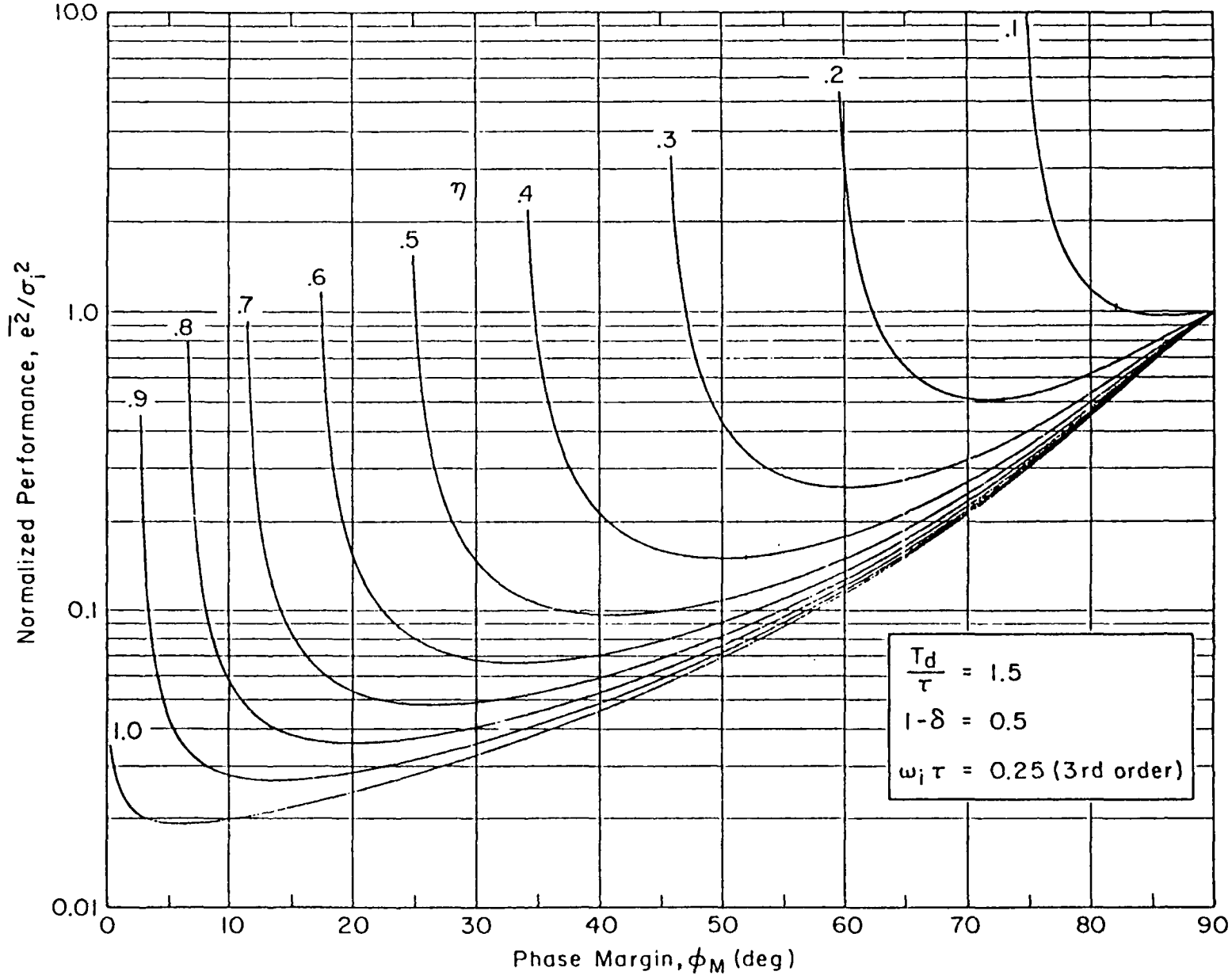

Figure 13b. Effect of Divided Attention Remnant on System Performance as a Function of Phase Margin

"instability in the mean square." This is associated with the inequality constraint

$$F = 1 - p_e = \frac{\overline{e_n^2}}{\overline{e^2}} < 1 \tag{12}$$

The bases for this phenomenon and other divided attention analytical relationships will be summarized below.

Note that mean-square error instability occurs at progressively increasing phase margins as the attentional dwell fraction on the control task decreases. Furthermore, the phase margins for minima in normalized error variance are even greater, and the minima are broad. Typically, the "blow up" phase margin is less than the phase margin for best performance by 10 to 16 deg. Figure 14 puts these points into context by showing the phase margins for the blow up condition ($F = 1$), the phase margins for the minima (from Fig. 13), and the phase margins for a value of error coherence, ρ_e^2, of 1/2 (corresponding to $F = 0.5$). The latter curve nearly coincides with the minimum mean-squared error curve when the control dwell fraction is less than 1/2. For larger control dwell fractions, say from 1/2 to 1, the phase margin for minimum mean-squared error is essentially a linear function of dwell fraction, as indicated by the fit on Fig. 14.

Analytical formulas (derived in Ref. 34), on which constructions such as Figs. 13 and 14 are based, are summarized in Table 4. The phase margin-dependent function $\underline{A}$ (ϕ_M, τ_e/T_d) [or normalized crossover frequency-dependent function $\underline{A}$ ($\tau_e\ \omega_c$, τ_e/T_d)] is shown in Fig. 15. The curves are given as families with two parameters: (a) the normalized control dwell time T_d/τ_e, and (b) the nondimensional variable $\beta\tau_e$, where $\beta = 2/T_d$. The $T_d/t_e = 0$ ($\beta\tau_e = \infty$) curve is the simplified function $A(\phi_M)$. As phase margin increases, this becomes a reasonable approximate bound for the more complete function.

One of the most interesting features provided by the formulas is the limit associated with the fundamental constraint, i.e., the

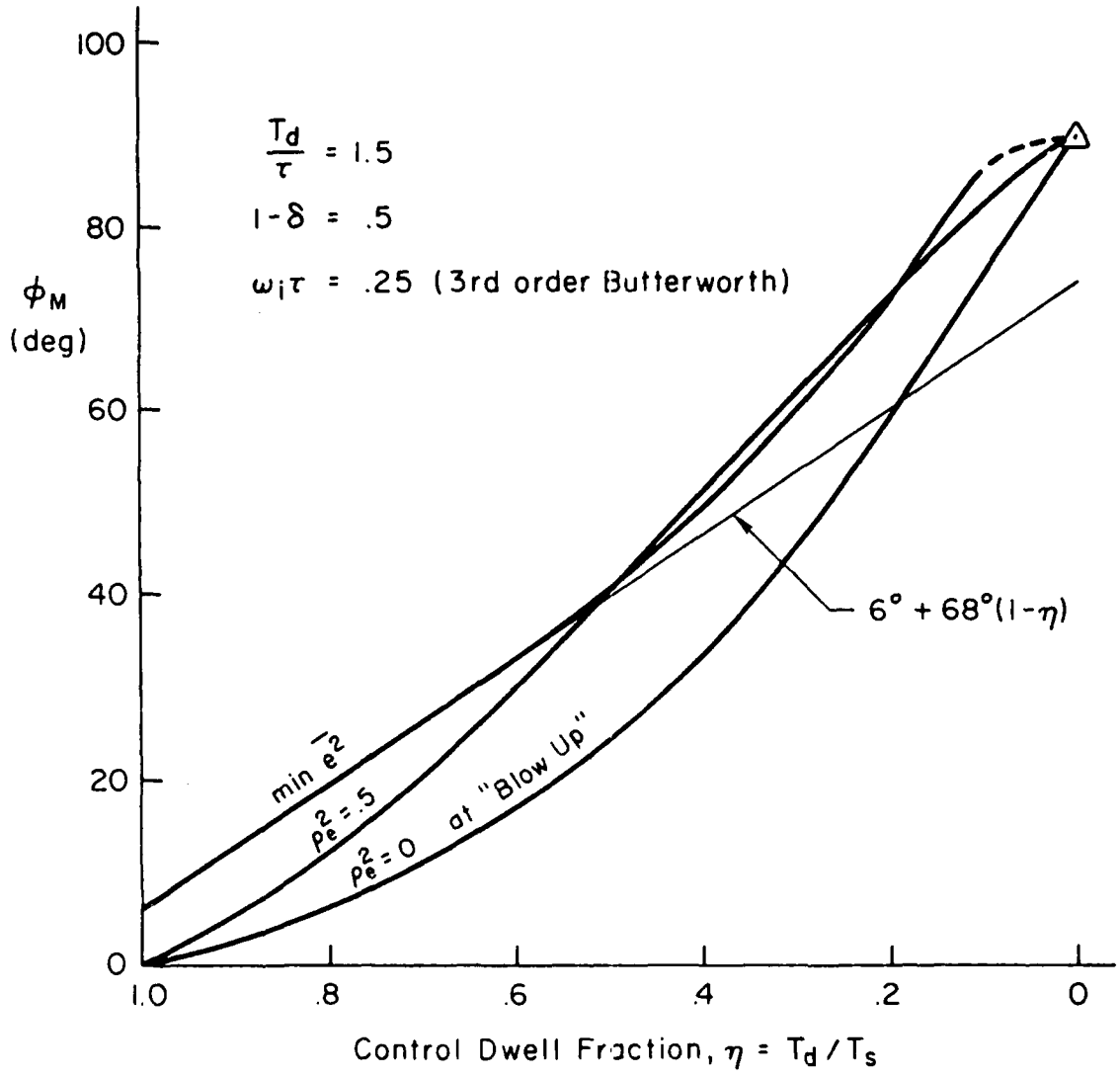

Figure 14. Effect of Divided Attention on Phase Margins for Minimum Mean-Squared Error

TABLE 4. BASIC DIVIDED ATTENTION RELATIONSHIPS

DIVIDED ATTENTION REMNANT POWER SPECTRAL DENSITY

$$\phi_{nn}(\omega) \doteq \frac{T_s(1-n)(1-\delta)}{\pi\left[1+\left(\frac{\omega T_d}{2}\right)^2\right]}\,\overline{e^2}, \qquad \begin{array}{l} 0 < \delta = T_o/T_s < 1 \\ 0 < n = T_d/T_s < 1 \end{array}$$

where $\overline{e^2} \triangleq \int_0^\infty \phi_{ee}(\omega)\,d\omega$

T_o is the lower bound on the attentional scanning or sampling interval

T_s is the mean value of the attentional scanning or sampling interval

T_d is the mean value of the attentional dwell interval

$\phi_{ee}(\omega)$ is the error power spectral density, (units of error)^2/(rad/sec)

SYSTEM PERFORMANCE

$$\underbrace{\overline{e^2}}_{\substack{\text{Total}\\\text{System}\\\text{Mean-Squared}\\\text{Error}}} = \underbrace{\overline{e_i^2}}_{\substack{\text{Input-and}\\\text{Disturbance-}\\\text{Correlated}\\\text{Mean-Squared-Error}}} + \underbrace{\overline{e_n^2}}_{\substack{\text{Uncorrelated}\\\text{Mean-Squared-Error}\\\text{Caused by}\\\text{Divided Attention}}}$$

$$= \int_0^\infty \left|\frac{1}{1+G}\right|^2 \phi_{ii}\,d\omega + \frac{T_s\overline{e^2}(1-n)(1-\delta)}{\pi}\int_0^\infty \left|\frac{G}{1+G}\right|^2 \frac{d\omega}{\left[1+\left(\frac{\omega T_d}{2}\right)^2\right]}$$

where G is the open-loop describing function of the pilot vehicle system (Fig. 10)

$$\frac{\overline{e^2}}{\overline{e_i^2}} = 1/1 - F$$

$$F = \frac{\overline{e_n^2}}{\overline{e^2}} = 1 - \rho_e^2 = \frac{T_s(1-n)(1-\delta)}{\pi}\int_0^\infty \left|\frac{G}{1+G}\right|^2 \frac{d\omega}{\left[1+\left(\frac{\omega T_d}{2}\right)^2\right]}$$

FUNDAMENTAL CONSTRAINTS

$$\tau_e\omega_u = \pi/2 \qquad \text{(Full Attention)}$$

$$F = \overline{e_n^2}/\overline{e^2} < 1 \qquad \text{(Divided Attention)}$$

BASIC RELATIONSHIPS FOR ERROR INCOHERENCE IN TERMS OF THE CROSSOVER MODEL FOR G

$$F = \frac{\overline{e_n^2}}{\overline{e^2}} = \frac{(T_s - T_d)}{\tau_e}(1-\delta)\,\mathcal{X}(\phi_M, T_d/\tau_e)$$

$$\mathcal{X}(\phi_M, T_d/\tau_e) = A(\phi_M)\left\{\frac{A(\phi_M) + \gamma(\phi_M)(T_d/4\tau_e)}{A(\phi_M)[1+\gamma(\phi_M)(T_d/2\tau_e)^2] + \gamma(\phi_M)(T_d/4\tau_e)}\right\}$$

$$A(\phi_M) = \frac{\ln(\pi e/2)}{4}\,\frac{[(e\pi/2)[1-(\phi_M/(\pi/2))]^{2[(\ln\pi/2)/(\ln\pi e/2)]}}{-\ln[1-(\phi_M)/(\pi/2)]}$$

$$= 0.676\,[(\pi/2-\phi_M)^{0.622}]/[-\ln(1-\phi_M/(\pi/2))]$$

$$\gamma(\phi_M) = [e\pi/2\,(1-\phi_M/(\pi/2))]^{2[(\ln\pi/2)/(\ln\pi e/2)]}$$

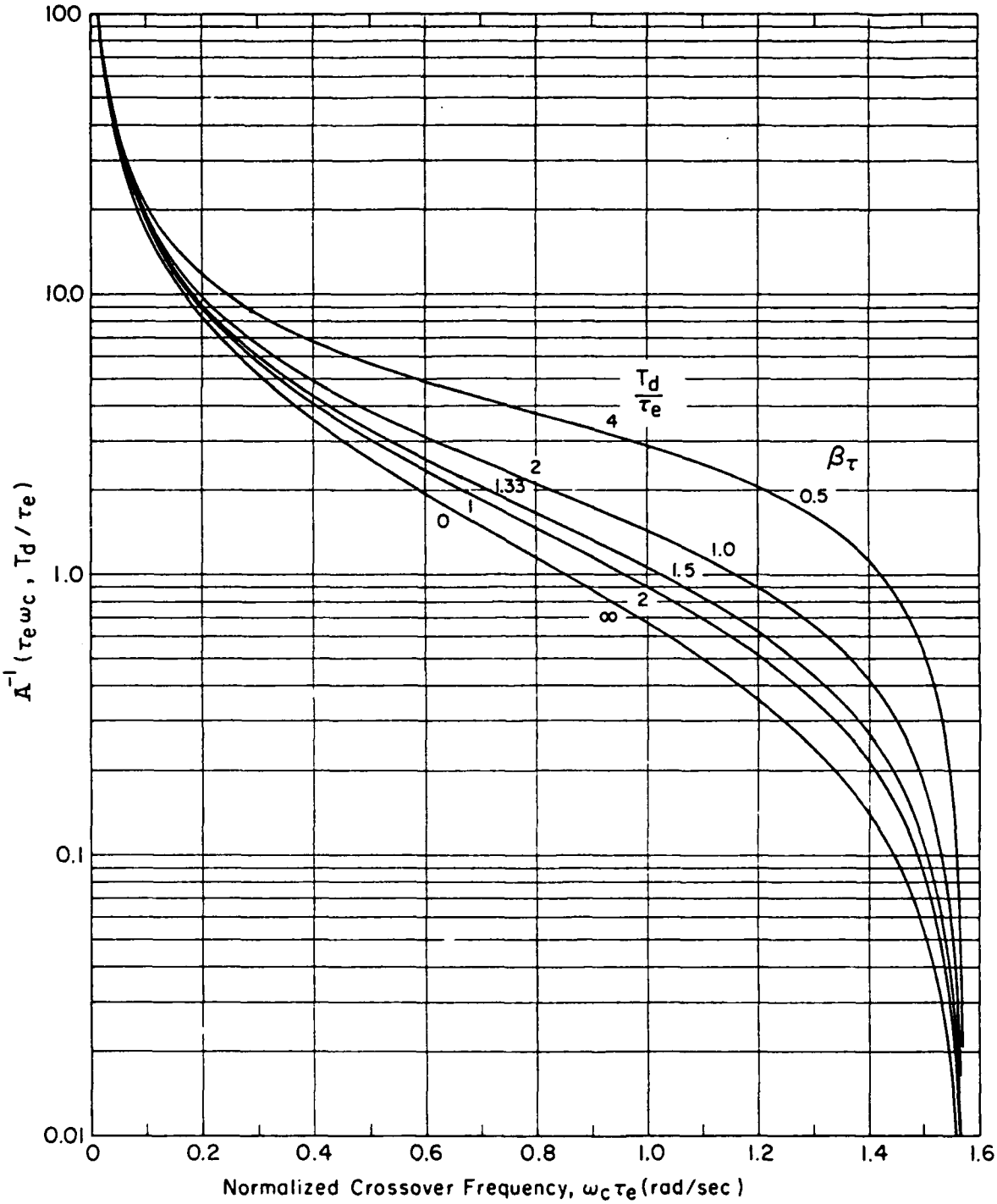

Figure 15a. $\underline{A}^{-1}(\phi_M, \tau_e/T_d)$ as a Function of Normalized Crossover Frequency

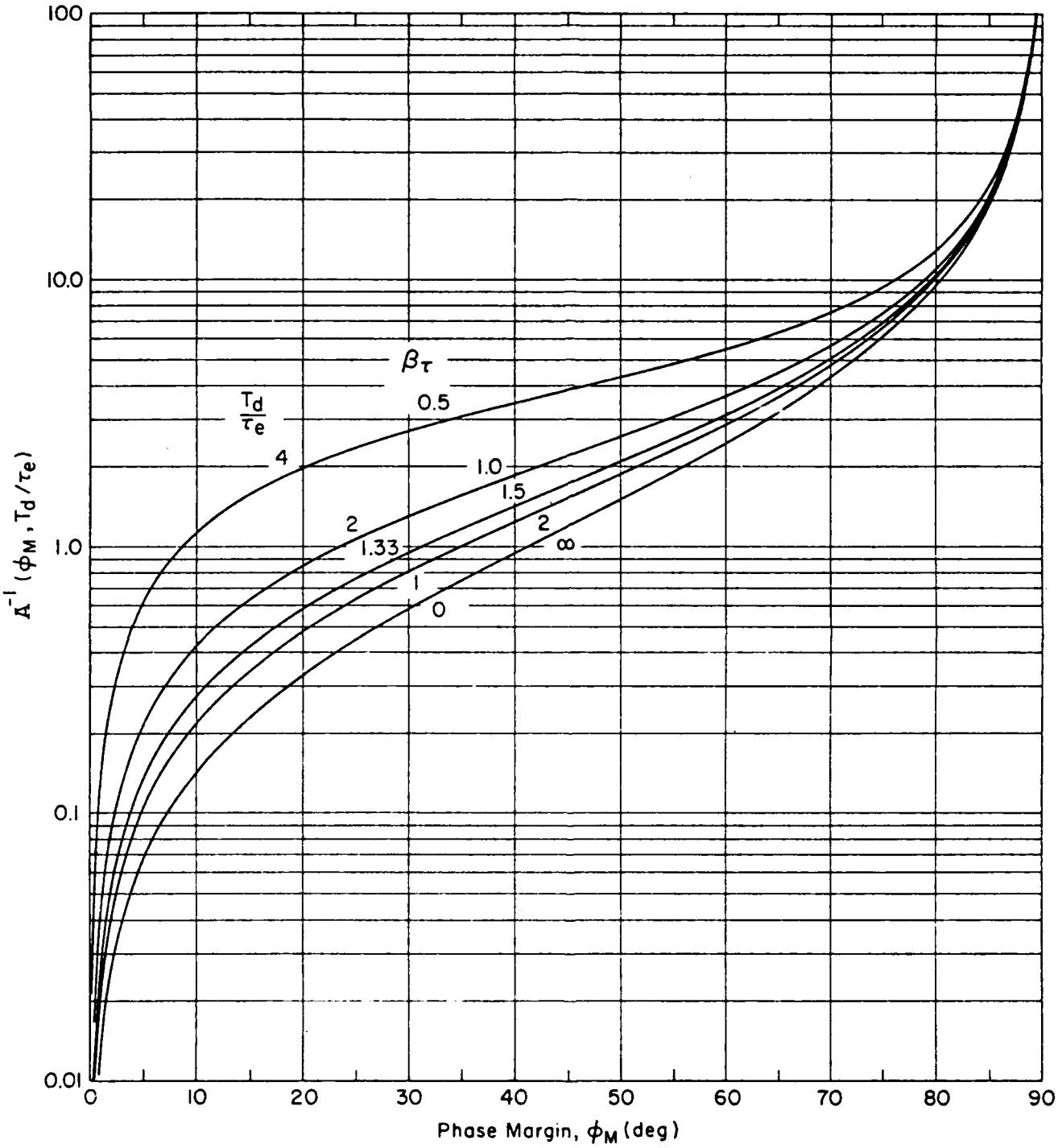

Figure 15b. $\underline{A}^{-1}(\phi_M, \tau_e/T_d)$ as a Function of Phase Margin

Divided Attention Error Stability Limit:

$$F = \frac{\overline{e_n^2}}{\overline{e^2}} \leq 1, \qquad \text{or}$$

$$\underline{A}\left(\phi_M, \frac{T_d}{\tau_e}\right) \geq \frac{(T_s - T_d)(1 - \delta)}{\tau_e} \tag{13}$$

The curves of Fig. 15 can be used directly in conjunction with Eq. (13) to determine the minimum phase margin or maximum normalized crossover frequency available for a given level of divided attention. The maximum value of $\underline{A}(\phi_m, T_d/T_e)$ must be less than $\tau_e/(T_s - T_e)(1 - \delta)$. With an appropriate change of labeling on the ordinate, the curves then become boundaries for stability in the mean-square, with locations below the curves corresponding to allowable phase margins.

For some purposes, the inequality of Eq. 13 may be awkward to work with because of the dependence of both sides on T_d. The simpler, more approximate form using the $A(\phi_m)$ may therefore be more useful. With this approximation, the Eq. 13 condition becomes

$$\frac{1}{A(\phi_m)} > \frac{(T_s - T_d)(1 - \delta)}{\tau_e} = \frac{T_d}{\tau_e}(1 - \delta)\left(\frac{1 - \eta}{\eta}\right) \tag{14}$$

These last relationships emphasize the need to constrain the system phase margin to keep the error in divided attention operations within bounds. This follows because $(1-\eta)/\eta$ increases as the managerial demands increase. [For a given control task, the overall system latency is the sum of the net high-frequency system lag and the pilot's effective delay. The control task dwell time, T_d, defines how long the pilot must fixate on various "display" elements to assimilate the information needed for control. Thus T_d/τ_e is approximately constant for a given control-display task, and $(1-\eta)/\eta$ governs the inequality]. Then, as the maximum allowable value of $\underline{A}(\phi_M, \tau_e/T_d)$ is reduced to maintain the inequality, Fig. 13 indicates that the divided attention control task phase margin must be increased. Because the normalized crossover frequency, $\tau_e\,\omega_c$, is directly related to the phase margin by $\phi_M = (\pi/2) - \tau_e\,\omega_c$, this can also be

interpreted as indicating that the control task crossover frequency is reduced.

The implications of these statements include:

- The control task error has an extremely strong dependence on the control task dwell fraction. (The pilot-vehicle system gain is reduced and the system "remnant" or effective uncorrelated input due to lack of attention to the control task is increased as control task attention decreases).

- If the task complex requires significant division of pilot attention between managerial and control tasks, the dynamics of the system being controlled by the pilot must be able to support very large pilot-vehicle system phase margins. As a corollary, the controlled system must possess dynamic properties that require little attention to control.

These implications are, of course, consistent with the conventional wisdom that attitude control and path control functions are among the highest priorities for automation as means to reduce pilot control workload. Steps in this direction cut down the control dwell fraction directly, and increase the fraction of attention that can be devoted to managerial task sequences.

SECTION IV

ALGORITHMIC HUMAN PILOT MODEL

A. OVERVIEW OF THE MODEL

An alternative approach to the estimation and description of human control behavior has been the application of modern optimal control theory. The starting points in this process are the well-founded theory of the linear-quadratic-gaussian stochastic control problem, and manual control theory and data. To successfully marry these two elements is not easy, yet great progress has been made (e.g., Refs. 37-47) over the past twenty years. Some notable applications to flying qualities problems have also been published (e.g., Refs. 48-50). The concept rests on the presumption that human operator responses can be emulated by an analogous optimal control system. The optimal system operates to minimize a quadratic performance index in the presence of various system inputs and noises. In doing so it provides a representation for at least some of the adaptive characteristics of the human operator. The basic consideration in this algorithmic approach is the provision of techniques for imposing those characteristics of the human which represent both favorable (e.g., adaptation) and unfavorable (e.g., time delay and remnant) features so they are consonant with experiment. Related techniques must account for certain very fundamental human characteristics, such as the effective time delay and neuromuscular delays.

A general picture of the algorithmic or optimal control (OCM) model is shown in Fig. 16. At the top are the machine properties involving the controlled element and display as acted on by disturbances. These are represented by linear state vector and display vector-matrix equations. The disturbance, $\mathbf{w}(t)$, is a vector of white gaussian noise processes. This represents both forcing functions and disturbances impacting the controlled element. If the forcing functions are colored, they are represented by filtered white gaussian noise. The additional states required to represent the filter dynamics are appended to the controlled element state vector and result in expanded $\mathbf{A}$, $\mathbf{B}$, $\mathbf{C}$, and $\mathbf{E}$ matrices. Deterministic disturbances can be modeled by adding non-zero mean

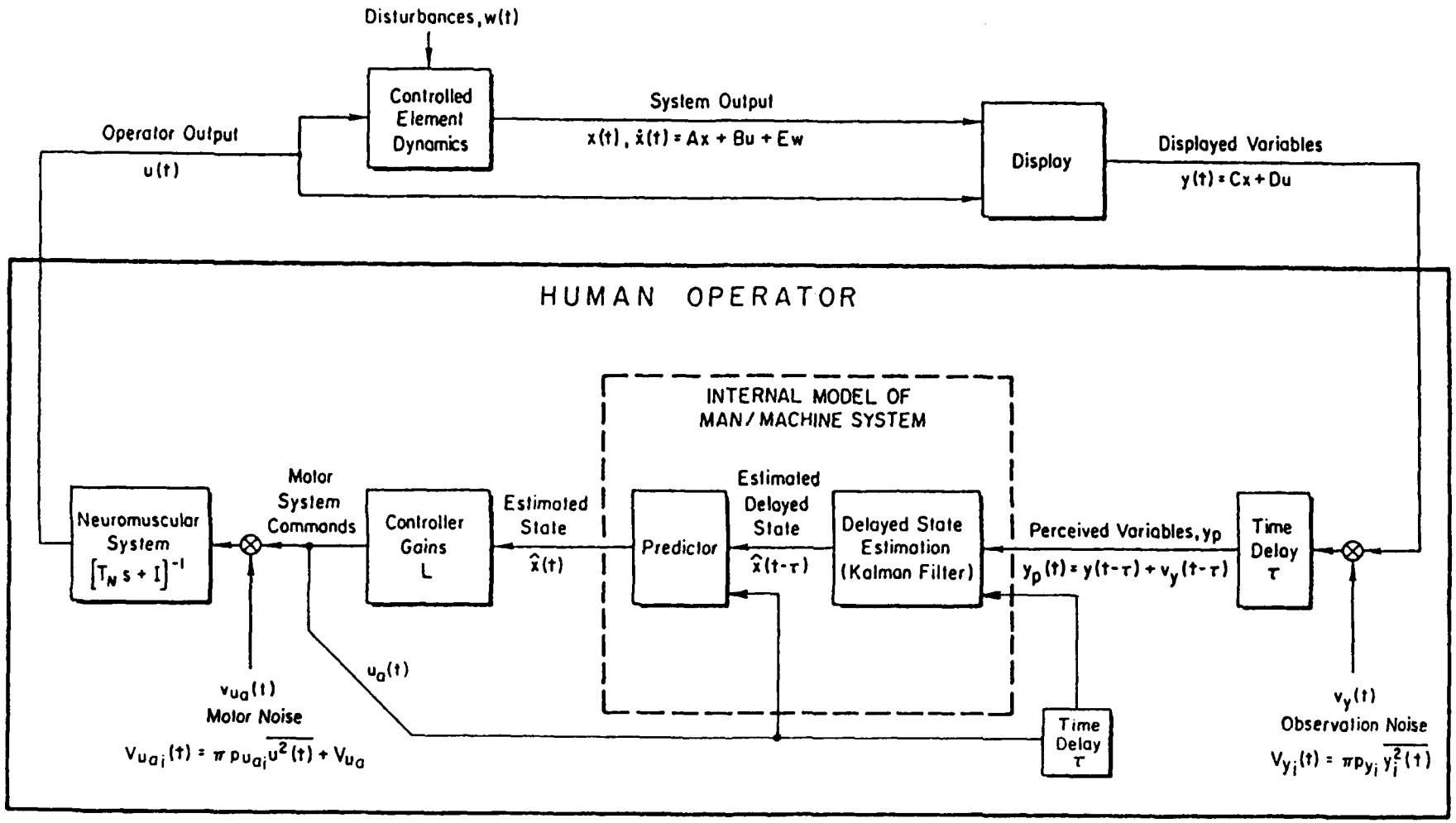

Figure 16. Algorithmic (Linear Optimal Control) Model of Man-Machine System

components to the disturbance vector, with the addition of still more elements to the state vector and associated matrices. The display variables are linear combinations of the system states and the pilot output.

In the optimal control formulation the human pilot's characteristics can be divided into two categories -- those which represent intrinsic human limitations, and thus which are not subject to optimization, and those properties which are subject to adaptation and thus optimization. In the first category are the effective time delay and the remnant. To some extent the neuromuscular system properties and/or the pilot-vehicle system crossover form and bandwidth also fall into this category, although their connections in the OCM formulation are somewhat obscure. (This will be illustrated later.) In the optimal control model the remnant is accounted for by observation noise and motor noise, shown respectively at the pilot's input and neuromuscular command output points. The observation noise vector is added to the display output $\mathbf{y(t)}$. A separate noise component, $v_{y_i}(t)$ is associated with each display output component, $y_i(t)$. As noted in Fig. 7a, the remnant added at the operator's input is relatively wideband, so each component is assumed to be an independent gaussian white noise process. The spectral density is proportional to the mean-squared value of the displayed component, with a proportionality factor P_{y_i}, which is a noise-to-signal ratio. In general, the human operator is presumed to obtain both displacement and rate information from a single display variable, and good results have been obtained by assuming that P_{y_i} for the position and rate variables is the same. In single-loop control situations numerical values of P_{y_i} of about 0.01 are typical. As can be appreciated from Fig. 7a, this is relatively invariant over a wide range of system dynamics and input spectra. To the extent that this is so, the normalized observation noise can be considered to be primarily operator-dependent.

The many internal time delays associated with visual, central processing, integrative, and other operations are combined into a lumped perceptual delay, τ. For simplicity, it is assumed in the current optimal control model that all outputs are delayed by the same amount. (As noted previously in connection with the structural isomorphic model, there is a delay increment associated with rate perception.)

The "motor noise," like the observation noise, is assumed to be a zero-mean gaussian white noise with spectral density proportional to the mean-squared operator output. An additional component, $V_{u_{a_o}}$, is sometimes included to account for the fact that the human operator introduces noise into an undisturbed system. A motor noise/signal ratio, $\rho_{u_{a_i}}$, of 0.003 has been found to provide a good match to some experimental data.

The neuromuscular system is represented by a lag matrix, T_N. This is not explicitly modeled as an inherent limitation. Instead, it is imposed by weighting control rate terms in the cost function used to generate the optimal control. For single-loop control problems with linear, wide bandwidth manipulators, this weighting is purposely selected to yield T_N of approximately 0.1 sec to represent this inherent limitation. As will be seen later, this weighting tends to set the frequency range over which the pilot-vehicle system may approximate the crossover model in a single input, single output system. When everything is taken into account in an effective pilot describing function Y_p the direct neuromuscular lag represented by T_N will be cancelled by other quantities, although the total effective time delay may reflect some neuromuscular lag.

The remaining elements of the human operator are adaptive to the system characteristics and to changes in the explicit human operator limitations described above. Estimation of the delayed state vector is accomplished via a Kalman filter. This delayed state estimate is fed to a least-mean-squared predictor to yield the estimated state vector, $\hat{x}(t)$. The optimal gain matrix, L, is generated by solving the optimal regulator problem for a quadratic cost function of the form

$$J(u) = E\left\{\lim_{T \to \infty} \frac{1}{T} \int_0^T (y'Qy + u'Ru + \dot{u}'G\dot{u})\, dt\right\} \tag{15}$$

Because the cost functional weightings preordain the details of the controller gain matrix, L, the selection of weightings is critical to the model's success. This is particularly the case when the model's purpose is to simulate human operator responses. For simple single-loop control situations, excellent agreement with experimental measurements has been obtained with a cost functional of the extremely simple form:

$$J(u) = E\left\{\lim_{T \to \infty} \frac{1}{T} \int_0^T (e^2 + G\dot{c}^2)\, dt\right\} \tag{16}$$

where e is the compensatory system error and $\dot{c} = \dot{u}$ is the operator's control rate. The value of G is selected as described above to yield an appropriate neuromuscular delay, T_N. For more complex situations, the relative weights are determined based either on maximum allowable deviations or limits, or from a knowledge of human preferences and capabilities. This is similar to the technique suggested by Ref. 51, wherein the weighting on each quadratic term is simply the inverse of the square of the corresponding allowable deviation. The solutions for this modified Kalman filtering prediction and optimal control problem are given by, for example, Refs. 38, 39, 42, 47, and 52.

Because the power spectral densities of the observation and motor noises scale with mean-squared values of variables within the system, an iterative solution method is required to achieve a solution with prescribed noise ratios. This, and other complications, make application of the OCM dependent on computer implementation. Although open literature implementations exist, notably PIREP (Ref. 47), they are not readily available or suitable for PC style calculations. Here we will describe an implementation of the OCM using Program CC (Ref. 53), which is anticipated to greatly increase the availability and understanding of the OCM.

Transfer functions of the operator dynamic characteristics obtained using the OCM are intrinsically very high order. For example, for single loop systems as treated later the human transfer function denominator is of order 2n + 5, where n is the order of the system which models the controlled element plus the driving noise. This contrasts markedly with such simple descriptions of human dynamic behavior as the crossover model (Ref. 1). Both the crossover model and the OCM can describe experimental data fairly well, so it follows that OCM results should be susceptible of considerable simplification. This possibility will be explored below. The approach to simplification is to include in the Program CC implementation of the OCM a novel transfer function approximation of the OCM's pilot describing function. This is expected to greatly enhance understanding and interpretation of OCM results

Additional features and numerous applications have appeared in the years following the OCM's introduction, notably (Refs. 54-56). The additional features included in Program CC's implementation are visual indifference thresholds and fractional attention parameters. Notably absent is the use of pseudo-noise to induce low frequency phase droop, and the optimization of fractional attention for multi-input problems. Article B will present a single axis version of the OCM, including a description of time and frequency domain performance measures and a novel transfer function approximation of the algorithmic model's pilot describing function. To later handle divided attention situations attentional fractions are incorporated in the model. These permit a relatively simple extension to cover the multi-axis case, which is done at the end of the article. Article C provides an outline of the implementation of the OCM using Program CC. This is more thoroughly treated in Volume III. In Article D the OCM is exercised in a single axis example which is used to compare with the crossover model.

B. *DETAILS OF THE HUMAN OCM*

1. Single Axis Problem Statement

In full attention operations the human operator manually controls a system with the objective of minimizing the system error in some sense. For a simple mathematical formulation we will presume that imprecisely stated objective will be satisfied by minimizing a mean square error. This is the situation for many standard tracking tasks. A state space model of the controlled system has n states, 1 input, 2 outputs, and 2 observations:

$$\dot{x} = Ax + Bu + Ew \tag{17}$$

$$y = Cx + Du \tag{18}$$

$$y_p = y(t - \tau) + v_y\,(t - \tau) \tag{19}$$

The 2 outputs are error y_e and error rate $\dot{y}_e$, and the observations are delayed by the human's assumed visual delay of $\tau = .2$ seconds. The source of the error is modelled by a white noise source w(t) with intensity V_w, passed through a shaping filter which has its dynamics included in the A matrix.

The observation noise is modelled by a white noise source $v_y(t)$ with intensity $V_y = \mathrm{diag}(v_{u_1}\ v_{y_2})$, where:

$$v_{y_i} = \frac{\rho_{y_i}\pi}{f} \frac{\sigma_{y_i}^2}{E(\sigma_{y_i}, T_i)^2} \quad i = 1,2 \tag{20}$$

The observation noise ratio is $\rho_{y_i} = .01$. The attentional fraction is $0 \le f \le 1$, with the remainder devoted either to other control tasks or to non-control tasks such as communication. (In the crossover model for divided attention the attentional fraction was devoted as η, which is equivalent to the f used here. The notational change is made to keep these developments consistent with the literature from which they were derived.) No control action results from errors below the indifference threshold T_i, which is based on human eye perceptual levels (e.g., $.05^o$ and $.1^o$/sec). The mean square error of the output is $\sigma_{y_i}^2$, which is increased due to the indifference threshold via the erfc function, which ranges from 0 to 1:

$$E(\sigma_{y_i}, T_i) = \mathrm{erfc}\left(\frac{T_i}{\sigma_{y_i}\sqrt{2}}\right) = \mathrm{Prob}\ (|y_i| > T_i) \tag{21}$$

It is important to note that v_{y_i} is proportional to the mean square error, which makes an iterative KBF/linear predictor solution necessary.

According to the human OCM, the human operator exerts control actions which minimize the performance index:

$$J = \lim_{T \to \infty} \left\{ \frac{1}{T} \int_0^T \left(y_e^2 + G\dot{u}^2\right) dt \right\} \tag{22}$$

The control action is a linear combination of the estimated state of the system. The linear combination is determined via a Linear Quadratic Regulator (LQR) problem, and the state estimation is determined via a Kalman Bucy Filter (KBF) and a linear predictor.

The LQR problem is solved by augmenting the input with an integrator and minimizing an equivalent performance index (using $\mu = \dot{u}$):

$$\dot{x}_o = A_o x_o + B_o \mu \tag{23}$$

$$x_o = \begin{bmatrix} x \\ u \end{bmatrix}; \quad A_o = \begin{bmatrix} A & B \\ 0 & 0 \end{bmatrix}; \quad B_o = \begin{bmatrix} 0 \\ I \end{bmatrix} \tag{24}$$

The solution is:

$$\mu = -[L_1 \quad L_2]\, x_o \tag{25}$$

$$L = G^{-1} B_o' K_o \tag{26}$$

$$0 = A_o' K_o + K_o A_o + Q_o - K_o B_o G^{-1} B_o' K_o \tag{27}$$

The weight G on the control rate $\dot{u}$ is chosen in an iterative fashion so that $L_2^{-1} = T_N = .1$, i.e., so that the state feedback around the integrator models the neuro-muscular mode with a time constant of .1 seconds.

The KBF/linear predictor problem estimates the state of the controlled system augmented with the neuromuscular mode and noise driven by an additional noise source:

$$\dot{x}_1 = A_1 x_1 + B_1 u_a + w_1; \quad y = C_1 x_1 \tag{28}$$

$$x_1 = \begin{bmatrix} x \\ u \end{bmatrix}; \quad w_1 = \begin{bmatrix} w \\ v_{u_a} \end{bmatrix}; \quad A_1 = \begin{bmatrix} A & B \\ 0 & -L_2 \end{bmatrix} \tag{29}$$

$$B_1 = \begin{bmatrix} 0 \\ L_2 \end{bmatrix}; \quad C_1 = (C \quad D) \tag{30}$$

$$W_1 = \begin{bmatrix} EV_w E' & 0 \\ 0 & L_2 V_{u_a} L_2' \end{bmatrix} \tag{31}$$

The white noise source $w_1(t)$ has intensity W_1 as shown above and incorporates the motor noise $v_{u_a}(t)$, which is inserted before the neuromuscular mode, and has its intensity defined as a ratio:

$$v_{u_a} = \rho_{u_a} \pi \sigma_{u_a}^2 \tag{32}$$

with the noise ratio $\rho_{u_a} = .01$ or $.003$. It is not physically possible to experimentally verify this motor noise model, but it is commonly accepted for reasons of mathematical tractability.

The KBF computes p(t), the linear mean-square estimate of $x_1(t - \tau)$, based on observations $y_p(\sigma)$ for $\sigma \leq t$.

$$\dot{p}(t) = A_1 p(t) + H_1[y_p(t) - C_1 p(t)] + B_1 u_a(t) \tag{33}$$

$$H_1 = \Sigma_1 C_1' V_y^{-1} \tag{34}$$

$$0 = A_1\Sigma_1 + \Sigma_1 A_1' + W_1 - \Sigma_1 C_1' V_y^{-1} C_1 \Sigma_1 \tag{35}$$

The linear predictor updates p(t) to obtain $\hat{x}_1(t)$, the linear mean-square estimate of $x_1(t)$ based on observations $y_p(\sigma)$ for $\sigma \le t$. Note that $p(t - \tau) \neq \hat{x}_1(t)$.

$$\dot{\xi}(t) = A_1 \xi(t) + B_1 u_a(t) \tag{36}$$

$$\hat{x}_1 = \xi(t) + e^{A_1 \tau}\,[p(t) - \xi(t - \tau)] \tag{37}$$

The LQR control weights are applied to $\hat{x}_1(t)$, but only to the portion which estimates the system states:

$$u_a(t) = -L^* \hat{x}_1(t); \quad L^* = (L_2^{-1} L_1 \quad 0) \tag{38}$$

A block diagram of the human optimal control model is presented in Fig. 17.

2. Time Domain Performance

Time domain performance measures are the mean square errors and the optimal cost. Define the estimation error $e_1 = x_1 - \hat{x}_1$, then:

$$E_1 = E\{e_1 e_1'\} = e^{A_1\tau}\Sigma_1 e^{A_1'\tau} + \int_0^\tau e^{A_1\sigma}\, W_1 e^{A_1'\sigma}\, d\sigma \tag{39}$$

$$\hat{X}_1 = E\{\hat{x}_1 \hat{x}_1'\} = \int_0^\infty e^{(A_1 - B_1 L^*)\sigma}\, e^{A_1\tau} H_1 V_y H_1' e^{A_1'\tau} e^{(A_1 - B_1 L^*)\dot{\sigma}} d\sigma \tag{40}$$

$$X_1 = E\{x_1 x_1'\} = E_1 + \hat{X}_1 \tag{41}$$

$$Y = E\{yy'\} = C_1 X_1 C_1' \tag{42}$$

$$U_a = E\{u_a u_a'\} = L^* \hat{X}_1 L^{*\prime} \tag{43}$$

The KBF/linear predictor solution is iterative due to the definition of these noise intensities. Use the mean square value Y and U_a to update the noise intensities, and stop the iteration when the achieved noise ratios are within about .1 power dB of the desired values (i.e., within .01 of $20 \log_{10}[\rho]$).

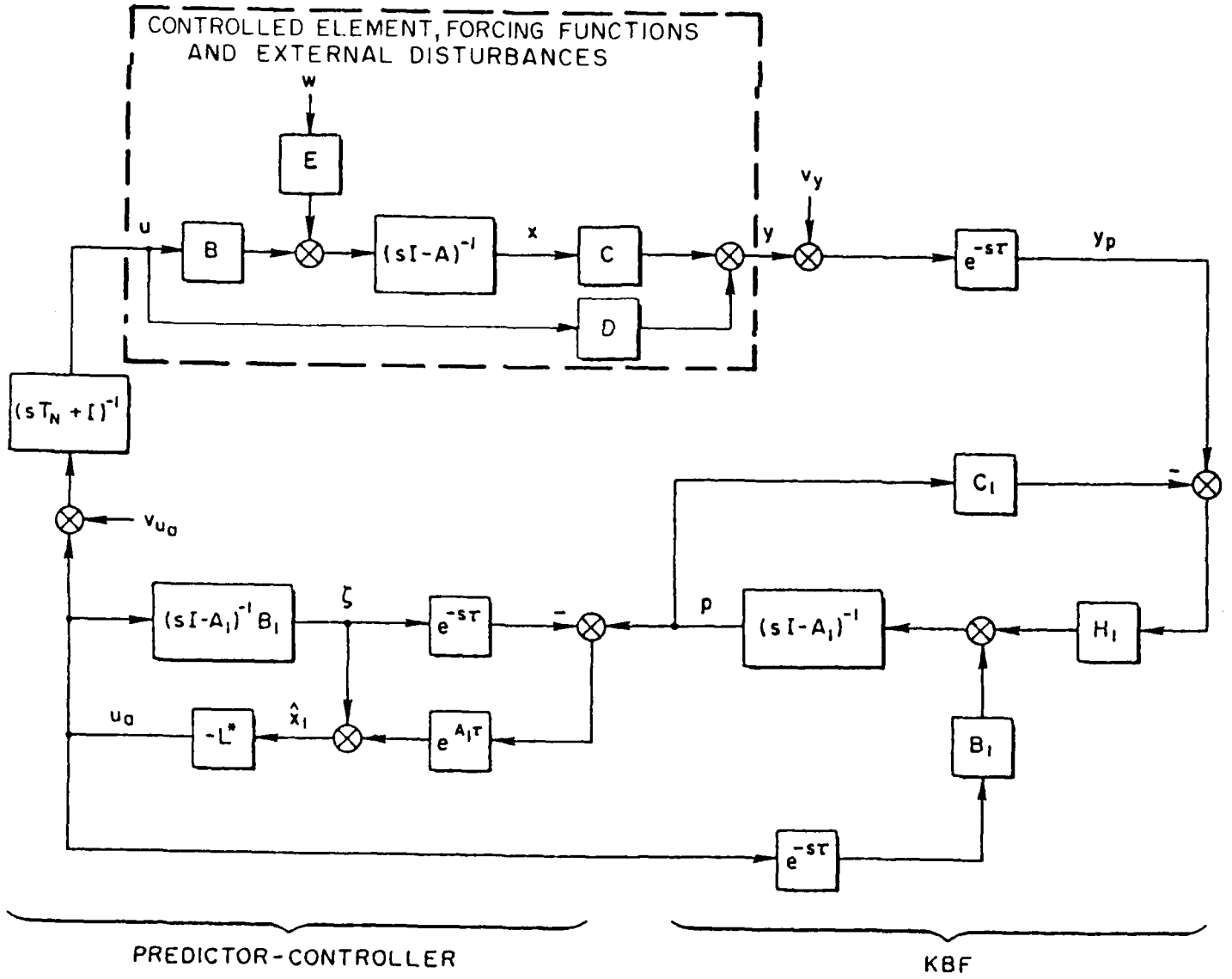

Figure 17. The Human Optimal Control Model

Strictly speaking, the performance index J is infinite, because the motor noise feeds directly into $\dot{u}$. Circumvent this problem by using $\dot{\hat{u}}$ instead. The optimal cost is:

$$\dot{\hat{U}} = E\{\dot{\hat{u}}\dot{\hat{u}}'\} = L\hat{X}_1L' + (0 \quad L_2)E_1(0 \quad L_2)' \tag{44}$$

$$J = Tr(YQ) + Tr(\dot{\hat{U}}G) \tag{45}$$

3. Frequency Domain Performance

Classical studies of human operator models use transfer function models. The controlled system has just the error as its output, i.e., $Y_c(s) = y_e/u$, and the pilot describing function is defined just from the error, i.e., $Y_p(s) = (u/y_e) + s(u/\dot{y}_e)$. Frequency domain performance measures are based on Y_p and Y_pY_c, for example

$$\omega_c = \text{system crossover frequency} \tag{46}$$

$$\phi M = \text{phase margin} \tag{47}$$

$$\tau_e = (\pi/2 - \phi_{Pm})/\omega_c = \text{effective delay} \tag{48}$$

$$\phi_{pc} = Arg[Y_p(j\omega_c)] - \omega_c\tau_e - \arctan[\omega_c\tau_N] \quad \text{pilot phase compensation} \tag{49}$$

Due to the observation delay the optimal solution incorporates a linear predictor. It is therefore not possible to express Y_p as a simple transfer function, and this has been a major impediment to understanding the OCM from a classical point of view.

The following new result gives an approximate transfer function for Y_p. Use a Padé approximation for the delay, where $u_p(t) \approx u_a\ (t - \tau)$:

$$\dot{x}_p(t) = A_px_p(t) + B_pu_a(t) \tag{50}$$

$$u_p(t) = C_px_p(t) + D_pu_a(t) \tag{51}$$

It then follows that the combined KBF/linear predictor/neuro-muscular system is approximated by:

$$\dot{x}_2 = A_2x_2 + B_2(y + v_y) + E_2v_{u_a}; \quad u = C_2x_2 \tag{52}$$

$$A_2 = \begin{bmatrix} A_1 - H_1C_1 & -B_1D_pL^* & B_1C_p & 0 \\ -e^{-A_1\tau}H_1C_1 & A_1 - B_1L^* & 0 & 0 \\ 0 & -B_pL^* & A_p & 0 \\ 0 & -L_2D_pL^* & L_2C_p & -L_2 \end{bmatrix} \tag{53}$$

$$x_2 = \begin{bmatrix} p \\ \hat{x}_1 \\ x_p \\ u \end{bmatrix} \quad B_2 = \begin{bmatrix} H_1 \\ e^{A_1\tau}H_1 \\ 0 \\ 0 \end{bmatrix} \quad E_2 = \begin{bmatrix} 0 \\ 0 \\ 0 \\ L_2 \end{bmatrix} \tag{54}$$

$$C_2 = (0 \quad 0 \quad 0 \quad 1) \tag{55}$$

The derivation is tedious but straightforward (replace $\dot{\xi}$ with $\hat{\dot{x}}_1$). A state space realization for Y_p is:

$$\dot{x}_2 = A_2x_2 + (B_{2_1} + A_2B_{2_2})y_e \tag{56}$$

$$u = C_2x_2 + C_2B_{2_2}y_e \tag{57}$$

The 2nd subscript indicates columns of the input matrix, and is based on the state space derivative:

$$s\gamma(sI - \alpha)^{-1}\beta = \gamma\beta + \gamma(sI - \alpha)^{-1}\alpha\beta \tag{58}$$

The state space realization for Y_p can be converted to a transfer function by standard techniques such as Fadeeva's method or eigenvalue and generalized eigenvalue problems. The order of $Y_p(s)$ will be $2n + 5$, and will contain many exact and approximate pole/zero cancellations.

4. Multi-Axis Extension

The human OCM formulation naturally extends to the multi--axis case. Here we are concerned with the case of multiple independent axes. The human operator scans several error indicators, each of which is controlled by only one input. Further, the operator is instructed to minimize the errors in all axes and not to give preference. These conditions can be

forced experimentally, and are a very good approximation of a pilot separately controlling longitudinal and lateral motion.

The assumptions of the human OCM problem for these conditions are (1) the single axis tasks are separately optimized, and (2) the attentional fractions are allocated so as to minimize the following total cost:

$$J_{total} = \sum_{i}^{N_{axes}} \frac{1}{\sigma_{c_i}^2} J_{axis}(f_i) \tag{59}$$

The axes are normalized with respect to the mean square command $\sigma_{c_i}^2$, defined to be $\sigma_{y_i}^2$ due to the driving noise. Note that these assumptions allow the operator to pay more attention to an axis which is difficult to control. The attention is apportioned across axes, so the same attention within an axis is paid to the error and error rate. The attentional sum across axes is ≤ 1, depending on whether a non-control task is required.

The multi-axis problem can be set up and solved as a multivariable problem. PIREP, one of the few currently available implementations of the OCM, solves the multivariable problem for given set of attentional fractions, and then optimizes over the f_i's using a gradient technique which iteratively computes at each step J_{total} and an estimate for $\partial f/\partial J_{total}$. PIREP's implementation is very involved, and is not suitable for personal computers. The multi-axis example of Appendix A is based on PIREP.

A different solution to the multi-axis problem which requires far fewer calculations is presented here. This approach is exemplified in Appendix B using the same data as Appendix A. The single axis problems are separately solved, and then the final optimization over the f_i's is computed by hand. The final optimization is based on the empirical observation that:

$$\frac{1}{\sigma_{c_i}^2} J_{axis_i} \approx a_i \frac{1}{f_i} + b_i \quad \text{for } i = 1,\ldots,N_{axis} \tag{60}$$

This approximation has been observed to hold (for the experimental systems used by Dander (Ref. 57) in a range varying from $f_i \geq .5$ to $f_i \geq .1$, depending on the amount of lead required by the operator. Each single

axis problem is solved for enough values of f_i to be able to estimate the a_i and b_i coefficients and to determine the range of validity. The final optimization over the f_i's can then be explicitly solved for the important cases of 2 and 3 axes.

The multi-axis optimization problem is to minimize with respect to the f_i's:

$$J_{total} = \sum_{i}^{N_{axes}} \frac{a_i}{f_i} + b_i \tag{61}$$

subject to constraint

$$\sum_{i}^{N_{axis}} f_i = 1 \tag{62}$$

The problem is solved using standard Lagrangian/Hamiltonian techniques. For 2 axes:

$$1/f_1 = 1 + \sqrt{a_2/a_1} \tag{63}$$

$$1/f_2 = 1 + \sqrt{a_1/a_2} \tag{64}$$

and for 3 axes:

$$1/f_1 = 1 + \sqrt{a_2/a_1} + \sqrt{a_3/a_1} \tag{65}$$

$$1/f_2 = 1 + \sqrt{a_1/a_2} + \sqrt{a_3/a_2} \tag{66}$$

$$1/f_3 = 1 + \sqrt{a_1/a_3} + \sqrt{a_2/a_3} \tag{67}$$

A final check should be made to see if the f_i's lie in range for which the approximations using a_i and b_i are valid. If not, a gradient search technique using piecewise linear approximations can be implemented, but we have yet to find this necessary.

C. IMPLEMENTATION

The human OCM is a variant of the standard Linear Quadratic Gaussian (LQG) problem, with the following distinctions. The algorithm for solving the human OCM is summarized in Fig. 18.

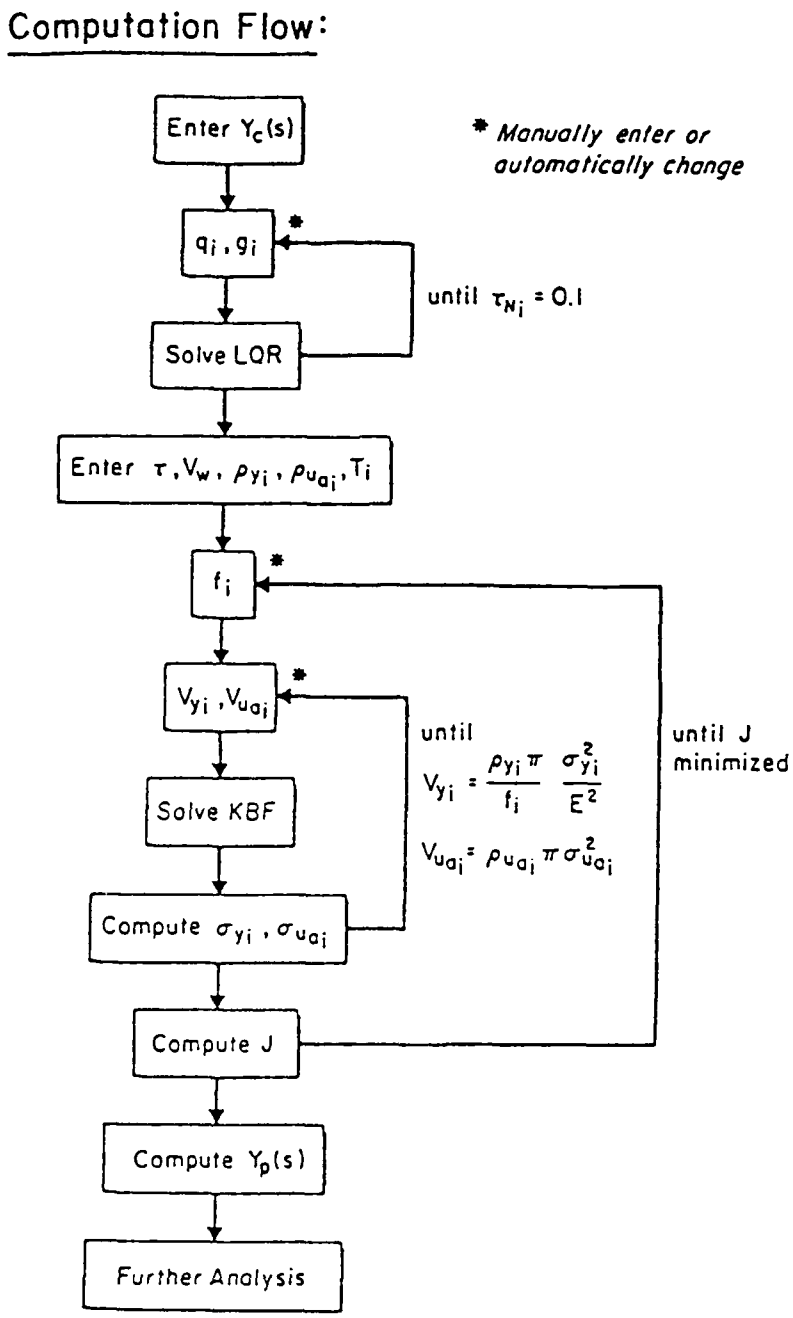

Figure 18. Iterative Algorithm for Solving the OCM

- The performance index weights $\dot{u}$, not u. The LQR problem is solved by augmenting the system with an integrator, and the feedback around the integrator models a neuro-muscular mode.

- The observations are delayed, hence the need for a linear predictor.

- The KBF uses the controlled system augmented with the neuro-muscular mode, not the system alone or the system with the integrator.

- The observation and motor noise intensities are defined as a ratio of the respective mean square outputs and inputs. An iteration is required to achieve this ratio.

- An additional iteration is required to minimize the multi-axis problem with respect to the attentional fractions.

Program CC contains all of the required low and high level routines for solving the OCM in a command driven, user friendly environment. It is significant that Program CC is implemented on a personal computer, thus greatly increasing the availability of the OCM. Program CC is used for design and analysis of a wide range of classical, digital, sampled-data, state space, and optimal control systems. The state space optimal control part of the package are used to solve the OCM problem, the state space realization for Y_p can be converted to a transfer function, and then Bode plots (also Nichols, Nyquist, root loci, and Bode-root-loci plots) can be used to analyze Y_p just like any other classical compensator. The interactive graphics makes the classical analysis particularly insightful.

The low level numerical routines which are required to solve the OCM are:

1. Block matrix manipulation
2. Riccati equation
3. Lyapunov equation
4. Matrix exponential
5. erfc function
6. iteration control

Elaborating further: (1) Block matrix manipulation is symbolically implemented, so that equations can be entered and solved in a very natural fashion. State space systems or quadruples are treated as a single data element, which greatly decreases bookkeeping. (2) Riccati equations are

used to solve the LQR and KBF problems. Potter's method is used, which computes the stable invariant subspace of a Hamiltonian matrix. Schur vectors are used for the required matrix decomposition, which is numerically better conditioned then the more standard eigenvector methods. (3) Lyapunov equations are used to compute mean square errors. A variant of the Bartel-Stewart method is used. The Bartel-Stewart method decomposes the linear Lyapunov matrix equation into a form which can be recursively solved. The variant uses Schur vectors instead of eigenvectors. (4) The matrix exponential is needed as part of the linear predictor. The matrix exponent is first scaled, a Pade approximation is computed, and then the result is unscaled. More information on matrix algorithms is available from Thompson (Ref. 53) and Golub and Van Loan (Ref. 58).

The many commands needed for the solution are combined into several macros and one user-defined-command. A macro is a sequence of commands which allows nesting and parameter insertion. A user-defined-command is a separate program callable from within Program CC, which is this case computes the erfc function and controls the LQR and KBF iterations.

There are many parameters in the OCM which define human behavior, yet there are generally accepted values for each. It is easiest to use the default values, but any other values may be substituted. Considerable work may be needed to characterize the controlled system and the driving noise, but the solution of the OCM is for the most part a turn-the-crank type operation.

The OCM problem stretches the limits of personal computers, even for relatively small order problems. There is no problem with memory size, disk size, and numerical accuracy; but there realistically is a problem with computation time, becoming quite noticeable for systems above 15th order, with the number of LQR and KBF iterations being the bottleneck. The number of iterations can be reduced by using good starting value for the noise intensities, which is feasible if the same or similar problems have been solved. Low order effective models of the controlled system can be used for most flying qualities problems.

Solving the multi-axis as several single axis problems requires fewer total calculations (i.e., flops), as now conservatively estimated. Several of the individual steps such as Riccati solutions are n^3 operations, so call the entire OCM solution an n^3 operation with a large multiple. If the 3 axis multivariable problem is solved in one step this takes $27n^3$ operations, and if there are 5 iterations for the f_i gradient search routine then the total is $135n^3$. On the other hand if the single axis problems are solved this requires $3n^3$ operations, and each axis must be solved say 5 times for different f_i's for a total of $15n^3$ operations; a nine-fold savings.

D. AN EXAMPLE FOR $Y_c = K_c/s$

To give an idea of the procedure and some of the results that can be obtained, an example with a very simple plant comprising a pure integrator is presented. Although this is a first-order approximation to many practical manual control systems, such as aircraft roll control, it is selected here to permit a fine-grained focus on the OCM version of the operator's dynamics without distortion of the numerical results from higher order controlled element complications. The controlled system and driving noise are:

$$y_e(s) = Y_c(s)\,[u(s) + Y_w(s)w(s)] \tag{68}$$

$$Y_c(s) = \frac{1}{s}; \quad Y_w(s) = \frac{1}{s+2} \tag{69}$$

Note that the driving noise is added to the input of Y_c. Use the following parameters (as in Ref. 44):

W	τ	T_N	ρ_{y_1}	ρ_{y_2}	ρ_{y_a}	f	T_1	T_2
8 8	.15	.1	.01	.01	.003	1	0	0

The command and macro calls for Program CC are:

```
CC>g=1/s                    enter Yc
CC>g1=3/(s+2)               enter Yw
CC>@ocmyc2,g,g1,p40         create s.s. p40 = Yc
CC>@ocmall,p40              solve OCM
CC>@ocmg,g2                 compute g2 = Yp
```

The time domain results are:

G	$\sigma^2_{y_e}$	$\sigma^2_{\dot{y}_e}$	σ^2_u	$\sigma^2_{u_a}$	$\sigma^2_{\dot{u}}$	J
.00017	.12	3.1	3.9	4.8	242	.16

The pilot describing function is:

$$Y_p(s) = \frac{179(0)(2)(3.25)(6.39)(12.4)(12.6)[-.866,23.1]}{(0)(1.99)(2)(6.46)(12.4)(12.4)[.367,23.3](42.5)} \qquad (70)$$

where the notation (a) = (s + a) and $[\zeta,\omega_n] = (s^2 + 2\zeta\omega_n s + \omega^2)$. With a ninth-order denominator this transfer function is of very high degree indeed. Explanations for each of these factors is now provided.

Two orders stem from the ratio of second-order Pade factors representing the pure time delay. This is reflected in exact form in the numerator [-.866, 23.1], which represents 0.075 sec of the given $\tau = 0.15$ sec pure time delay. The denominator quadratic [.367,23.3] is the other half of this Pade approximate as it is shifted from its open loop value of [.866, 23.1] by the loop closure. At low frequencies [.367,23.3] can be replaced by a pure time delay of 2[.367,23.3] = 0.032 sec. Thus 0.107 sec of the initially prescribed time delay of 0.15 sec is "recovered" by the shifted version of the Pade approximation. If the high frequency lag at (42.5) is treated as a pure delay at low frequencies it will add 0.023 sec, giving a total of 0.130 sec for the effective human operator pure time delay.

The terms associated with the driving noise Y_w and with the neuromuscular lag at T_N sec will be exactly cancelled; in this example these terms are (2)(12.4)/(2)(12.4). These exact cancellations can be explained by the way in which the $(sI - A_1)^{-1}B_1$ block appears in the linear-predictor portion of the OCM in Fig. 17. The driving noise terms cancel because the input to this block does not excite these terms. The neuromuscular mode cancels because this mode is redundant with the $sT_N + 1)^{-1}$ block appearing above the v_{u_a} input.

An exact cancellation also occurs in this example at the controlled element dynamics: (0)/(0). The Y_c dynamics occur in both the KBF and

linear-predictor portions of the OCM. This redundancy gives rise to cancellations. Despite the exact cancellation in this and other examples, we conjecture that in general this cancellation is only approximate.

Of the remaining terms in the describing function, (6.39)(12.6)/[(6.46)(12.4)] are close approximations and can be dropped in any rational simplifying procedure. The (12.4) derives from the desire to set up a first-order neuromuscular lag of T_N = .08 sec (see Fig. 17). In the OCM this is supposed to be accomplished by the selection of the weight G on the control rate in the performance index of Eq. 22. Interestingly, the neuro-muscular mode does not survive the process of reducing all the OCM elements to a transfer function. Clearly the selection of G has a different effect than was intended by the OCM's originators in this respect.

When all of these cancellations and near cancellations are taken into account the describing function for pilot dynamics for frequencies less than about 15 rad/sec is:

$$Y_p(s) \approx \frac{4.17(3.25)}{(1.99)} e^{-.130s} \tag{71}$$

This result agrees remarkably well in form with the crossover model:

$$Y_p Y_c = \frac{\omega_c}{s} e^{-\tau} e^{s} \tag{72}$$

The close to cancelling low-frequency lag-lead, (3.25)/(1.99) in the OCM can be rationalized as a slight improvement on the simple crossover model in that a tiny bit of the so-called low-frequency phase droop will also be picked up. This is, of course, handled in the extended crossover and the structural-isomorphic models by the "alpha" or "low-frequency trimming" terms (Ref. 59).

If the control rate weight doesn't really "adjust the neuro-muscular time constant", what does it do? For this case, at least, we can speculate that the value of G and the use of control rate in the performance index implicitly "specifies" a frequency range in the region of crossover where the OCM will behave similarly to the crossover model. Other examples we have worked tend to support this speculation, although still others, such as cases which involve controlled elements of the form

$\frac{(a)}{[\zeta, \omega_n]}$, don't work out as well. Consequently this is currently an open issue. But this Program CC-based version of the OCM, with its features to determine the dynamic form of the pilot's describing function and to reduce it to essentials, permits a much wider cadre of researchers to easily examine such issues.

E. CONCLUDING REMARKS

The algorithmic and computational advantages of the optimal control model make it extremely valuable as a means to make quantitative estimates of the human operator's dynamic response in control tasks for which the model is appropriate. Besides the need to simplify, as illustrated above, there are three other aspects which give some difficulty. The first is philosophical and relates to the explicit requirement that the human operator description contain a complete internal model of the human's intrinsic characteristics and the system dynamics and disturbances. Thus, for the state estimation to be accomplished, the **A**, **B**, **C**, **D**, and **E** matrices plus the system disturbances and the human time delay, observation noise, and motor noise must all be known. Further, for the controller equalization adjustments, the **A** and **B** matrices plus the weights in the cost functional are needed. All of this amounts to an essentially complete "knowledge" by the human of the man-machine system characteristics. Internal models have a long history in psychology for several purposes. For instance, their elaboration and refinement have served as a useful construct for the development of skill by dint of training. In fact, even the simple crossover model can be interpreted as an implicit internal model of the human and controlled element dynamic characteristics in the crossover region. The key problem is thus not with the concept of an internal model, but rather its degree of perfection, especially in extremely complex systems where the required internal model is equally complicated. This philosophical point is more sophistic than practical as long as the OCM is considered to be only a mimic rather than an indication that all good human operators incorporate a Kalman Bucy filter as a component of their neurological apparatus!

The second difficulty is that of attempting to identify the underlying model parameters from experimental data. Not only is this inverse problem fundamentally difficult, but the optimal control model reviewed here suffers from overparameterization. Thus, from an identification viewpoint, the observation and motor noises are not resolvable, and the feedback matrix and the observer gain matrix can only be determined up to a similarity transformation of the model (Ref. 60).

The third problem area is specification of the cost function. The teleological character of the linear quadratic optimal model is imperfect because the performance criterion must be shaped to the task. As a practical matter, this has seldom posed a serious problem when the model has been applied by an experienced practitioner. Nonetheless, an aura of artistry is present in this requirement.

In the structural isomorphic model, a very large number of experimentally observed phenomena are accounted for. Since its inception, a great deal of effort has been devoted to similarly account for human operator behavior with the algorithmic model. This has required, in the main, adjustments in the cost function or in those properties associated with the human operator's limitations, such as normalized observation or motor noise. The model has proved to be quite flexible in accommodating most of the many behavior changes desired. Table 5 summarizes some procedures and techniques which have been found suitable to accomplish this accommodation (Refs. 36-38, 41-45). Thus advanced modeling features, can be handled with the OCM. Consequently both the structural and algorithmic forms of pilot model are now quite mature and can be used in a complementary fashion to solve pilot-vehicle analysis problems and to help resolve data interpretation issues.

TABLE 5. PROCEDURES FOR ADJUSTMENT OF THE ALGORITHMIC MODEL

FEATURES TO BE MODELED	SUITABLE PROCEDURES AND MEANS
Effective time delay accomodation	Least squares prediction applied to output of Kalman estimate of delayed states
Basic crossover behavior	Use of control rate weighting in distinction to control weighting in cost function
Effective neuromuscular lag T_N	Select ratio of control weighting to control rate weighting (e.g., "g") in cost function
Selection of cost function weights on states and control	Choose weights to be inverse of squares of the respective maximum allowable values
Remnant	Observation noise covariances scaled with mean-squared state. Residual (non-scaled) observation noise component to account for imprecision due to lack of references. Motor noise to reflect inability to generate control motions precisely. Residual motor noise to reflect human's introduction of noise into an undisturbed system.
Low-frequency phase lag	Use larger motor noise level than actually present in determining Kalman filter gains
Perceptual and indifference thresholds	Scale observation noise inversely with equivalent gain (random input describing function for threshold)
Scanning effects	Scale observation noise inversely with attentional fraction (f_i) of each display, subject to the constraint that $(\Sigma f_i) + f_{margin} < 1$, $f_i > 0$. Different noise levels for foveal and parafoveal viewing.
Workload (attentional)	Attentional workload effects evaluated by examining performance as a function of the reserved workload margin, f_{margin}
Motion cues	Add model of human motion sensory apparatus (e.g., vestibular system, proprioception) to state and output equations.

SECTION V

ESTIMATION OF PILOT RATINGS

In the previous sections we have described techniques for the estimation of pilot dynamics in closed-loop tasks. Because aggressively performed closed-loop tasks are ordinarily critical from the standpoint of pilot compensation or skill required, and are usually high workload flight phases, they tend to be dominant discriminators in flying qualities assessments. The assessments themselves are provided by pilot comments and associated ratings, such as the Cooper-Harper scale (Ref. 61) shown in Fig. 19. It is apparent that pilot compensation (equalization) and effort (workload) and task performance are major constituents of the rating scheme. When the task variables (effective vehicle dynamics, forcing functions and disturbances, etc.) are well-defined the pilot-vehicle system dynamic models presented in Sections II-IV can be used to make quantitative estimates of pilot compensation and task performance. Workload, on the other hand, is much more difficult to quantify. Still, we can expect some connections between the subjective pilot ratings and comments, which are subjective workload indices, and the pilot and pilot-vehicle system dynamics and performance. These connections are intrinsically empirical. They are also awkward theoretically because the rating scale is ordinal. Consequently averages, standard deviations, etc. are not legitimate statistics, although this has never stopped flying qualities engineers from using them! (Fortunately the scales seem to be close to interval in some ranges or, for the purist, data can be converted to an underlying interval scale wherein all the parametric statistics can be applied and then converted back -- see Ref. 62.)

Our goal in this section is to summarize the available connections between pilot and pilot-vehicle system dynamics and pilot ratings. There are fundamentally two approaches which have been used with some success. The first directly associates pilot and system dynamic and performance characteristics with the pilot rating via a functional relationship. Such functionals have been developed for use with both the classical and OCM

Aircraft Characteristics	Demands on the Pilot in Selected Task or Required Operation*	Pilot Rating
Excellent Highly Desirable	Pilot Compensation Not a Factor for Desired Performance	1
Good Negligible Deficiencies	Pilot Compensation Not a Factor for Desired Performance	2
Fair - Some Mildly Unpleasant Deficiencies	Minimal Pilot Compensation Required for Desired Performance	3
Minor But Annoying Deficiencies	Desired Performance Requires Moderate Pilot Compensation	4
Moderately Objectionable Deficiencies	Adequate Performance Requires Considerable Pilot Compensation	5
Very Objectionable But Tolerable Deficiencies	Adequate Performance Requires Extensive Pilot Compensation	6
Major Deficiencies	Adequate Performance Not Attainable With Maximum Tolerable Pilot Compensation. Controllability Not in Question	7
Major Deficiencies	Considerable Pilot Compensation Is Required for Control	8
Major Deficiencies	Intense Pilot Compensation Is Required to Retain Control	9
Major Deficiencies	Control Will Be Lost During Some Portion of Required Operation	10

*Definition of required operation involves designation of flight phase and/or subphase with accompanying conditions.

Figure 19. Cooper-Harper Handling Qualities Rating Scale

versions of pilot models. The actual connections which have been established are based on specific tasks and circumstances.

The second approach is more clinical in style. It takes into account the pilot and pilot-vehicle system characteristics in terms of their implications for control. A list of assessment features is considered to reveal symptoms of flying qualities problems. Some quantitative aspects can be set forth, but others are only qualitative. Consequently this approach is more the basis for a pseudo pilot commentary rather than a means to make numerical rating estimates directly. Of course, if the "commentary" is sufficiently complete it can be converted to a rating by working through Fig. 19. The clinical technique is especially useful to define possible flying qualities problems and key effective airplane dynamic parameters, or as a means of interpreting experimental data.

The two approaches described are currently most useful for single axis situations. Multi-axis rating estimates can be developed from single axis results using a "product rule," which is described in the third article. OCM-based multi-axis results can also be the basis for direct estimates of multi-axis ratings. This is summarized in the third article as well, and is developed in Appendix A.

A. PILOT RATING FUNCTIONALS

A direct approach is to formulate a functional which incorporates the pilot and system dynamic and performance quantities which are presumed to underlie the pilot rating. A general form which explicitly contains some, and implicitly contains all of the desired features is given by,

Mission/Task Performance	Pilot Workload	
Dominant Aircraft Motion Quantities and Task Measures	Pilot Activity (Scale of Pilot Effort)	Pilot Equalization (Dynamic Quality of Pilot Effort)

$$R = R\left[\ \lambda_i \overline{q_i^2}\ ;\ \overline{\delta_j^2}\ ,\ \overline{\dot{\delta}_j^2}\ ;\ \frac{d\ |Y_p|_{dB}|}{d(\text{lag}\ \omega)}\Big|_{\omega_{1_k}}\ ;\ \cdots\ \right]_{i,j,k} \tag{73}$$

The subscript notation used is intended to imply that $i \epsilon I$ motion and task measures are controlled by $k \epsilon K$ pilot loops actuating $j \epsilon J$ control points. This functional form is general enough to include the existing (e.g., Refs. 62-72) approaches to quantitative flying qualities rating functions. The key closed-loop system quantities in the rating functional are measures of mission/task performance. These are conveniently described by a set of dominant weighted aircraft motion deviations and total task accuracy or error indications (represented by the q_i).

The pilot activity component of pilot effort, $\overline{\delta_j^2}$ (either force or displacement, as pertinent to the manipulator involved) and $\overline{\dot{\delta}_j^2}$ are particularly dependent on the level of pilot gain. For a given gain, these will increase directly with gust disturbance spectrum amplitude and remnant amplitude. Accordingly, both the mission/task and pilot activity quantities will reflect turbulence and remnant levels.

The pilot equalization component of pilot workload is represented in Eq. 18 by the slope (in dB per octave or decade) of the pilot's amplitude ratio evaluated at a particular frequency (generally near crossover). This is by no means the only measure available to describe the dynamic quality of the pilot's effort, others (e.g., Refs. 64-68) use pilot lead time constants, a desirable alternative for particular situations with a sufficient data base. Then the rating functional takes the very useful form illustrated in Fig. 20. At present, adequate functions of this form exist for precision hover tasks (Refs. 62-68), pitch attitude control (Ref. 66), and roll attitude control based on Refs. 69 and 70. In addition, the Ref. 71 data provide a base for a multiloop functional.

The technique pioneered in Ref. 64 actually used the pilot rating functional as a performance index, as well as a rating estimator. That is, the pilot model parameters (Fig. 20a) were adjusted to minimize R, the pilot rating functional.

The follow-on work of Ref. 68, which was dedicated to experimentally verifying the Ref. 64 result, produced a "modified" pilot rating functional for the $R_2 + R_3$ component, as shown in Fig. 21. The correlation between predicted and actual ratings shown in Fig. 22 are reasonably good.

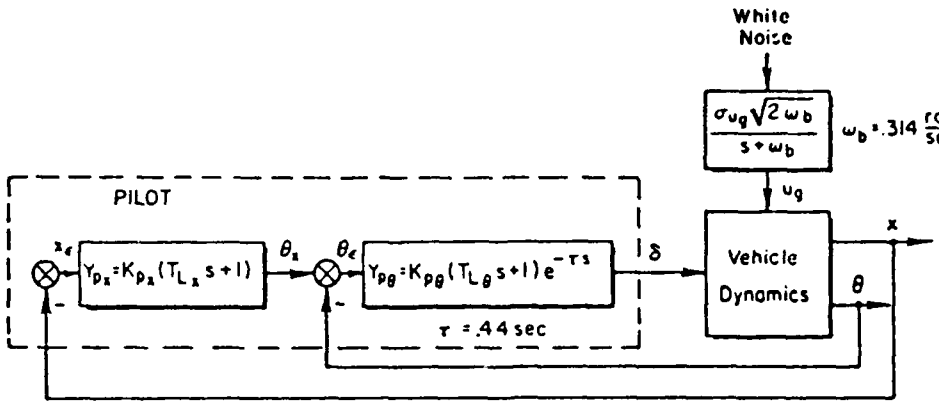

a) Pilot / Vehicle Model

$$R = 1 + R_1 + R_2 + R_3$$

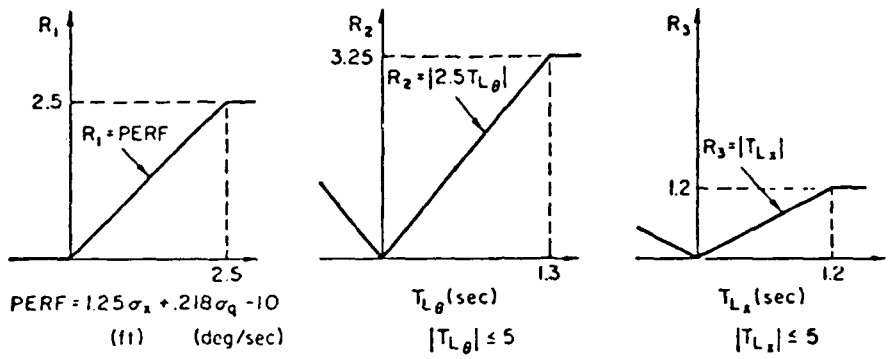

$PERF = 1.25\sigma_x + .218\sigma_q - 10$
(ft) (deg/sec)

$T_{L\theta}$(sec)
$|T_{L\theta}| \leq 5$

T_{L_x}(sec)
$|T_{L_x}| \leq 5$

b) Pilot Rating Functional

$$J = 1 + PERF + R_2 + R_3$$

PERF, R_2, R_3 – as defined in b)

1) K_{P_x}, T_{L_x}, $K_{P\theta}$, $T_{L\theta}$ found to minimize J

2) K_{P_x}, $K_{P\theta}$ simultaneously increased by 20%.
If system asymptotically stable, performance and rating computed based on values found in 1). If system not stable, go to 3).

3) $T_{L\theta}$, T_{L_x} held fixed at values found in 1). K_{P_x}, $K_{P\theta}$ simultaneously decreased until values found for which a 20.3% increase would result in an unstable system while a 20% increase would result in a stable system. These values are used to compute performance and rating.

c) Minimum Pilot Rating Concept For Pilot Model Parameter Adjustment

Figure 20. The Elements of the "Paper Pilot" for the Hover Task (Ref. 64)

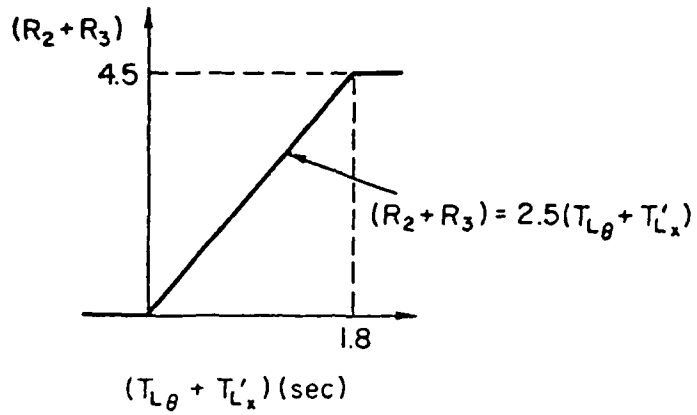

Modification for Hover Paper Pilot Rating Functionals (Ref. 68)

Figure 21. "Paper Pilot" Rating Functionals

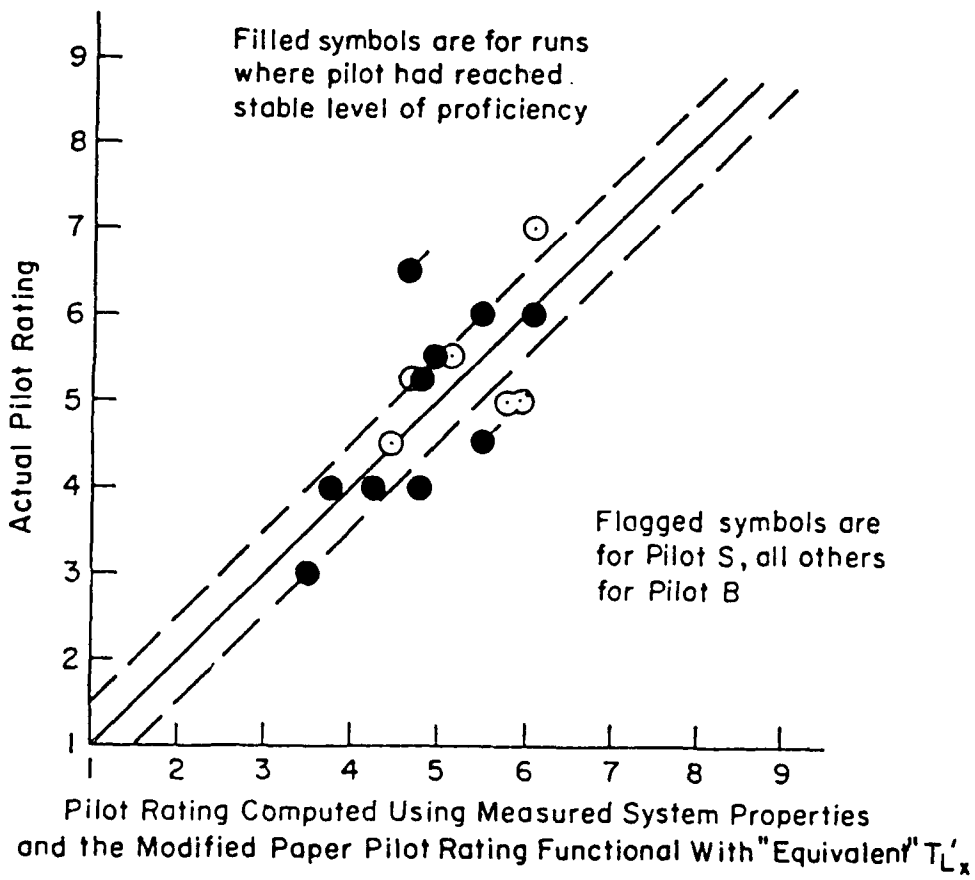

Figure 22. Comparison of Actual Pilot Ratings with Ratings Computed Using Modified Hover "Paper Pilot" Rating Functional (Ref. 68)

In Ref. 66 the task was changed to pitch attitude control and the resulting pilot rating functional evolved to:

$$R = \underbrace{\frac{0.1}{.974-\sigma}}_{R_1} + \underbrace{2.5T_L + 1.0}_{R_2}$$

where $\sigma = \sigma_e/\sigma_1$ = ratio of error variance to input variance

T_L = pilot lead, seconds

and $R \leq 10$, $0 \leq R_2 \leq 3.25$, $0 \leq R_1$

(If a value of $\sigma < .974$ cannot be obtained, $R = 10$)

Yet another way to estimate pilot ratings is to use correlations developed for the algorithmic pilot model. (Refs. 72 through 75.) This pilot rating estimation procedure is based on the hypothesis that the pilot rating for a particular task and set of vehicle dynamics can be correlated with the numerical value of the index of performance (minimum values of the OCM Cost Function) resulting from the optimal pilot modeling procedure. As indicated in Fig. 23, this has worked fairly well for some single-axis cases (e.g., helicopter hover and longitudinal approach).

The extension of the OCM performance-index-based pilot rating estimating procedure to the multi-axis case has been addressed as part of this project. The basic developments are given in Appendix A and Volume III. Reference 76 is the primary source of connected single and multi-axis rating data, although no pilot dynamic information is available. Consequently the OCM was used to establish pilot and system dynamics estimates. For the rating estimates only the performance index is needed. The appropriate performance index for each single axis was chosen to be,

$$J_{axis_i} = \left[\frac{\sigma^2_{\epsilon_i}}{\sigma^2_{c_i}} + \frac{\sigma^2_{\dot{\delta}_i}}{g_i}\right] \tag{74}$$

And for a multi-axis task, the objective function used was

$$J_{task} = \sum_{i}^{N_{axes}} J_{axis\ i} \tag{75}$$

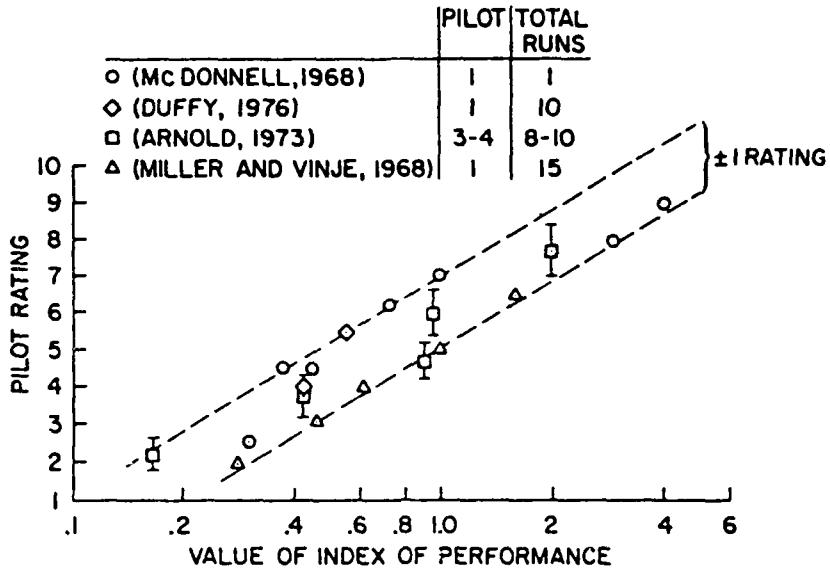

Model Parameters for Hover Task of Miller and Vinje (1968)

Parameter	*Value*
Time delay τ	0.2 s
Neuromuscular time constant T_N	0.2 s
Visual thresholds	None
"Full-attention" noise-signal ratio for observation noise	0.0025
Fraction of attention on control task f_c	0.25 → 1.0 (configuration dependent)
Noise-signal ratio for motor noise	0.003

Index of Performance

$$J = E\left\{\lim_{T\to\infty} \frac{1}{T}\int_0^T \left[\mathbf{y}^T(t)\mathbf{Q}\mathbf{y}(t) + \mathbf{u}^T(t)\mathbf{R}\mathbf{u}(t)\right]dt\right\}$$

$y_1 = \dot{\theta}$	$q_{11} = (1/0.0873)^2\ s^2/rad^2$
$y_2 = x$	$q_{22} = (1/3.5)^2/ft^2$
$y_3 = \dot{x}$	$q_{33} = (1/3.5)^2\ s^2/ft^2$
u_1 = commanded control	$r_{11} = (1/0.138)^2/ft^2$

Figure 23. Pilot Rating vs. Value of Model Index of Performance (Ref. 72)

The justification of this selection involves three considerations. The first relates to the selection of equal (unity) weighting on each $J_{axis\ i}$ in the definition of J_{task} in multi-axis tasks. This decision was based on the instructions given to the subjects in the Ref. 64 experiment. They were to attempt to minimize the errors in all controlled axes. That is, they were instructed that no axis was to be given preference, which would then define primary and secondary sub-tasks.

Secondly, the normalization of the mean-square error with the mean-square command deals nicely with the fact that different units and different command-signal strengths were used in the axis.

Finally, the interpretation of g_i requires some discussion. In the OCM, the selection of g_i defines the frequency range over which the open-loop system amplitude ratio approximates a K/s-like form. In connection with the OCM it is often cited that g_i is selected to yield a desired neuromotor time constant, T_n, in the pilot's describing function obtained from the model. But, as indicated in Section IV, when the total pilot describing function, Y_p, is actually constructed from its various elements in the OCM, the T_n established in this fashion is canceled by a directly compensating lead, leaving the actual estimated Y_p with no $(T_n\ s + 1)^{-1}$ lag. Still it has been convenient to adjust g_i in this fashion even though the lag will later disappear. In this vein, the value of the desired neuromotor time constant used is either 0.1 sec, <u>or</u> the T_n that yields the lowest error (e.g., best performance), whichever is <u>greater</u>. Notice that after T_n is determined in the above fashion, this "operating point" is associated with some weight g_i in $J_{axis\ i}$. This value may also infer the subject's subjective trade between performance (σ_ϵ) and workload ($\sigma_{\dot{\delta}}$). And since pilot lead and $\sigma_{\dot{\delta}}$ are correlated, this procedure maximizes the possibility of relating the resulting value of J_{task} to the subjective rating of the task.

Shown in Fig. 24 is the correlation between J_{task}, as modeled, and the subjective ratings of the task. The correlation between J_{task} and POR from the single-axis results appears to hold for the multi-axis results as well. This result seems to indicate that the ratings reflect the actual performance and workload (stick rate) in the overall task. The results

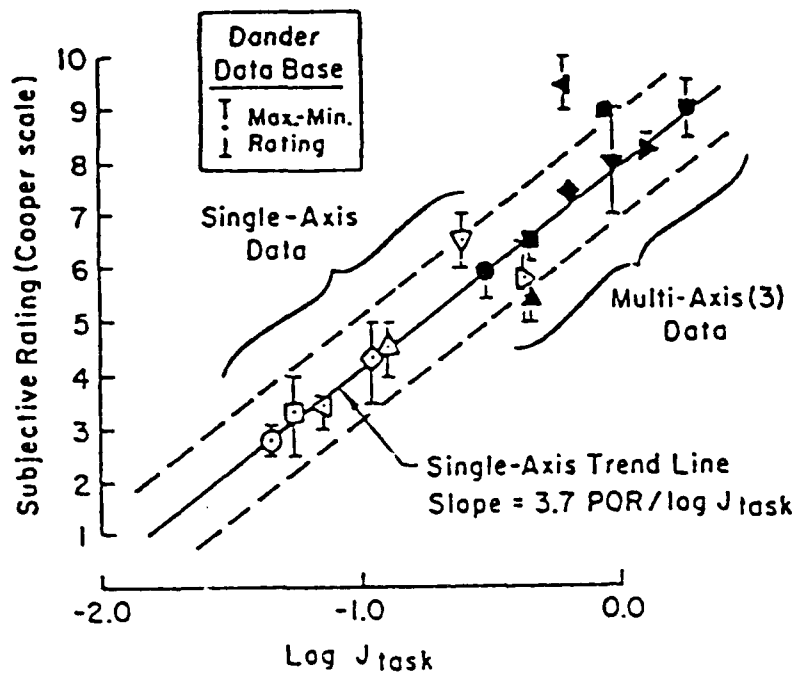

Figure 24. Pilot Rating vs. Performance Index for Dander Single and Multi-Axis Tasks (See Appendix)

also tend to support the hypothesis that determining the weightings g_i in the manner discussed leads to the "correct" relative weightings on control rate in the axis, and the relative weight between control rate and normalized error. Because the multi-axis correlations follow the same trend as the single-axis data this study indicates that the objective function for multi-axis situations can be extrapolated (or calibrated) from single axis correlations.

B. WORKLOAD, ATTENTIONAL DEMANDS, AND THE PRODUCT RULE FOR MULTI-AXIS RATINGS

There is a strong connotation of increasing pilot effort and workload in the phrases of the Cooper-Harper Scale (Ref. 61) which invoke levels of "pilot compensation," but workload is difficult to define and, con-

sequently, to quantify. A general definition that can be measured and predicted is workload margin, defined as the ability (or capacity) to accomplish additional (expected or unexpected) tasks. The pilot opinion rating scale satisfies this definition up to its "uncontrollable" limit point. It is, therefore, a key workload measure, easy to obtain in some experimental circumstances.

Auxiliary tasks have been developed that satisfy the workload margin definition given above and that permit more objective measurements. One such task provides a complementary pair of measures suitable for integrating many workload concepts and factors into one basic context. These are the "attentional demand" and the "excess control capacity."

The attentional demand and excess control capacity measures have been connected with pilot rating in a multiaxis experiment using the so-called cross-coupled subcritical task (see, for example, Refs. 15 and 62). A block diagram of the general experimental setup is shown in Fig. 25. The pilot first performs the primary task alone, attempts to achieve satisfactory levels of performance, and provides a Cooper-Harper pilot rating.

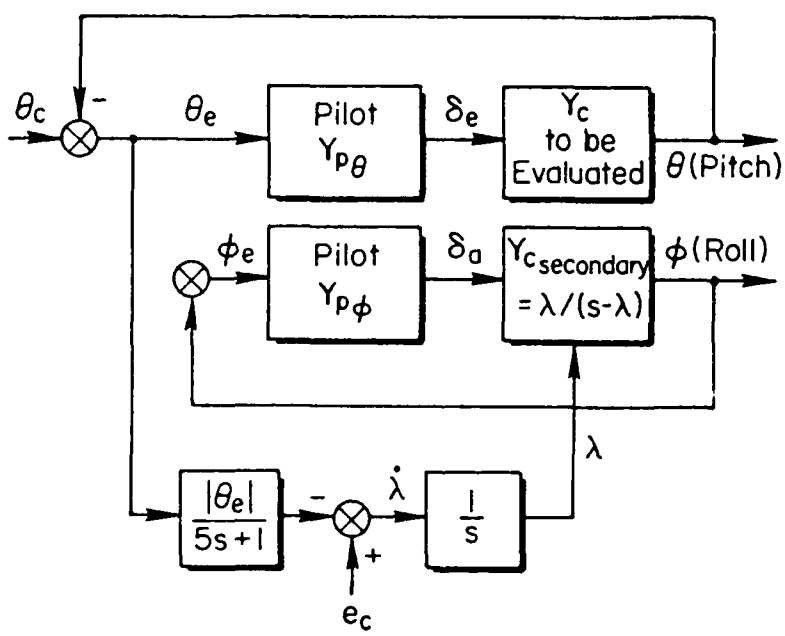

Figure 25. Single-Loop Primary Task with Secondary Cross-Coupled Loading Task

The secondary subcritical tracking task is then connected in order to "load" the pilot. The difficulty of the secondary task is made proportional to primary task performance via the cross-coupling. Thus, when the pilot keeps primary task performance less than a criterion value (based on the runs with the primary task alone), the secondary task difficulty is automatically increased by increasing the rate of divergence of the secondary task instability. Conversely, when the pilot becomes so busy with the secondary task that the primary task error becomes larger than the criterion value, the secondary task difficulty is automatically decreased. The final "score" is γ_s, the stationary value of the secondary unstable pole (γ) in rad/sec. The scores obtained from this cross-coupled secondary task represent its difficulty; consequently, they also represent the "degree of ease" of the primary task or the excess control capacity available with respect to the primary task. The γ_s scores can be appropriately scaled into proportional workload indices by normalizing them with respect to the maximum sidetask score attainable under full attention conditions (no primary task). In this case, γ_s approaches γ_c, the "critical task" score. The attentional demand of the primary task is then given by

$$AD = 1 - \frac{\lambda_s}{\lambda_c} \tag{75}$$

The attentional demand, AD, is a dimensionless decimal fraction that can be equated with the average primary control task attentional dwell fraction, η. Its complement, the excess control capacity, which measures the average fraction of time available for other than the primary task, is

$$XSCC = \frac{\lambda_s}{\lambda_s} \tag{76}$$

If the side task is taken to be a surrogate for all of the managerial functions, XSCC will be just the average managerial task dwell time fraction $1-\eta$.

Achieving the critical limiting score in the cross-coupled secondary task indicates a condition of maximum available excess control capacity; the secondary task is a "critical" task in this limiting case. The critical task provides a divergent controlled element form that tightly constrains allowable pilot equalization near the region of gain crossover so

that the pilot's effective time delay, τ_e, is the sole determinant of system stability. Thus, pilot activity that demands an increase in τ_e on the <u>whole</u> task will prevent the attainment of the pilot's critical limiting score on the cross-coupled secondary task.

Secondary scores obtained for a variety of primary controlled elements are presented in Ref. 62. Figure 26 shows how the scores for the best gain configurations of each controlled element compare with the Cooper-Harper ratings. In Fig. 26 a score of $\lambda_s = 0$ corresponds to 100 percent of the pilot's attention being devoted to the primary task or <u>no</u> excess control capacity; whereas, a limiting score ($\lambda_s \doteq 5.5$) means that no attention is required to maintain primary task performance or that <u>100</u> percent of excess control capacity is available.

These relationships show that subjective pilot ratings, can be associated closely with the objective measures of workload provided by the attentional demand and the excess control capacity. The lower (better) values of pilot rating correspond to low attentional demands and large excess capacity to perform other functions. More difficult effective vehicle dynamics that receive poorer pilot ratings of their flying qualities, require much more of the pilot's attention and hence leave less capacity for other tasks.

The excess control capacity concept also provides a potential basis for estimating ratings for multiloop situations Ref. 77. First, assume that the relationship between pilot rating and excess control capacity, $\lambda_n = \lambda_s/\lambda_c$ given by Fig. 26, is applicable to each axis in a multi-axis situation. Then, single-axis capacity, or attention, values can be combined to yield the combined axis value by a multiplication process, i.e., the multiaxis excess capacity, λ_{n_m}, is given by the product of the excess capacities for the individual axes:

$$\lambda_{n_m} = \prod^{m} \lambda_{n_i} \tag{77}$$

For $R = A + B\lambda_n$ as a linear fit of the Fig. 26 data, the multiaxis rating R_m will be given by,

$$R_m = A + B\lambda_{n_m} = A + B\prod^{m}\lambda_{n_i} = A + B\prod^{m}\left(\frac{R_i - A}{B}\right)$$

$$R_m = A + \frac{1}{B^m - 1}\prod^{m}(R_i - A) \tag{78}$$

Combined ratings are always greater than (or equal to) individual ratings, since combined λ_n's are always less than any individual λ_n. Also, the maximum value of R_m never exceeds A, i.e., for large $R_i < A$, $\prod^{m}(R - A) \rightarrow 0$.

The logical value for A is 10.0, and B is determined, using the empirical data, to be equal to -8.3. As depicted in Fig. 27, this results in a good, overall fit to all of the available multiaxis rating data (Ref. 77). Notice that in its final form the multi-axis rating, R_m, can be computed directly from the single-axis ratings R_i. Measures or computation of excess control capacity or attentional demand are not required.

C. THE CLINICAL APPROACH TO RATING ESTIMATION

The treatment above has the great merit that, when appropriate measures and experimental correlates are available, a set of pilot rating estimates can be made using relatively simple formulas. The detailed reasons for the rating estimates are inherently buried in the empirical data which serve as bases for the correlations. In other words, the pilot commentary and reasons behind whatever the rating estimate comes out may be quite obscure. To alleviate this difficulty, and to provide an alternative for situations where the data base is insufficient or non-existent, a clinical approach is indicated. Here the characteristics exhibited by the pilot and pilot-vehicle system dynamics are examined for "symptoms" of potential problems. These are then reflected into a summary of properties which amount to a pilot commentary expressed in technical terms.

Consider, for the most elementary situation, that the crossover model is used in accomplishing a pilot-vehicle analysis for a given set of

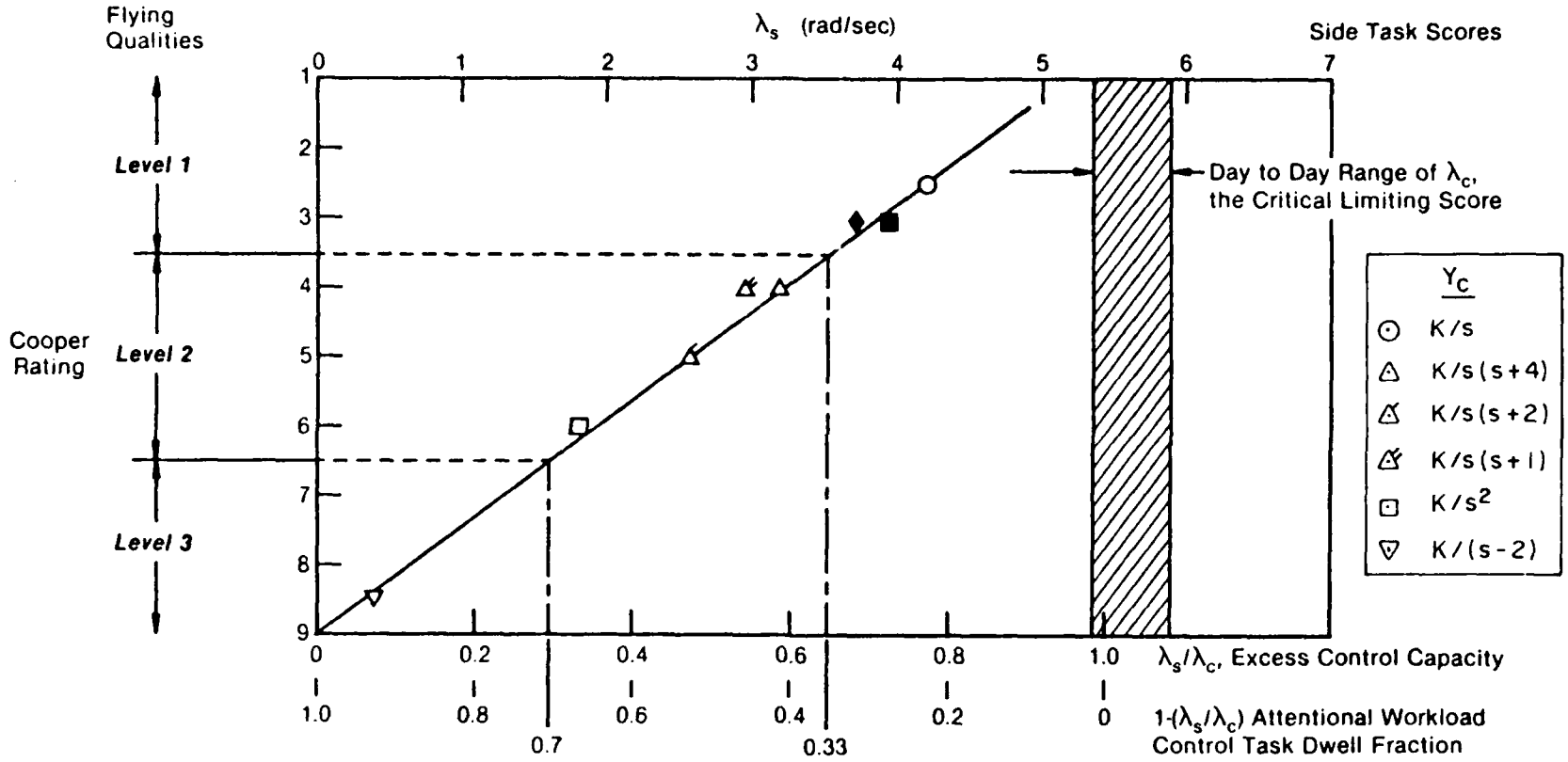

Figure 26. Calibration of Pilot Rating with Attentional Workload and Excess Control Capacity

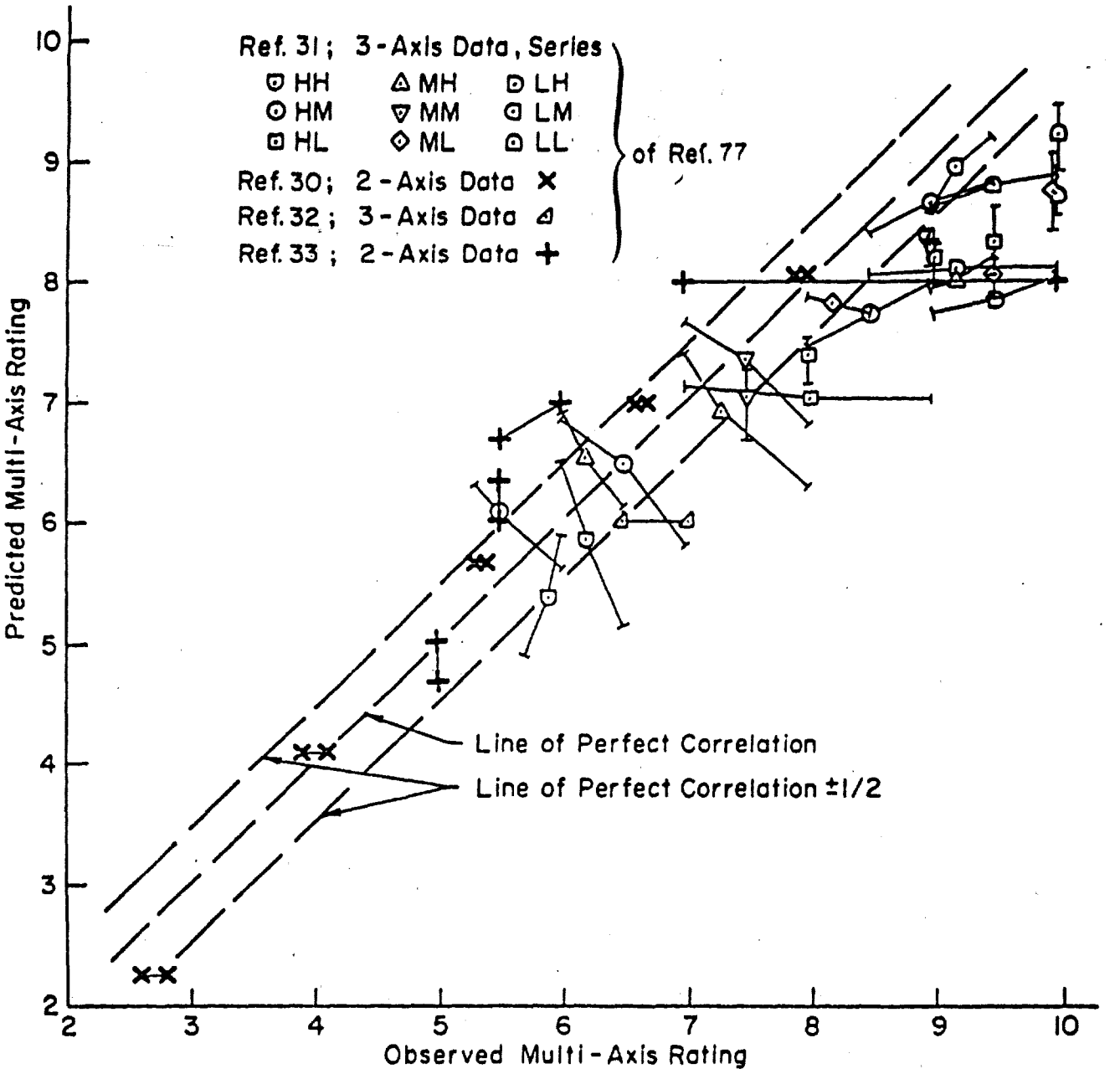

Figure 27. Correlations Obtained with Product Method

effective aircraft dynamics. The data directly available from the analysis includes an estimate of:

- the stability-limited maximum crossover frequency, ω_u;
- pilot lead equalization required in the region of crossover to make good the crossover law (measured in terms of pilot amplitude ratio slope, $[d|Y_p|_{dB}/d \log \omega]_{\omega c}$
- the nominal full-attention crossover frequency, ω_c;

The two crossover frequencies are closely related, i.e.

	ω_c/ω_u
No pilot lead	0.78
Low-frequency pilot lead	0.66

If, in addition, equivalent forcing function information is available the system steady-state performance can be determined easily (e.g. by using Figs. 9 or 13a).

As might be expected, the most important pilot dynamics correlates with pilot rating are pilot gain and pilot lead. Empirical connections between these are given in Fig. 28. For a particular controlled element there is an optimum controlled element gain which depends on the manipulator dynamics, controller sensitivity, control harmony among axes, etc. No theory yet exists to establish this optimum gain, so it must be determined empirically. Then, curves such as those shown in Fig. 28 can be used to assess any rating decrements from the optimum. By virtue of the ω_c-K_c independence property any change in K_c will be countered by a change in K_p to keep the crossover frequency approximately constant. However, either too-sluggish (K_c too small, K_p too large) or too-sensitive conditions can give rise to major decrements. This can be greater than 6 rating points even for the $Y_c = K_c/s$ controlled element dynamics. As can be appreciated from Fig. 28 the optimum is quite broad (changes of plus or minus 50% in either direction are less than 1 rating point for even the narrowest U-shaped curve), so once the controlled element sensitivity is properly adjusted minor controlled element gain changes are not major factors in pilot rating.

The pilot lead equalization required to make good the crossover model

has a major effect on the pilot rating. For example, Fig. 28 indicates that the difference between a $Y_c = K_c/s$ controlled element, which requires no pilot lead, and $Y_c = K_c/s^2$, which demands +1 lead units, is a pilot rating decrement of about 3 Cooper-Harper rating points. Considered as idealized systems these correspond, respectively, to "rate command" and "acceleration command" effective vehicle characteristics. Re-examining Fig. 26, the rate command system data point shows a pilot rating, PR = 2 1/2 with an attentional demand of 0.2 while the acceleration command system data point has PR = 6 and a control task dwell fraction of about 0.65. The primary reasons for rating shifts for these data are the amount of lead required and the reduction in system performance (the attainable crossover frequency for the acceleration case is less than that for the rate command situation because of the increased τ_e due to the need for lead generation). In any event, even a best gain acceleration command system will be Level 2 (3 1/2 < PR < 6 1/2) from a flying qualities standpoint. From the descriptive adjectival phrases of Fig. 19 this level of low frequency lead generation would therefore be interpreted as "considerable pilot compensation" required to achieve adequate performance.

There are, of course, factors other than pilot lead and gain adjustment that affect the pilot rating. In general, flying qualities ratings tend to be given on a global basis which may include several maneuvers in a task complex. Both open-loop (unattended) and closed-loop (attended) piloting operations will be considered in the rating. In the present work we are, of course, concerned primarily with the closed-loop piloting aspects. In fact, for stability and control flight testing the important connection is with "flying qualities while tracking" aspects and other precision and/or aggressive tasks which involve tight closed-loop pilot-vehicle control.

The unattended category can be the major factor in determining the acceptable values of very low frequency divergences such as the spiral or a divergent phugoid. It can also be decisive in setting the nature of the "hold" characteristic built into the stability augmentation system. For example, for many up and away tasks the attended longitudinal pitch attitude system should, ideally, require no pilot lead equalization. In

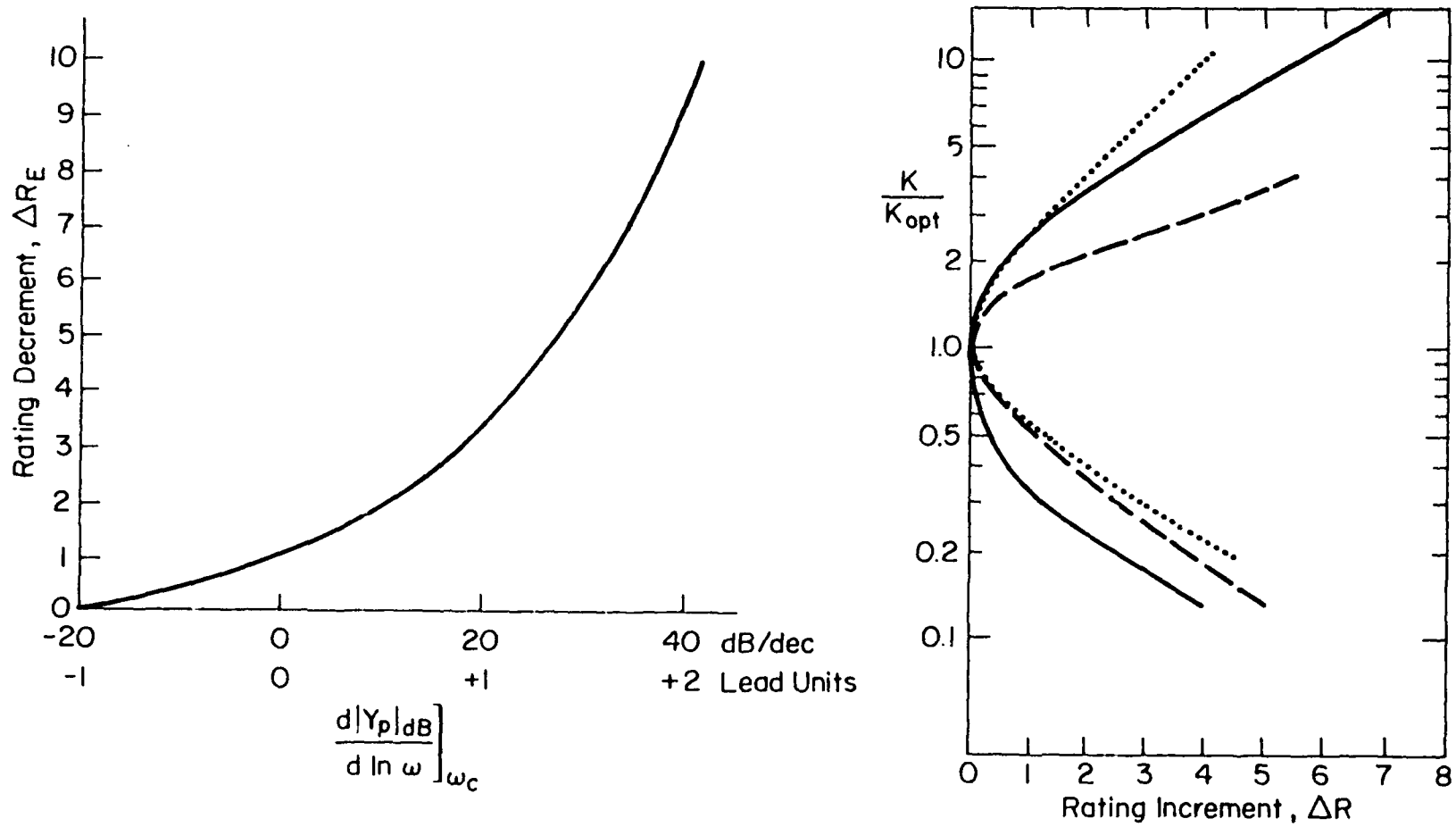

Figure 28. Pilot Rating Decrements as Functions of Lead Equalization and Gain Tracking with Full Attention, Single Axis

terms of ideal effective airplane dynamics this would approximate $Y_c = K_c/s$ in the region of crossover. But for unattended operations a rate command system is not ideal in that an attitude-stable platform is desired. Thus a rate-command/attitude-hold system has superior pilot ratings to rate-command/rate-hold.

Another major facet in nearly unattended operations is "commandability", the ability of the airplane to respond in a precise, orderly, and predictable manner to highly skilled, precognitive pilot command inputs. These inputs are pure commands, functions of time alone, and, as such, are basically open-loop in character. Typical examples are turn entries, step-like (for attitude command systems) or pulse-like (for rate command systems) inputs to adjust attitude, etc. These maneuvers may have to be fine-tuned at the end via closed-loop control, but for an ideal vehicle and a skilled pilot this will not ordinarily be necessary. Again, to the extent that this feature of the airplane's characteristics enter into the rating game, closed-loop dynamics considerations are not explicitly involved.

An important distinction about the unattended factors in the current context is that they may set a base for the pilot rating which does not depend on closed-loop factors. This base can itself shift as the divided attention requirements shift. For example, if managerial tasks take up almost all the available time the effective vehicle dynamics in the unattended state may have to be highly automated even including path, altitude, or position control. In any event, the closed-loop effects should be thought of as increments from the base level determined from the unattended operation requirements.

Table 6 presents listing of primary factors to which the pilot is sensitive and which, accordingly, underlie pilot rating. Except for pilot lead and gain variation from optimum these factors are not individually quantifiable in ratings terms. On the other hand, with modern flight control system technology most of them can be modified by design. Consequently these system aspects can be profitably compared in competing system studies, and also serve as a useful checklist for interpreting manned simulation or flight test results. As remarked earlier, a pseudo

pilot commentary can be constructed by considering them.

In Table 6 both items under "Unattended Operations" and the "Pilot Lead" and "Pilot Gain/Optimum" parts of the "Attended Operations" list have been covered above. The remaining items will be discussed below. Some of the considerations can be developed from the crossover model, while others will require application of the structural-isomorphic pilot model in some form or other.

TABLE 6. PILOT-VEHICLE SYSTEM FACTORS IN PILOT RATING

- ATTENDED OPERATIONS
  - -- Pilot Lead
  - -- Pilot Gain/Optimum
  - -- Urgency Adjustment Gain Tolerance Without Changing Closed-Loop Dynamic Form
  - -- Stability Margin Gain Tolerances Including Total Available Gain Range
  - -- Neuromuscular System Coupling
  - -- Attentional Demands/Excess Control Capacity
  - -- Closed-Loop System Performance
- UNATTENDED OPERATIONS
  - -- Allowable Fluctuations in Pilot-Control-Precision Demands
  - -- Equilibrium/Trim Properties (Effective "Hold" Characteristics)

The "Urgency Adjustment Gain Tolerance" factor can best be understood by considering two limiting cases of controlled element. For the first, consider a K_c/s controlled element form. From the crossover model The pilot dynamic characteristic for this system will be a pure gain plus effective time delay. The closed-loop system for this case can support a range of pilot gains which correspond to crossover frequencies from zero to an octave or so below ω_u with only minor changes in the basic dynamic form of the closed-loop system. In terms of pilot-vehicle system input/output characteristics this will be approximately,

$$\frac{M(s)}{I(s)} \doteq \frac{1}{(s/\omega_c + 1)}$$

As the pilot urgency or aggressiveness modifies his gain, ω_c will increase or decrease, with the dominant closed-loop system time constant, $1/\omega_c$, waxing and waning in corresponding fashion. Thus there is a very wide range of excellent closed-loop dynamic response properties available to the pilot which is easily adjusted in direct proportion by his effort. In the words of Fig. 19 "pilot compensation is not a factor for desired performance", and the configuration will highly rated. For the other extreme imagine a set of effective airplane characteristics which has dynamics in the region of crossover which require precise adjustment of the pilot's lead-lag equalization and gain to close the loop in a stable manner. The pilot can exert closed-loop control, but the dynamic quality and even closed-loop system stability require that his describing function be precisely tuned to offset the controlled element deficiencies. The pilot's compensation in this case will range from "considerable" to "intense", and the configuration will be rated very poorly.

The "Stability Margin Gain Tolerances" factor is most easily described when the pilot-vehicle system is conditionally stable. In this situation the system becomes unstable if the gain is either too low or too high. When the pilot lead-lag equalization is adjusted to maximize this range (which will ordinarily provide crossover model-like features in the nominal crossover region), there is a "total available gain range" (TAGR) through which the pilot can maintain some semblance of closed-loop control. Clearly, the more narrow this range becomes the more difficult the pilot's adjustment and the worse his rating will become.

The "Neuromuscular System Coupling" factor can become important when the low-frequency effective airplane dynamics are excellent but the closed-loop system gain margin in the region of the neuromuscular actuation mode is reduced. This was touched on briefly in Section III, and is covered in Refs. 12 and 13. The resulting closed-loop system instability is high frequency, 2-3 hz. It is one explanation for "roll ratchet".

The "Attentional Demands/Excess Control Capacity" factor is primarily related to divided attention operations. When the control task itself is responsible for using most of the pilot's excess control capacity the reasons for this are invariably due to factors already covered. When the managerial, communication, planning, and other non-control tasks consume too much of the pilot's available attention pilot ratings will suffer. The obverse of this is that the effective vehicle dynamics must very good in order to require a minimum of attention. The ratings for control alone should, in general, be superior and the unattended operations factors would be good as well.

The last Table 6 factor to be discussed is "Closed-Loop Performance". Many facets of task performance stem directly from mission requirements and are hence mission-specific. The status of the pilot-vehicle system relative to mission requirements is the very first thing the pilot assesses before he even establishes more detailed ratings. Average error performance in command and regulation tasks can be calculated with all the pilot models once these inputs are defined. These estimates can serve as one basis for flying qualities assessments.

There are other, more general, closed-loop dynamic performance aspects which should also be considered in flying qualities assessments. Four of these are listed in Table 7. The first two are simple statements of closed-loop dynamic response quality. They, in essence, suggest that there be one dominant closed-loop mode which can have a damping ratio greater than 0.35 to 0.5. (It could also be a dominant first-order mode.) The requirement to avoid a closed-loop mid-frequency droop is tantamount to the one dominant mode prescription, for the droop will show up as an additional minor mode with a longer time constant. The Neal-Smith criteria (Ref. 78), for example, call specific attention to the mid-frequency droop and require that it be less than 3 dB to achieve

TABLE 7. DESIRABLE CLOSED LOOP DYNAMIC FEATURES

- ADEQUATE CLOSED-LOOP DAMPING, $\zeta_{CL} \geq 0.35\text{-}0.50$
- AVOIDANCE OF CLOSED-LOOP MID-FREQUENCY DROOP
- MULTILOOP CONTROL VIA SERIES STRUCTURE FOR SINGLE CONTROL
- FREQUENCY SEPARATION OF INNER, OUTER LOOPS, E.G., $\omega_{c_i} = 2.3 \quad \omega_{c_o} - 0.5\text{-}1.0$
- SIMPLE CROSSFEEDS TO DIRECTLY NEGATE SUBSIDIARY RESPONSES
- CONTROL HARMONY

Level 1 ratings. By way of example a 3 dB mid-frequency droop can be associated with the presence of a minor mode comprising a single dipole pair in the closed-loop pilot-vehicle system (with the |zero/pole| < 1.41) supplementing the major dominant mode.

The remaining two desirable closed-loop dynamic features are associated with multi-loop, single control axis situations. Common examples of this include: 1) the control of altitude wherein altitude error is the outer loop feedback and pitch angle is an inner loop; and 2) hover control, as shown in Fig. 20. "Desirable" aspects of such systems include the qualitative feature that a "series" (rather than parallel) closure of the outer loop is possible in the presence of an inner loop system which serves both independently and as a means to equalize the outer loop. Thus the pilot closure of a pitch attitude loop satisfies an attitude control function and gives rise to an effective outer, altitude control, loop which needs very little if any further pilot equalization. This is supported in a more quantitative sense by the suggestion for the separation of crossover frequencies in multiloop systems with series pilot elements.

The desirable crossfeed feature listed accounts for the possibility of pilot-induced crossfeeds to reduce or eliminate subsidiary modes or response quantities. A common example of this is an aileron to rudder crossfeed for turn coordination. The last feature on the list of desires is control harmony, which relates to multi-axis control conditions. Force and position gradients, pre-loads and centering springs and other manipulator features between elevator and aileron need to be in proper balance so that the effective controlled element gains in each axis are near optima, interaxis crosstalk is minimized, etc. Just as with the setting of controlled element optimum gain, control harmony is a subject of experimental determination.

As a consequence of flying qualities analyses using pilot-vehicle analysis to examine the factors of Tables 6 and 7, the analyst can develop a set of conclusions and arrive at a wide variety of issues and possible problems. Table 8 illustrates the type of problems that might be uncovered by such examinations for the case of longitudinal attitude and path control.

TABLE 8. TYPICAL PILOT CENTERED PATH REGULATION PROBLEMS

ATTITUDE CONTROL

- INADEQUATE BANDWIDTH
- INNER-OUTER LOOP EQUALIZATION CONFLICT
- LOW STATIC GAIN
- OVER-SENSITIVITY TO GAIN/EQUALIZATION

PATH CONTROL

- PERFORMANCE REVERSALS
- INADEQUATE BANDWIDTH
- INADEQUATE SEPARATION OF PATH AND ATTITUDE RESPONSES
- DIFFICULT OR CONFLICTING CROSSFEEDS
- EXCESSIVE DEPLETION OF SAFETY MARGINS
- LOW (HIGH) EFFECTIVE PATH GAINS

REFERENCES

1. McRuer, D. T., and E. S. Krendel, Mathematical Models of Human Pilot Behavior, AGARDograph No. 188, Jan. 1974.

2. McRuer, D. T., D. Graham, E. S. Krendel, et al, "System Performance and Operator Stationarity in Manual Control Systems," Third IFAC Congress, London, Feb. 1965.

3. Bekey, G. A., and J. M. Biddle, "The Effect of a Random-Sampling Interval on a Sampled-Data Model of the Human Operator," Third Annual NASA-University Conference on Manual Control, NASA SP-144, Mar. 1967, pp. 247-258.

4. Jex, H. R., and R. E. Magdaleno, "Corroborative Data on Normalization of Human Operator Remnant," IEEE Trans. Man-Machine Syst., Vol. 10, No. 4, Dec. 1969, pp. 137-140.

5. Levison, W. H., S. Baron, and D. L. Kleinman, "A Model for Controller Remnant," IEEE Trans. Man-Machine Syst., Vol. 10, No. 4, Oct. 1969, pp. 101-108. (Also, Bolt, Beranek, and Newman, Inc., Rept. 1731, Oct. 1968.)

6. Schweizer, G., "Some Contributions to the Theory of Linear Models Describing the Control Behavior of the Human Operator," R. K. Bernotat and K. P. Gartner (Eds.), Displays and Controls, Swets and Zeitlinger N.V., Amsterdam, 1972, pp. 327-348.

7. Allen, R. W., H. R. Jex, D. T. McRuer, et al, "Alcohol Effects on Driving Behavior and Performance in a Car Simulator," IEEE Trans. Syst., Man & Cybern., Vol. SMC-5, No. 5, Sept. 1975, pp. 498-505.

8. McRuer, D. T., "Human Operator System and Subsystem Dynamic Characteristics," A. S. Iberall and A. C. Guyton (Eds.), Regulation and Control in Physiological Systems, Instrument Society of America, Pittsburgh, PA, May 1973, pp. 230-235.

9. Magdeleno, R. E., D. T. McRuer, and G. P. Moore, Small Perturbation Dynamics of the Neuromuscular System in Tracking Tasks, NASA CR-1212, Dec. 1968. (Also, "A Neuromuscular Actuation System Model," IEEE Trans. Man-Machine Syst., Vol. 9, No. 3, Sept. 1968, pp. 61-71.)

10. Magdaleno, R. E., and D. T. McRuer, Experimental Validation and Analytical Elaboration for Models of the Pilot's Neuromuscular Subsystem in Tracking Tasks, NASA CR-1757, Apr. 1971.

11. Jex, H. R., and R. E. Magdaleno, "Biomechanical Models for Vibration Feedthrough to Hands and Head for a Semisupine Pilot," Aviat., Space and Environ. Med., Vol. 49, No. 1, Jan. 1978, pp. 304-316.

REFERENCES (CONTINUED)

12. Johnston, D. E., and D. T. McRuer, Investigation of Interactions Between Limb-Manipulator Dynamics and Effective Vehicle Roll Control Characteristics, NASA CR-3983, May 1986.

13. Johnston, D. E., and B. L. Aponso, Design Considerations of Manipulator and Feel System Characteristics in Roll Tracking, NASA CR 4111. Feb. 1988.

14. McRuer, D. T., H. R. Jex, W. F. Clement, et al, A Systems Analysis Theory for Displays in Manual Control, Systems Technology, Inc., TR-163-1, June 1967.

15. Allen, R. W., W. F. Clement, and H. R. Jex, Research on Display Scanning, Sampling, and Reconstruction Using Separate Main and Secondary Tracking Tasks, NASA CR-1569, July 1970.

16. Levison, W. H., and J. I. Elkind, Studies of Multivariable Manual Control Systems: Two-Axis Compensatory Systems with Separated Displays and Controls, NASA CR-875, Oct. 1967.

17. Levison, W. H., and J. I. Elkind, Studies of Multivariable Manual Control Systems: Four-Axis Compensatory Systems with Separated Displays and Controls, Bolt Baranek and Newman, Inc., Rept. No. 1695, Mar. 1969.

18. Weir, D. H., and R. H. Klein, The Measurement and Analysis of Pilot Scanning and Control Behavior During Simulated Instrument Approaches, NASA CR-1535, June 1970.

19. Meiry, J. L., The Vestibular System and Human Dynamic Space Orientation, MIT, Man-Vehicle Control Lab., Thesis T-65-1, June 1965.

20. Peters, R. A., Dynamics of the Vestibular System and Their Relation to Motion Perception, Spatial Disorientation, and Illusions, NASA CR-1309, Apr. 1969.

21. Ringland, R. F., and R. L. Stapleford, Experimental Measurements of Motion Cue Effects on STOL Approach Tasks, NASA CR-114458, Apr. 1972.

22. Shirley, R. S., Motion Cues in Man-Vehicle Control, MIT, ScD Thesis, MVT68-1, 1968. (Also R. S. Shirley and L. R. Young, Motion Cues in Man-Vehicle Control: Effects of Roll-Motion Cues on Human Operator's Behavior in Compensatory Systems with Disturbance Inputs, IEEE Trans., Vol. MMS-9, No. 4, Dec. 1968, pp. 121-128.)

23. Stapleford, R. L., R. A. Peters, and F. R. Alex, Experiments and a Model for Pilot Dynamics with Visual and Motion Inputs, NASA CR-1325, May 1969.

REFERENCES (CONTINUED)

24. McRuer, D. T., and R. E. Magdaleno, Human Pilot Dynamics with Various Manipulators, AFFDL-TR-66-138, Dec. 1966.

25. Gordon-Smith, M., "An Investigation into Some Aspects of the Human Describing Function While Controlling a Single Degree of Freedom," 5th Annual NASA-Univ. Conference on Manual Control, NASA SP-215, 1970, pp. 203-240. (Also An Investigation Into Certain Aspects of the Describing Function of a Human Operator Controlling a System of One Degree of Freedom, Univ. of Toronto, Inst. for Aerospace Studies, Toronto, Canada, Rept. #149, Feb. 1970.)

26. Hess, R. A., "Structural Model of the Adaptive Human Pilot," J. Guidance and Control, Vol. 3, No. 5, Oct. 1980, pp. 416-423.

27. Hess, R. A., "A Model-Based Investigation of Manipulator Characteristics and Pilot/Vehicle Performance," J. Guidance, Vol. 6, No. 5, Oct. 1983.

28. Hess, R. A., "Investigating Aircraft Handling Qualities Using a Structural Model of the Human Pilot," AIAA GMC Guidance, Navigation and Control Conference Proceedings, AIAA-87-2537-CP, Monterey, CA, Aug. 1987.

29. Smith, R. H., "A Unifying Theory for Pilot Opinion Rating," Proceedings of the 12th Annual Conference on Manual Control, May 1976, pp. 542-554.

30. Reason, J., and K. Mycielska, Absent-Minded? The Study of Mental Lapses and Everyday Errors, Prentice-Hall, Inc., Englewood Cliffs, NJ, 1982.

31. McRuer, D. T., H. R. Jex, W. F. Clement, et al, Development of a Systems Analysis Theory of Manual Control Displays, Systems Technology, Inc., TR 163-1, Oct. 1967.

32. Jex, H. R., R. W. Allen, and R. E. Magdaleno, Display Format Effects on Precision Tracking Performance, AMRL-TR-71-63, Aug. 1971.

33. Clement, W. F., "A Theory for the Human Operator's Remnant in Multi-Loop Display-Control Tasks," Fifth NASA-University Conference on Manual Control, NASA SP-215, 1970, pp. 637-654.

34. McRuer, D. T., W. F. Clement, and R. E. Magdaleno, Simplified Pilot-Modeling for Divided Attention Operations, Systems Technology, Inc., TR-1219-1, Vol. II, May 1987.

35. McRuer, D. T., Chapter 2.0 of "Improved Guidance and Control Automation at the Man-Machine Interface" Allocation of Human and Automatic Resources in the Cockpit, AGARD Advisory Report AR-228, Dec. 1986.

REFERENCES (CONTINUED)

36. Allen, R. W., D. T. McRuer, R. E. Magdaleno, and H. R. Jex, "Computer Aided Procedures for Analyzing Pilot/Vehicle/System Interactions," NAECON, 1986, Dayton, Ohio, Systems Technology, Inc., P-385, May 1986.

37. Baron, S., and D. L. Kleinman, The Human As An Optimal Controller and Information Processor, NASA CR-1151. (Also IEEE Trans. Man-Machine Syst., Vol. 10, No. 1, Mar. 1969, pp. 9-17.)

38. Baron, S., D. L. Kleinman, D. C. Miller, W. H. Levison, and J. I. Elkind, Application of Optimal Control Theory to the Prediction of Human Performance in a Complex Task, AFFDL-TR-69-81, Mar. 1970.

39. Curry, R. E., W. C. Hoffman, and L. R. Young, Pilot Modeling for Manned Simulation, AFFDL-TR-76-124, Vol. 1, Dec 1976.

40. Elkind, J. E., P. L. Falb, D. Kleinman, et al., An Optimal Control Method for Predicting Control Characteristics and Display Requirements of Manned-Vehicle Systems, AFFDL-TR-67-187, June 1968.

41. Kleinman, D. L., "Optimal Control of Linear Systems With Time-Delay and Observation Noise," IEEE Trans. Autom. Control, Vol. 14, Oct. 1969, pp. 524-527.

42. Kleinman, D. L., and S. Baron, Manned Vehicle Systems Analysis by Means of Modern Control Theory, NASA CR-1753, June 1971.

43. Kleinman, D. L., and S. Baron, "A Control Theoretic Model for Piloted Approach to Landing," Automatica, Vol. 9, No. 3, May 1973, pp. 339.

44. Kleinman, D. L., S. Baron, and W. H. Levison, "An Optimal Control Model of Human Response, Parts 1 and 2, Automatica, Vol. 6, May 1970, pp. 357-383.

45. Kleinman, D. L., S. Baron, and W. H. Levison, "A Control Theoretic Approach to Manned-Vehicle Systems Analysis," IEEE Trans., Vol. AC-16, No. 6, Dec. 1971, pp. 824-832.

46. Kleinman, D. L., and T. Perkins, "Modeling the Human in a Time-Varying Anti-Aircraft Tracking Loop", IEEE Trans., Vol. AC-19, No. 4, Aug. 1974, pp. 297-306.

47. Doyle, K. M., and W. C. Hoffman, Pilot Modeling for Manned Simulation, Volume II: Program User's Manual (PIREP), AFFDL-TR-76-124, Dec. 1976.

REFERENCES (CONTINUED)

48. Hess, R. A., "Aircraft Control-Display Analysis and Design Using the Optimal Control Model of the Human Pilot", IEEE Trans. on Systs., Man, and Cybernetics, Vol. SMC-11, No. 7, July 1981, pp. 465-480.

49. Schmidt, D. K., "Optimal Flight Control Synthesis via Pilot Modeling," J. Guidance and Control, Vol. 2, Aug. 1979, pp. 308-312.

50. Bacon, B. J., and D. K. Schmidt, "An Optimal Control Approach to Pilot/Vehicle Analysis and the Neal-Smith Criteria," J. Guidance, Vol. 6, No. 5, Sept-Oct. 1983, pp. 339-347.

51. Bryson, A. E., and Y. C. Ho, Applied Optimal Control, Blaisdell, Waltham, MA., 1969.

52. Thompson, P. M., "Program CC's Implementation of the Human Optimal Control Model," AIAA Guidance, Navigation and Control Conference, Monterey, CA, Systems Technology, Inc., Paper No. 411, Aug. 1987.

53. Thompson, P. M., Program CC Version 4 Tutorial and Reference Manuals, Systems Technology, 1989.

54. Levision, W. H., J. I. Elkind and J. L. Ward, Studies for Multivariable Manual Control Systems: A Model for Task Interference, NASA CR-1746, May 1971.

55. Hoffman, W. C., R. E. Curry, D. L. Kleinman, and W. M. Hollister, Display/Control Requirements for VTOL Aircraft, ASI-TR-75-26, Aug. 1975.

56. Levison, W. H., S. Baron, and A. Junker, Modeling the Effects of Environmental Factors on Human Control and Information Processing, AMRL-TR-76-74.

57. Dander, V., An Evaluation of Four Methods for Converting Single Axis Pilot Ratings to Multi-Axis Pilot Ratings Using Fixed Base Simulation Data, M.S. Thesis, AFIIT GE/EE/62-4, Dec. 1962.

58. Golub, G. H., and C. F. Van Loan, Matrix Computations, John Hopkins University Press, Baltimore, 1983.

59. McRuer, D. T., "Human Dynamics in Man Machine Systems," Automatica, 1980.

60. van Wyjk, R. A., and J. J. Kok, "Theoretic Aspects of the Identification of the Parameters in the Optimal Control Model," 13th Annual Conference on Manual Control, MIT, Cambridge, MA, NASA CR-158107, 1977, pp. 27-34.

REFERENCES (CONTINUED)

61. Cooper, G. E., and R. P. Harper Jr., The Use of Pilot Ratings in the Evaluation of Aircraft Handling Qualities, NASA TN D-5153, Apr. 1969.

62. McDonnell, J. D., Pilot Rating Techniques for the Estimation and Evaluation of Handling Qualities, AFFDL-TR-68-76, Dec. 1968.

63. Ashkenas, I. L., and D. T. McRuer, "A Theory of Handling Qualities Derived from Pilot-Vehicle System Considerations," Aerospace Eng., Vol. 21, No. 2, Feb. 1962, pp. 60, 61, 83-102.

64. Anderson, R. O., A New Approach to the Specification and Evaluation of Flying Qualities, AFFDL-TR-69-120, June 1970.

65. Dillow, J. D., The "Paper Pilot" -- A Digital Computer program to Predict Pilot Rating for the Hover Task, AFFDL-TR-70-40, Mar. 1971.

66. Anderson, R. O., A. J. Connors, and J. D. Dillow, Paper Pilot Ponders Pitch, AFFDL/FGC-TM-70-1, Nov. 1970.

67. Anderson, R. O., "Theoretical Pilot Rating Predictions," Handling Qualities Criteria, AGARD Conf. Proc. No. 106, June 1972, pp. 19-1 to 19-14.

68. Teper, G. L., An Assessment of the "Paper Pilot" -- An Analytical Approach to the Specification and Evaluation of Flying Qualities, AFFDL-TR-71-174, June 1972.

69. Onstott, E. D., and E. P. Salmon, Airplane Flying Characteristics in Turbulence, AFFDL-TR-70-143, Feb. 1971.

70. Onstott, E. D., E. P. Salmon, and R. L. McCormick, Prediction and Evaluation of Flying Qualities in Turbulence, AFFDL-TR-71-162, Feb. 1972.

71. Clement, W. F., R. Wade Allen, and D. Graham, Pilot Experiments for a Theory of Integrated Display Format, Systems Technology, Inc., Technical Report 183-1, Oct. 1971 (Also JANAIR Report 711107).

72. Hess, Ronald A., "Prediction of Pilot Opinion Ratings Using an Optimal Pilot Model," Human Factors, Vol. 19, Nov. 5, 1977, pp. 459-475.

73. Schmidt, D. K., "On the Use of the OCM's Quadratic Objective Function as a Pilot Rating Metric," Proceedings of the 17th Annual Conference on Manual Control, JPL Publication 81-95, Oct. 1981.

REFERENCES (CONCLUDED)

74. Schmidt, D. K., "Time Domain Identification of Pilot Dynamics and Control Strategy," Proceedings of the 18th Annual Conference on Manual Control, AFWAL TR-83-3021, June 1982.

75. Anderson, M. R., and D. K. Schmidt, "Closed-Loop Pilot Vehicle Analysis of the Approach and Landing Task," J. of Guidance, Control, and Dynamics, Vol. 10, No. 2, 1987, pp. 187-194.

76. Dander, V., An Evaluation of Four Methods for Converting Single Axis Pilot Ratings to Multi-Axis Pilot Ratings Using Fixed Base Simulation Data, M.S. Thesis, AFIT, GE/FE/62-4, Dec. 1962.

77. Ashkenas, I. L., R. H. Hoh, and S. J. Craig, Section III Requirements for Airplane Normal and Failure States -- in Recommended Revisions to Selected Portions of MIL-F-8785B (ASG) and Background Data, AFFDL-TR-73-76, Aug. 1973.

78. Neal, T. P., and R. E. Smith, An In-Flight Investigation to Develop System Design Criteria for Fighter Airplanes, Vol. I, AFFDL-TR-7074, Dec. 1970.

APPENDIX A

AIAA Paper No. 87-2538-CP

"PILOT-VEHICLE ANALYSIS OF MULTI-AXIS TASKS"

PILOT-VEHICLE ANALYSIS OF MULTI-AXIS TASKS

Duane McRuer*
Systems Technology, Inc.
Hawthorne, California

David K. Schmidt**
Purdue University
West Lafayette, Indiana

Abstract

In missions where high cognitive and managerial requirements are placed on the pilot, or where failures may significantly degrade one or more aircraft control axes, the pilot must divide his attention among several tasks. The pilot and system behavior in such divided attention conditions, and the combination of pilot ratings from single to multi-axis conditions are treated using classical and optimal control models for the human in a complementary fashion. It is shown that the crossover frequency and closed-loop system performance for a given axis under divided attention will be less than full attention values while the remnant and the phase margin will be greater, and that the model-based trends are consistent with experiment. Also, the optimal control performance index used in the pilot and system behavioral modeling, when "calibrated" with single-axis correlations, shows potential for the development of subjective rating estimates for multi-axis tasks.

Introduction

The pilot of a modern high-performance aircraft must perform both control and managerial functions in most mission phases. In some, such as final approach and landing or a variety of air-to-air or air-to-ground tracking tasks, the control function is paramount and requires most of the pilot's available attention. In the past the more difficult of these control tasks have tended to expose whatever unfavorable effective aircraft dynamic (flying quality) problems were present. Consequently, pilot modeling for the consideration of critical flying qualities has tended to be focused on full attention or nearly full attention control operations. Further, the vast majority of pilot dynamics and pilot rating data used to develop flying quality boundaries have been obtained for situations where the dynamic properties of one control axis are varied while maintaining the dynamics of other axes at "good" levels.

With modern missions in which high cognitive and managerial requirements are placed on the pilot, or where failures may significantly degrade one or more aircraft control axes, the pilot must divide his attention among several axes or, more generally, between control and other tasks. In such situations the vehicle dynamics in each axis being controlled by the pilot must be superior to those which would be suitable if the pilot could devote almost full attention to just one axis.

This state of affairs brings two key issues to the fore. The first is pilot and system behavior in divided attention or task interference situations, where several tasks compete for the pilot's attention. Critical questions in these situations relate to the standards that should be set for both desirable and minimum flying quality levels in a given axis when these standards are conditioned by the other control and managerial tasks at hand. The second is the subjective assessment, or rating, of effective vehicle dynamics in multi-axis control or multiple task conditions.

This paper will treat both of these issues for multi-axis control tasks. It begins with a review of pilot modeling for divided attention conditions, developing the differences to be expected in pilot and pilot-vehicle system behavior for single-axis (full attention) and multi-axis control tasks. The major data source for which pilot ratings for both single and multi-axes are available is then used as a basis for the estimation of pilot and system behavior data. The estimates are obtained using an optimal control model and serve to augment the pilot rating "data set" by providing estimates for these quantities (which were not available from the original experiments). The estimates are compared with the theoretical expectations and with the limited experimental evidence available. The estimation of pilot ratings is then treated using an extension of previously available correlations. Important features in these developments are the complementary connections of classical theory and optimal control modeling techniques.

Divided Attention and Task Interference Modeling

The classical theory of pilot-vehicle system dynamics is based on the well-known "Crossover Model" (see, e.g., Ref. 1). In this theory the human pilot's behavior is characterized in mathematical terms as a random-input describing function, Y_p, plus pilot-induced "noise" expressed as a power spectral density, Φ_{nn}, commonly referred to as "remnant." In a specified task with the effective vehicle dynamics described by the transfer function Y_c, the crossover model open-loop describing function, G, takes the form shown in Fig. 1. This form is established by appropriate adjustment of Y_p by the pilot.

In the crossover model there are three key variables -- the crossover frequency ω_c, the effective system latency τ, and the remnant power spectral density, Φ_{nn}. The crossover frequency is sometimes loosely referred to as the pilot-vehicle system "bandwidth." It has the usual feedback system physical interpretation as the metric which divides the world of the control system into two frequency regimes: below ω_c the benefits of

*President and Technical Director. Fellow AIAA.
**Professor, School of Aeronautics and Astronautics. Associate Fellow AIAA.

feedback are present (e.g., output follows input, error is reduced, etc.) while above ω_c the system becomes essentially open-loop. The system latency theoretically appears as a pure time delay, although it is actually a low frequency approximation to all the high frquency (i.e., well above ω_c) net lags and delays in the system. It includes time delays and neuromuscular lags contributed by the pilot as well as net lags from manipulators and other manual controller elements, higher frequency effective aircraft dynamics, etc. The effective aircraft dynamics include aircraft plus stability augmentation plus display, etc., dynamics. By using the effective system latency as a normalizing variable the crossover model dynamic properties can be given in more general terms as either a normalized crossover frequency, $\tau\omega_c$, or a phase margin, $\phi_M = \pi/2 - \tau\omega_c$.

The remnant power spectral density depends on the amount of pilot-generated lead required to make good the crossover model form, the nature of the manipulator, and other features of the system and task. It arises primarily from fluctuations of attention and other time-variations internal to the pilot.[1] When, as is usually the case, these time-variations are random the power spectral density is continuous and, more importantly, the remnant spectral density will scale with the mean-square error.[1-4] This is depicted in Fig. 1 by the dotted line introducing $\overline{e^2}$ into the remnant block.

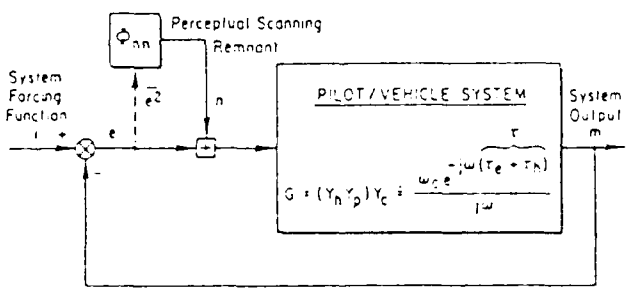

Y_c = Effective dynamics of vehicle (e.g., aircraft plus stability augmentation plus displays)

Y_p = Full attention pilot describing function

Y_h = Perceptual describing function to account for divided attention

Figure 1. Pilot-Vehicle System for Divided Attention Control Tasks

When the pilot's full attention is focused on a single-axis control task the crossover frequency of the pilot-vehicle system is maximized, and the remnant has a minimum value which is dependent on the details (pilot-lead, manipulator characteristics, etc.) of the particular task. When more than one axis is to be controlled, or when managerial tasks are present, or when both multi-axis control and managerial operations are to be accomplished, the pilot must share his attention among the several tasks. In these cases the crossover model will still hold for the control activities, but with some modifications. The possible nature of the changes is partially exhibited in Fig. 1 by the presence of a perceptual describing function, Y_h, an accompanying additional latency, τ_h, and a more general name ("Perceptual Scanning") for the divided attention or task-interference remnant to account for the divided attention.

Divided attention operations can be considered as an extension to the well-established theory of display scanning and signal sampling/reconstruction.[1,3,5,6] The most important and fundamental model change is the remnant. A theoretical model for remnant due to quasi-random task switching/sampling with a constant average dwell time on the task at hand, T_d, and a sampling/switching interval among tasks varying about some mean value T_s was derived by Clement[3] and validated for visual inputs.[6] This remnant form is

$$\Phi_{nn}(\omega) \doteq \frac{T_s \overline{e^2}\,(1-\bar{n})(1-\delta)}{\pi\left[1+\left(\frac{\omega T_d}{2}\right)^2\right]} \left(\frac{\text{units}^2}{\text{rad/sec}}\right) \qquad (1)$$

where $\overline{e^2}$ is the mean-square of the signal sampled

T_s is the mean sampling interval

$\bar{n}$ is effective control dwell fraction = T_d/T_s

T_d is effective dwell interval on the control task considered

δ is normalized lower bound on the domain of T_s: $T_o/T_s < 1$

This power spectrum is valid at frequencies well above the low-pass breakpoint, $2/T_d$, defined by the control dwell time. The variability of the switching interval is not purely random, but is subject to a lower bound, T_o. This is represented in Eq. 1 by the term $1 - \delta$. The numerical values in Table 1, based on the Ref. 6 experiments involving the visual modalities and attention switches between displays, provide some appreciation for the magnitudes of some of the quanities in Eq. 1.

TABLE 1. TYPICAL VALUES FOR DIVIDED ATTENTION REMNANT QUANTITIES

ITEM	NOMINAL	RANGE
$\delta = T_o/T_s$	1/2	1/3 to 2/3
Minimum T_d (sec)	0.4 - 0.5	
T_d for Velocity Detection (sec)	0.6 - 0.7	
T_d for Acceleration Detection (sec)	1.0	

The major low frequency remnant variations are with the control dwell fraction, $\bar{n}$, and the mean-square input to the pilot (shown as mean-square error, $\overline{e^2}$, in Fig. 1). Perceptual Scanning remnant

is reduced by increasing the dwell fraction, going to zero when the divided attention control task becomes full attention. (In this limiting case full attention remnant will still be present; this is not included in Eq. 1 because the perceptual scanning remnant is typically much larger for the divided attention conditions of interest here. It can easily be included because, as already noted the same scaling with $\overline{e^2}$, with a different proportionality factor, applies for the full-attention remnant.) Just as for full-attention remnant, the increase of remnant power with the magnitude of the pilot's input stems from time variations, in this case the time modulation of attention inherent in the perceptual scanning process.

The implications of divided attention have been explored theoretically and experimentally for almost two decades. (The classical theory described to this point stems from Ref. 5, and includes Refs. 1, 3-8). A quantitative example of the effects of divided attention on task performance is presented in Fig. 2, taken from Ref. 8. Here the forcing function is white noise through a third-order Butterworth filter with normalized breakpoint $\omega_i \tau = 0.25$. Full attention is the lowest curve. The divided attention conditions are then shown as a family with task dwell fraction, η, as the parameter. In this example the normalized control task dwell interval is set at $T_d/\tau = 1.5$, and the divided attention remnant normalized lower bound on the scanning interval, $\delta = 0.5$.

Figure 2 illustrates the profound effects of divided attention on task performance. The perceptual scanning penalizes the performance in three important ways:

- by reduction of the crossover frequency (and a concomitant increase in the phase margin)
- by increase in the remnant
- by the introduction of a new kind of "stability" constraint -- "instability in the mean-square"

While all of these are apparent in the figure, the third point requires some additional explanation. The full attention stability limit for the crossover model function, given by

$$\omega_c \longrightarrow \omega_u = \frac{\pi}{2\tau} \tag{2}$$

is approached by the full attention, $\eta = 1$ curve. In general the mean-squared error for the feedback system shown in Fig. 1 is given by,

$$\overline{e^2} = \overline{e_1^2} + \overline{e_n^2} \tag{3}$$

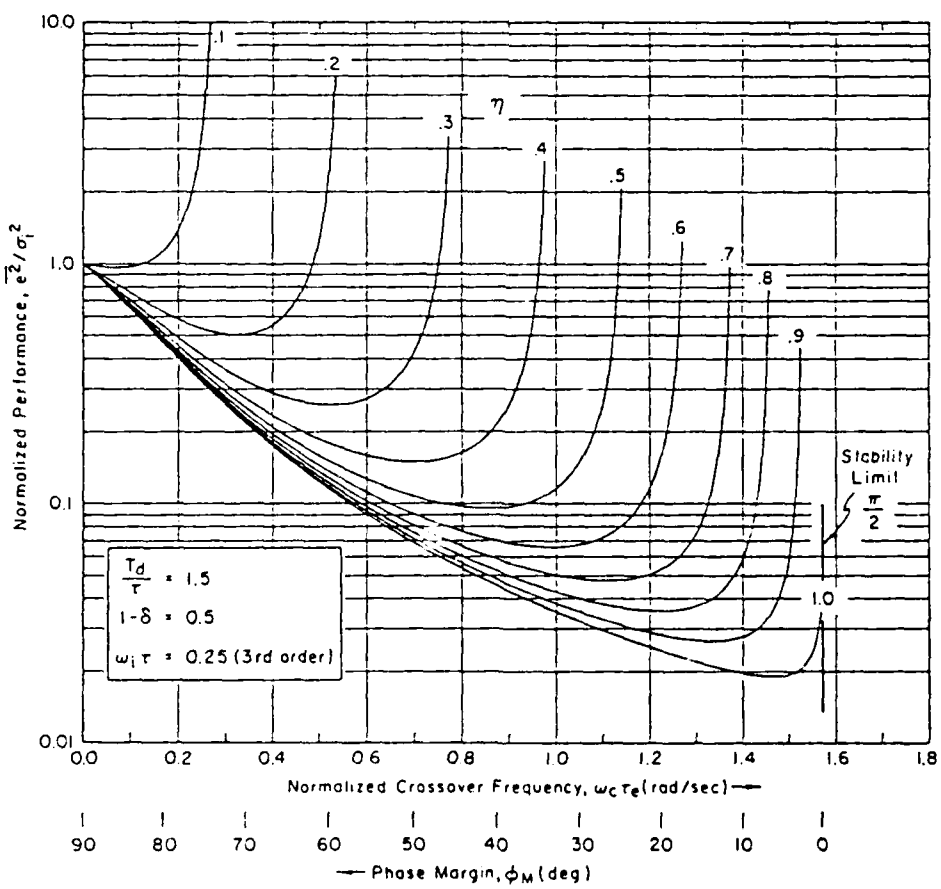

Figure 2. Effect of Divided Attention on Task Performance

where $\overline{e_i^2}$ is the error component correlated with the forcing function and $\overline{e_n^2}$ is due to the remnant. Because the remnant component is proportional to the total mean-squared error,

$$\overline{e^2} = \overline{e_i^2} + \left(\frac{\overline{e_n^2}}{\overline{e^2}}\right)\overline{e^2}$$

$$= \overline{e_i^2} + F\,\overline{e^2} \tag{4}$$

so that

$$\overline{e^2} = \frac{\overline{e_i^2}}{1 - F} \tag{5}$$

As $F \longrightarrow 1$, which is associated with the limit on the inequality constraint, $F = \overline{e_n^2}/\overline{e^2} < 1$, the blow-up in the mean-square occurs.

The performance data shown in Fig. 2 indicate that, as tasks require the pilot's attention the dwell fraction for the primary task must decrease, and the optimum operating point for the pilot shifts. This is further illustrated in Fig. 3, which shows an increase in the minimum mean-squared error and in phase margin and a decrease in the normalized crossover frequency as the task dwell fraction decreases.

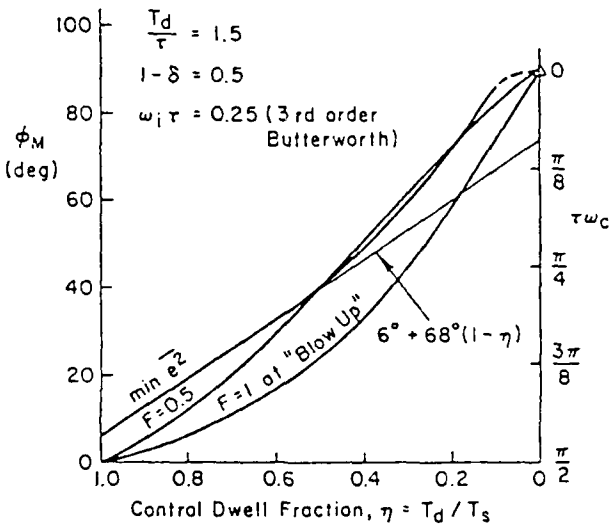

Figure 3. Effect of Divided Attention on Phase Margin and Crossover Frequency for Minimum $\overline{e^2}$ and F = 0.5 and 1 (from Ref. 8)

Divided attention effects can also be modeled with optimal control models for pilot behavior. Reference 9 is an early empirical/analytical study of task interference which took this approach. In this study, the simultaneous control of several independent axes was the situation creating the task interference. From two to four axes were controlled, each with an associated display. The results were compared to single-axis control results. A model for task interference was hypothesized, and this model also focuses on remnant-related parameters. The key parameters proposed in Ref. 9 to reflect task interference are centered on the increased "measurement noise" contaminating the subject's observations of sensed quantities.

Specifically, in the optimal-control modeling approach,[10] the human is considered to observe an array of system responses, which then comprise the subject's observation vector, $\bar{y}_p(t)$. These measurements are (each) contaminated with (white) observation noise, v_{y_i}, or

$$\bar{y}_p(t) = \bar{y}_{p_{true}}(t) + \bar{v}_y \tag{6}$$

Finally, the noise-intensity matrix of $\bar{v}_y$ is assumed diagonal, with elements equal to V_{ii}, where i corresponds to the ith observed variable (e.g., displayed error in one axis).

For a single-axis control task and display, V_{ii} is taken to be

$$V_{ii} = P_o \left[\frac{\sigma_{y_i}}{N(\sigma_{y_i}, T_i)}\right]^2 \tag{7}$$

where σ_{y_i} is the rms value of the response variable, y_{p_i}, and $N(\sigma_{y_i}, T_i)$ is the random-input describing function of a dead zone of half-width T_i. This dead-zone model represents the effect of perception or indifference thresholds in the subjects' observations. Finally P_o is the nominal, full-attention noise-to-signal ratio for the observed variable, y_i. This (full-attention) noise-to-signal ratio has been empirically shown to be relatively constant over a range of tasks and controlled element dynamics, and is usually measured (for foveal viewing in the case of visually sensed responses) to be approximately -20 dB (i.e., .01 units of normalized power per rad/sec, defined over positive frequencies).[4,9] Note that all the above is consistent with the "standard" optimal-control modeling approach described in Ref. 10, for example.

Now the interference model of Ref. 9 states that the effect of task interference is reflected in an increase in the effective P_o, the noise to signal ratio defining the observation noise intensity. With the description of task interference, the noise intensity becomes

$$V_{ii} = \frac{P_o}{f_i}\left[\frac{\sigma_{y_i}}{N(\sigma_{y_i}, T_i)}\right] \tag{8}$$

where f_i is the fractional attention devoted to task i (or more precisely, reponse i), and $0 < f_i < 1$. Also, since the human's capacity is finite, $\sum_i f_i = 1.0$ over all tasks and displays. This model was validated in Ref. 9 by comparing model-based tracking errors, pilot describing functions, and remnant (reflected to the displayed error) with experimental results. Because the filter dynamics which are a portion of the pilot (model)[10] dynamics depend on observation noises, variation in these noises manifest themselves in changes in pilot (model) dynamics and hence in pilot-vehicle closed-loop dynamics. (Note that in Ref. 9, the threshold effects were modeled as additional additive observation noise that did <u>not</u>

scale with σ_{y_i}. The threshold effects considered in this reference were primarily due to parafoveal viewing. The use of the dead-zone describing function did not appear until after Ref. 9 was published although its use is basically an extension of results presented in Ref. 9.)

Attention will now turn to the application of the optimal-control theoretic model for task interference to the modeling of other experimental situations involving single and multi-axis tasks. These are the multi-axis experiments of Dander (Ref. 11), which are the only data set currently available in which pilot ratings are available for single axis and multi-axes made up of the single axis. The model results will provide an "estimated pilot behavior and system performance data base," which is otherwise not available. These results can then be compared with the trends from the divided attention theory, and also with some of the experimental results of Ref. 6.

The Experimental Data

Dander[11] has reported experimental findings from single-axis as well as multi-axis tracking experiments. The only experimental results were in the form of subjective ratings, using the Cooper scale, but both single-axis and multi-axis ratings of the same dynamics were obtained.

Dynamically independent axes were considered in the tracking experiments. Single-axis as well as simultaneous two- and three-axis tracking tasks were performed, and the tasks were subjectively rated. For the two- and three-axis experiments, an overall rating was given, not a rating of an individual axis in the task. Although some of the two-axis cases will be discussed here, the ratings for these cases were considered by Dander to be inconsistent. This conclusion was reinforced by an independent analysis.[12] Consequently, the two-axis ratings will not be used in the analyses presented here.

The controlled-element dynamics in each axis were varied to obtain a wide variety of combinations of configurations. The dynamics for each axis were initially selected to yield Level 1, 2, and Level 3 ratings in the single-axis tracking task. So three different dynamic elements were selected for each axis, yielding a total of nine different dynamic elements. These transfer functions are listed in Table 2.

TABLE 2. DANDER CONTROLLED-ELEMENT DYNAMICS

Axis Transfer Functions	Good Dynamics (H)	Intermediate Dynamics (M)	Bad Dynamics (L)
$\frac{\theta}{\delta_{E_s}} = \frac{4.(.04)(0.9)}{(1/T_\theta)(5.)(.7,.25)}$	$1/T_\theta = 0$	$1/T_\theta = -.5$	$1/T_\theta = -.8$
$\frac{\phi}{\delta_{A_s}} = \frac{0.5(0.1)}{(1.5)(\zeta_\phi, 0.5)}$	$\zeta_\phi = .84$	$\zeta_\phi = -.3$	$\zeta_\phi = -.84$
$\frac{\beta}{\delta_{R_p}} = \frac{(0.(3..)}{(3.0)(\zeta_d, .5)}$	$\zeta_\beta = .5$	$\zeta_\beta = -.2$	$\zeta_\beta = -.5$

The configurations to be considered herein, along with the ratings obtained in the Ref. 11 experiments are listed in Table 3, with configuration symbols used in later graphical presentations.

TABLE 3. CONFIGURATIONS CONSIDERED

Configuration Identifyer	No. of Axes	Subjective Ratings	Graphical Symbol
θ-H	1	2.5,2.5,3.,3.,3.	⊙
θ-M	1	4.,4.5,4.5,5.,5.	△
θ-L	1	6.,6.,6.5,7.,8.	▽
φ-H	1	2.5,3.,3.,4.,4.	⊡
φ-M	1	3.5,4.,4.,5,5.,5.	◇
φ-L	1	5.0,5.5,6.0,6.5	▷
β-H	1	3.0,3.5,3.5,3.5,3.5	◁
θφ-HH	2	(2.,3.,3.,3.,3.5)*	⊙
θφ-HL	2	(6.,6.,6.5)*	▷
θφ-ML	2	(6.,7.,7.)*	△
θφ-LH	2	(4.,4.,4.)*	▽
θφβ-HHH	3	5.5,6.,6.,6.	●
θφβ-HMH	3	5.,5.5,6.	▲
θφβ-HLH	3	7.,9.	▼
θφβ-MHH	3	5.5,6.5,6.5	■
θφβ-MMH	3	7.5	◆
θφβ-MLH	3	8.,8.5	▶
θφβ-LHH	3	9.,10.	◀
θφβ-LMH	3	9.0	■
θφβ-LLH	3	8.5,9.5	▼

*Data considered inconsistent-not specifically used

The command signals in each axis consisted of sums of sinusoids, generating random-appearing signals. The amplitudes and frequencies of the sinusoids used in each of the three command signals are listed in Table 4 below, along with the approximate maximum command-signal amplitude. Note that

TABLE 4. DANDER COMMAND SIGNAL CONTENT

Axis	Frequency (r/s)	Unscaled Amplitude
θ_c	0.367	4.80
	0.483	5.50
($\theta_{c_{max}}$ = ±0.75 in.)	0.816	1.44
	1.32	1.64
ϕ_c	0.367	4.80
	0.483	2.20
($\phi_{c_{max}}$ = ±45 deg.)	0.816	1.15
	1.32	1.64
β_c	0.483	0.92
	0.816	0.33
($\beta_{c_{max}}$ = ±1.8 units)	1.32	0.33

the units of displayed commands are inches of command bar displacement on the display (θ_c), angle of rotation of the command bar (ϕ_c), and "display units" (approximately 7 degs of rotation of a needle on a circular dial = 1 unit) (β_c). Also it is noted that most of the power in the signals is in frequencies below 0.5 rad/sec., with the maximum frequency in the signals equal to 1.32 rad/sec.

Optimal-Control Modeling of the Experiment

The modeling process now involves representing the task in terms of the parameters in the optimal control framework.[10] These include the following:

1. An appropriate objective function representative of the task (or a generic task critical to the performance of the actual task).

2. The value for the neuromotor time constant in each axis.

3. The parameters that determine the observation noise intensities:

   a. Nominal noise-to-signal ratio (P_o)
   b. Perception/indifference threshold (T_i)
   c. Attentional allocation (may be optimized).

4. Vector of human operator observations in the task.

5. Observation time delay (routinely selected as $\tau = 0.2$ sec).

6. Neuromotor noise-to-signal ratio.

7. Characterization of the command signals.

For these experiments, the appropriate objective function for each axis was chosen to be

$$J_{axis_i} = \left[\frac{\sigma^2_{\varepsilon_i}}{\sigma^2_{c_i}} + \frac{\sigma^2_{\dot{\delta}_i}}{g_i}\right] \tag{9}$$

And for a multi-axis task, the objective function for the task was

$$J_{task} = \sum_{i}^{N_{axes}} J_{axis_i} \tag{10}$$

The justification of this selection involves three considerations. The first relates to the selection of equal (unity) weighting on each $J_{axis\ i}$ in the definition of J_{task} in multi-axis tasks. This decision was based on the instructions given to the subjects in the experiment. They were to attempt to minimize the errors in all controlled axes. That is, they were instructed that no axis was to be given preference, which would then define primary and secondary sub-tasks.

Secondly, the normalization of the mean-square error with the mean-square command deals nicely with the fact that different units and different command-signal strengths were used in the axes. This will be discussed further with regard to subjective ratings.

Finally, the interpretation of g_i requires some discussion. In the OCM, the selection of g_i defines the frequency range over which the open-loop system amplitude ratio approximates a K/s-like form. In connection with the OCM it is often cited that g_i is selected to yield a desired neuromotor time constant, τ_n, in the pilots's describing function obtained from the model. But, when the total pilot describing function, Y_p, is actually constructed from its various elements in the OCM, the τ_n established in this fashion is canceled by a directly compensating lead, leaving the actual estimated Y_p with no $(\tau_n s + 1)^{-1}$ lag. Still it has been convenient to adjust g_i in this fashion even though the lag will later disappear. In this vein, the value of the desired neuromotor time constant used is either 0.1 sec, or the τ_n that yields the lowest error (e.g., best performance), whichever is greater. Notice that after τ_n is determined in the above fashion, this "operating point" is associated with some weight g_i in $J_{axis\ i}$. This value may also infer the subject's subjective trade between performance (σ_ε) and workload ($\sigma_{\dot{\delta}}$). And since pilot lead and $\sigma_{\dot{\delta}}$ are correlated, this procedure maximizes the possibility of relating the resulting value of J_{task} to the subjective rating of the task. More about this later.

The parameters related to observation noise were selected as follows. For the experimental set-up considered, and using visual perception thresholds of 0.05 deg and 0.1 deg/sec of visual arc and arc rate at the pilot's eye, the dead-zone widths for the perception thresholds are

θ -- 0.03 in; 0.05 in/sec

ϕ -- 1.5 deg; 3.0 deg/sec

β -- 0.14 unit; 0.28 units/sec

The nominal full-attention foveal-viewing value of -20 dB was selected as the basic noise-to-signal ratio, P_o, for both perceived error and error rate in each axis. And finally, for multi-axis tasks, the attention was optimized among the observations for each axis, with the fractional attention f_i (see Eq. 8) constrained to be equal for both error and error rate in each axis. This optimization was performed using the criteria that f_i's were to be chosen such that J_{task} was minimized, subject to the constraint that

$$\sum_{axis} f_i = 1 \tag{11}$$

For further discussion of the attentional allocation, see Ref. 13.

The observations assumed available to the subjects were error and error rates in each axis. The displays were either integrated or considered sufficiently close together such that additional observation errors due to scanning or parafoveal viewing was neglected.

The neuromotor noise-to-signal ratio was established as -20 dB. In addition to neuromotor noise reflecting a source of remnant, the use of this noise has also been found to be necessary for the OCM to yield gain and phase margins appropriate for human operator modeling. For the relation between

this noise and stability margins of LQG controllers, the reader is referred to Ref. 14.

Finally, the command signal for each axis was modeled as a second-order Markov process, using the filter

$$F_c(s) = \frac{A_c}{s^2 + 2(.7)(.5)s + (.5)^2} \qquad (12)$$

Note that the break frequency of 0.5 rad/s corresponds to maximum command power below 0.5 rad/sec. The gain A_c was selected such that the maximum command amplitude listed in Table 4 was twice the standard deviation (2σ) of the random command generated with the above filter.

Results of the Model Analysis

The above OCM set-up data were then inserted into a version of the PIREPS computer program[13] to obtain OCM-based estimates for the pilot dynamic behavior and various system performance metrics. The model results obtained include both time- and frequency-domain quantities. The time-doman results include root-mean-square tracking error, σ_ϵ, control manipulation deflection rate, $\sigma_{\dot\delta}$, the objective function magnitude, J_{task}, and the optimized attentional allocation, f_i, for each axis (for multi-axis tasks). The frequency-domain results include pilot describing function $\delta_i/\epsilon_i(j\omega)$, and remnant, $\phi_{nn}(\omega)$, along with the controlled-element transfer function in Bode form, $\epsilon_i/\delta_i\,(j\omega)$. From this information, the crossover frequency, ω_{c_i}, pilot phase compensation at crossover, $\phi_p(\omega_c)$, phase margin, ϕ_M, effective pilot latency, τ_E, and closed-loop bandwidth may be determined. These parameters are defined graphically on some example results in the Appendix. This phase of the analysis is similar to that of Refs. 15 and 16. The pilot's describing function (in each axis) corresponds to the form

$$Y_p(j\omega) = \frac{e^{j\omega\tau_{obs}}}{j\omega\tau_n + 1}\hat{Y}_p(j\omega) \qquad (13)$$

And the pilot phase compensation is then

$$\phi_p(\omega_c) = \arg \hat{Y}_p(j\omega_c) \qquad (14)$$

The phase margin is determined from

$$\phi_M = \pi - \arg Y_p Y_c(j\omega_c) \qquad (15)$$

while effective pilot latency is

$$\tau_E = (\pi/2 - \phi_M)/\omega_c \qquad (16)$$

Finally, closed-loop bandwidth is defined as

$$\omega_{BW} = \omega\Big|_{\substack{\text{closed-loop}\\ \text{phase} = -90^0}} \qquad (17)$$

The key results are summarized in Tables 5, 6, and 7. Table 5 lists the single-axis results. When the single axis estimates are converted to classical forms the results show trends of rating with increased effective latency, τ_e, and reduced crossover frequency, ω_c, which are consistent with similar sets of vehicle dynamics considered in Refs. 1 and 17. Tables 6 and 7 summarize the two- and three-axis results, respectively. These results are discussed further below.

Since one of the fundamental effects of task interference is increased remnant, this area is the first to be discussed. Shown in Fig. 4 are the modeling results for the remnant ϕ_{nn}, normalized with mean-squared error for two cases considered. This figure does indeed indicate an increase in remnant at low frequencies for the two axis task over the single axis. Note that this two-axis task involves poor dynamics laterally, with the same good dynamics in pitch as the single axis case. As a result of the interference from difficult lateral dynamics, the attention allocated to the pitch axis reduces from 100 percent ($f_{pitch} = 1.0$) to 20 percent ($f_{pitch} = 0.2$).

TABLE 5. SINGLE AXIS SUMMARY

case*	ω_c(r/s)	ω_{BW}	$\phi_M(\tau_e)$	ϕ_p	σ_ϵ/σ_i	$\sigma_{\dot\delta}/g_i$	J	PCR
θ_H	3.2	3.7	37°(.289)	44.2°	.188	.103	0.46	2.5-3
θ_M	3.1	3.5	28.4(.346)	42.6	.295	.193	.124	4-5
θ_L	3.1	3.5	25.5(.363)	44.8	.413	.273	.245	6-8
ϕ_H	3.1	3.6	37.2(.297)	50.7	.202	.119	.055	2.5-4
ϕ_M	3.1	3.5	29.5(.335)	64.5	.281	.176	.110	3.5-5
ϕ_L (τ_n=.12)	2.8	3.1	21.5(.427)	64.0	.523	.385	.422	5-6.5
θ_H	2.9	3.6	43.4(.280)	38.9	.234	.125	.071	3-3.5

* τ_n = 0.1s, except as noted

TABLE 6. TWO-AXIS SUMMARY

case/axis*	ω_c	ω_{BW}	$\phi_M(\tau_e)$	ϕ_P	σ_ϵ/σ_i	$\sigma_{\dot\delta}/g_i$	Attn	J_{task}	POR
θφ,HH/θ	2.75	3.3	41.5(.308)	39.0	.230	.111	.5	.140	(2.9)
/φ	2.7	3.3	42.2(.308)	43.7	.242	.126	.5		
θφ,HL/θ	2.15	2.85	49.2(.331)	33.9	.315	.127	.2	.646	(6.2)
/φ	2.75	2.95	22.1(.431)	62.8	.594	.421	.8		
θφ,LH/θ	3.0	3.4	26.3(.371)	44.1	.472	.235	.8	.430	(4.0)
/φ	2.2	2.87	51.0(.309)	34.1	.306	.134	.2		

* τ_n in each axis as in Table 5

TABLE 7. THREE-AXIS SUMMARY

case/axis**	ω_c	ω_{BW}	$\phi_M(\tau_e)$	ϕ_{PC}	σ_ϵ/σ_i	$\sigma_{\dot\delta}/g_i$	attn	J_{task}	POR
θφβ,HHH/θ	2.5	3.1	45.(.314)	36.6	.262	.118	.33	.300	5.5-6
θφβ,HHH/φ	2.45	3.1	46.(.313)	39.1	.273	.130	.33		
θφβ,HHH/β	2.0	2.8	54.2(.312)	17.2	.330	.126	.33		
θφβ,HLH/θ	1.9	2.6	53.1(.339)	32.5	.368	.134	.15	.935	7.-9.0
θφβ,HLH/φ	2.65	2.9	23.5(.438)	61.3	.644	.445	.67		
θφβ,HLH/β	1.75	2.6	60.7(.292)	16.9	.389	.140	.18		
θφβ,LHH/θ	2.9	3.3	26.8(.380)	42.8	.505	.244	.67	.539	9.0-10.0
θφβ,LHH/φ	1.9	2.6	56.5(.308)	27.9	.360	.140	.15		
θφβ,LHH/β	1.63	2.6	60.2(.319)	4.4	.394	.132	.18		
θφβ,MMH/θ	2.6	3.0	32.3(.395)	36.0	.430	.165	.40	.631	7.5
θφβ,MMH/φ	2.7	3.1	34.5(.366)	58.5	.420	.186	.40		
θφβ,MMH/β	1.7	2.5	59.5(.318)	7.3	.380	.131	.20		
θφβ,MHH/θ	*	*	*	*	.370	.211	.48	.426	5.5-6.5
θφβ,MHH/φ	*	*	*	*	.293	.131	.27		
θφβ,MHH/β	*	*	*	*	.349	.138	.25		
θφβ,HMH/θ	*	*	*	*	.295	.126	.25	.421	5.0-6.0
θφβ,HMH/φ	*	*	*	*	.381	.210	.46		
θφβ,HMH/β	*	*	*	*	.333	.137	.29		
θφβ,LMH/θ	*	*	*	*	.533	.322	.54	.859	9.0
θφβ,LMH/φ	*	*	*	*	.490	.242	.28		
θφβ,LMH/β	*	*	*	*	.388	.140	.18		
θφβ,MLH/θ	*	*	*	*	.508	.257	.28	1.23	8.0-8.5
θφβ,MLH/φ	*	*	*	*	.695	.468	.59		
θφβ,MLH/β	*	*	*	*	.428	.142	.13		
θφβ,LLH/θ	*	*	*	*	.682	.386	.39	1.74	8.5-9.5
θφβ,LLH/φ	*	*	*	*	.788	.512	.51		
θφβ,LLH/β	*	*	*	*	.472	.143	.10		

* - not determined

** τ_n in each axis as in Table 5

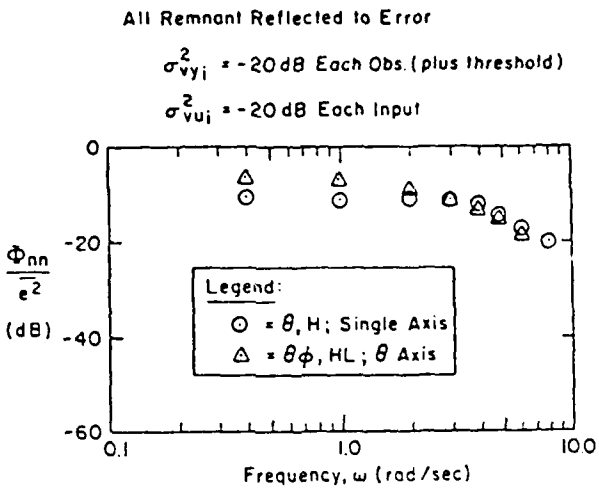

Figure 4. Model-Based Error Remnant Spectrum Task-Interference Effect

One reason the controlled elements of Fig. 4 were chosen for single axis, dual axis comparisons is the possibility to compare the estimation results with similar data. Reference 6 considered a two-axis case with one axis involving an unstable controlled element similar to the lateral dynamics for the two-axis case modeled here. Figure 5 shows that the remnant shown for the pitch axis in the two-axis task in Fig. 4 compares favorably with that from Ref. 6 for the natural-scanning case. To the extent that these remnant data from Ref. 6 are a reasonable surrogate for the Dander case this close correspondence is compelling. However, the key result involving remnant is that an increase in remnant is the model-based result of task interference, as expected from the theory reviewed earlier.

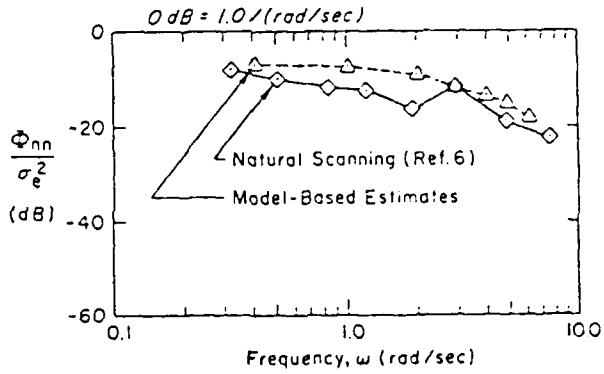

Figure 5. Comparison of Model-Estimated and Ref. 6 Normalized Remnant Spectra

Another effect of interference noted was ω_c regression. Shown in Fig. 6 are some results from Ref. 6 along with some model-based results generated in this study. The ratio of crossover frequency to that for a single-axis task is plotted versus effective dwell fraction, η_e, defined as

$$\eta_e = \eta - \Omega(1 - \eta) \qquad (18)$$

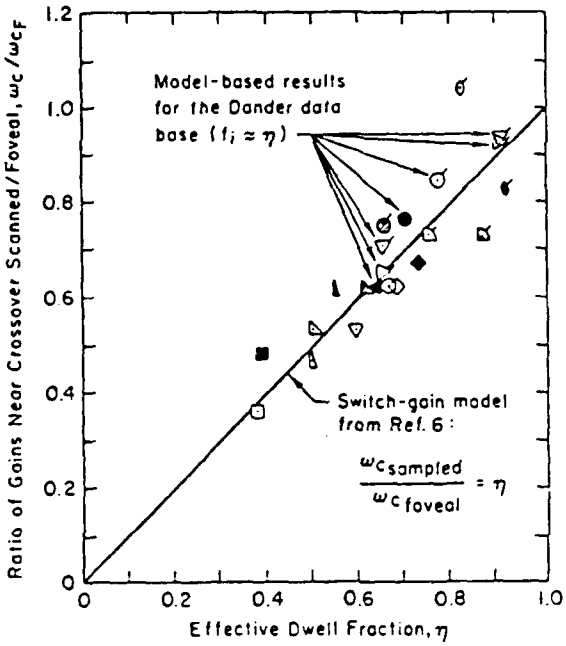

Figure 6. Crossover Regression with Task Interference (after Ref. 6)

where Ω = 0.566 from Ref. 6, and η = actual dwell fraction. If dwell fraction is taken to approximate fractional attention, f_i, as defined herein (or vice versa), one can compare model-based results to those of Ref. 6. The modeling results are in general agreement with the experimental data and exhibit the same trends as expected from the theory. Therefore, we can say that the task interference effect of ω_c regression is also observed in the modeling results.

Another comparison between the theory and the modeling results discussed herein is revealed in Fig. 7. The results in this figure are consistent

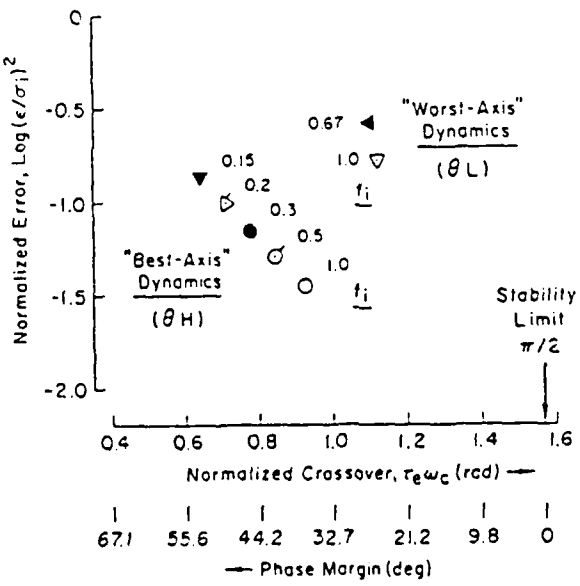

Figure 7. Trend of Optimal Operating Points

with the parametric results shown in Figs. 2 and 3. The minima in Fig. 2 represent the optimum performance σ_ϵ for a given dwell fraction, η. Again interpreting η to be analogous to fractional attention, f_i, the model based results for the Dander configuration in Fig. 7 corresponding to "best" dynamics, for example, are the model-based results that show trends comparable to the minimum mean-squared error points of Figs. 2 and 3. Listed alongside the data points in Fig. 7 is the fractional attention used for control of the "best" axis dynamics (θH) as well as some results for the "worst" axis dynamics (θL). Note that as fractional attention (dwell fraction) decreases for a given controlled element, (optimum) tracking performance is degraded, ω_c regresses, and phase margin increases -- all generally consistent with the divided attention theory.

Pilot Rating Estimation

Given the consistencies between full- and divided-attention behavior described above the next concern is the estimation of pilot workload associated with the multi-axis control tasks. This is quantified in the Dander data set by Cooper pilot ratings. It is well known (e.g., Refs. 1, 12, 17) that the subjective ratings of flying qualities provided by pilots depend on task performance and the pilot equalization needed to offset any deleterious vehicle dynamic characteristics. In tasks with a significant closed-loop tracking content these features can be reasonably represented by normalized tracking error and pilot lead equalization.

Pilot lead equalization will skew the pilot's output ("control input" in the OCM) spectrum toward higher frequency content. Consequently, lead equalization when reflected into a component of an integral performance index will be manifest as increased control input rate. Also, the task performance in terms of mean-squared error is a natural component of a system performance metric or index. With these two facts in mind, Hess[18] suggested that the combination of error squared and pilot-output-(control input)-rate-squared might be used as a metric giving an indication of the subjective rating. With a particular weighting (g) on the control rate term this is just the optimal control performance index in the OCM. Using the limited experimental data available Hess[19] was able to show that a reasonable linear correlation did indeed exist between the OCM performance index J and the pilot rating, and the basis for this correlation was extended further in Ref. 19. Indeed, one reason that the present study was undertaken was the hope that this relationship could be expanded to the multi-axis situation.

To determine if the (appropriately chosen) objective function did in fact correlate with multi-axis as well as single-axis ratings, the Dander results are again considered. In the task objective functions chosen in this modeling work, the error was normalized with the variance of the command signal in the respective axis. Not only does this offset the effects of different units in the axes, but it also cancels the effect of command signal strength on the ratings.[17] Finally, with the model-based determination of g_i, the weight on control rate in the objective function, one may consider the resultant weight as "normalizing" control rate. These normalized quantities, mean-square error and control rate, are tabulated in Tables 5, 6, and 7, along with J_{task}.

Shown in Fig. 8 is the correlation between J_{task}, as modeled, and the subjective ratings of the task. The correlation between J_{task} and POR from the single-axis results appears to hold for the multi-axis results as well. This result would seem to indicate that the ratings reflect the actual performance and workload (stick rate) in the overall task, or that the subject does not accept the fact that the performance should be worse since the task is more difficult. In other words, he does not accept worse performance and workload in a multi-axis task compared to single-axis results.

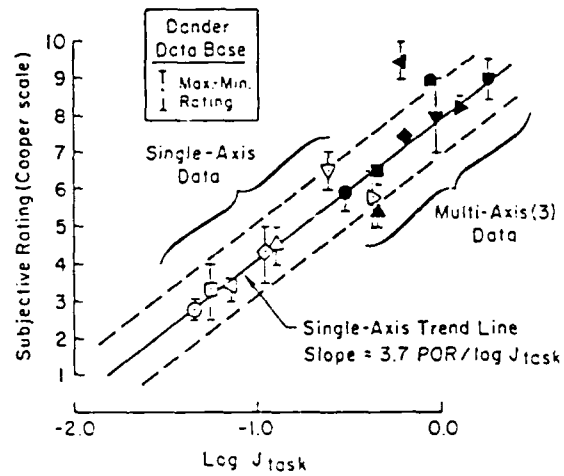

Figure 8. "Cost Function"/Rating Correlation

The results also tend to support the hypothesis that determining the weightings g_i in the manner discussed leads to the "correct" relative weightings on control rate in the axis, and the relative weight between control rate and normalized error.

Conclusions

This study has illustrated that:

1) When the pilot must divide his attention across several control axes the crossover frequency will be less than full attention values while the remnant, closed-loop system performance (error) and phase margin will be larger.

2) Pilot modeling estimates using the optimal control model adjusted to take into account divided attention or task interference among several control axes exhibit characteristics consistent with those listed above.

3) Comparison of the estimates and available data show similar trends.

4) The objective function (optimal control performance index) used in the pilot and system behavioral modeling, when "calibrated" with single-axis correlations, show potential for the development of subjective ratings estimates for multi-axis tasks.

Acknowledgement

This research was supported under Contract F33615-85-C-3610 from the Flight Dynamics Laboratory, Air Force Wright Aeronautical Laboratories, Wright Patterson Air Force Base, Ohio. The contract technical monitor was Mr. Thomas Gentry.

References

[1] McRuer, D. T., and Krendel, E. S., Mathematical Models of Human Pilot Behavior, AGARDograph No. 188, Jan. 1974.

[2] Bergen, A. R., "On the Statistical Design of Linear Random Sampling Systems," in J. F. Coales, et al., eds., Automatic and Remote Control (Proc. First Internatinal Congress IFAC), London, Butterworths, 1961, pp. 430-436.

[3] Clement, W. F., Random Sampling Remnant Theory Applied to Manual Control, Systems Technology, Inc., TM-183-A, Mar. 1969.

[4] Jex, H. R., Allen, R. W., and Magdaleno, R. E., Display Format Effects on Precision Tracking Performance, AMRL-TR-71-63, Aug. 1971.

[5] McRuer, D. T., Jex, H. R., and Clement, W. F., et al., Development of a Systems Analysis Theory of Manual Control Displays, Systems Technology, Inc., TR-163-1, Oct. 1967.

[6] Allen, R. W., Clement, W. F., and Jex, H. R., Research on Display Scanning, Sampling, and Reconstruction Using Separate Main and Secondary Tracking Tasks, NASA CR-1569, July 1970.

[7] Hollister, W. M. (Editor), Improved Guidance and Control Automation at the Man-Machine Interface, AGARD Advisory Report 228, Dec. 1986.

[8] McRuer, D. T., Clement, W. F., and Magdaleno, R. E., "Simplified Pilot-Modeling for Divided Attention Operation," Vol. II of Computer-Aided Procedure for Analyzing Man-Machine System Dynamic Interactions, STI TR 1219-1, Apr. 1987.

[9] Levison, W., Elkind, J., and Ward, J., "Studies of Multivariable Manual Control Systems: A Model of Task Interference," NASA CR-1746, May 1971.

[10] Kleinman, D., Baron, S., and Levison, W., "An Optimal Control Model of Human Behavior," Automatica, Vol. 6, 1970, pp. 357-369.

[11] Dander, V., "An Evaluation of Four Methods for Converting Single Axis Pilot Ratings to Multi-Axis Pilot Ratings Using Fixed Base Simulation Data," M.S. Thesis, AFIT, GE/EE/62-4, Dec. 1962.

[12] Ashkenas, I. L., Hoh, R. H., and Craig, S., Recommended Revisions to Selected Portions of MIL-F-8785B (ASG) and Background Data, AFFDL-TR-73-76, Aug., 1973.

[13] Curry, R., Hoffman, W., and Young, L., Pilot Modeling for Manned Simulation, AFFDL-TR-76-124, Vols. 1 and 2, Dec. 1976.

[14] Doyle, J., and Stein, G., "Robustness with Observers," IEEE Trans. on Automatic Control, August, 1979.

[15] Bacon, B., and Schmidt, D., "A Modern Control Approach to Pilot/ Vehicle Analysis and the Neal-Smith Criteria," Journal of Guid., Control, and Dynamics, Vol. 19, No. 5, 1983, pp. 339-347.

[16] Anderson, M. R., and Schmidt, D. K., "Closed-Loop Pilot Vehicle Analysis of the Approach and Landing Task," Journal of Guid., Control, and Dynamics, Vol. 10, No. 2, 1987, pp. 187-194.

[17] McDonnell, J., Pilot Rating Techniques for the Estimation and Evaluation of Handling Qualities, AFFDL-TR-68-76, May 1968.

[18] Hess, R., "Prediction of Pilot Opinion Ratings Using an Optimal Pilot Model," Human Factors, Vol. 19, No. 5, 1977.

[19] Schmidt, D. K., "On the Use of the OCM Objective Function as a Pilot Rating Metric," 17th Annual Conf. on Manual Control, UCLA, June, 1981.

Appendix

Included in Figs. A.1 and A.2 are the open- and closed-loop Bode plots, and the pilot describing function $Y_p(j\omega)$, respectively. Shown on these figures are the frequency-domain measures determined from the modeling process. The measures, specifically, are gain crossover frequency, ω_c, phase margin, ϕ_M, closed-loop bandwidth, BW, and pilot phase compensation, ϕ_{PC} (including the phase due to τ_{OBS} at ω_c and $(1 + j\tau_n\omega_c)^{-1}$).

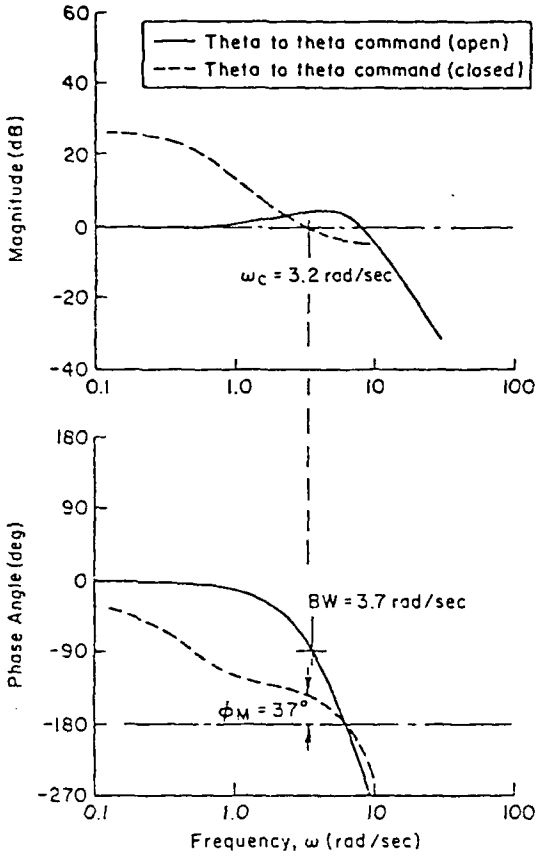

Figure A.1

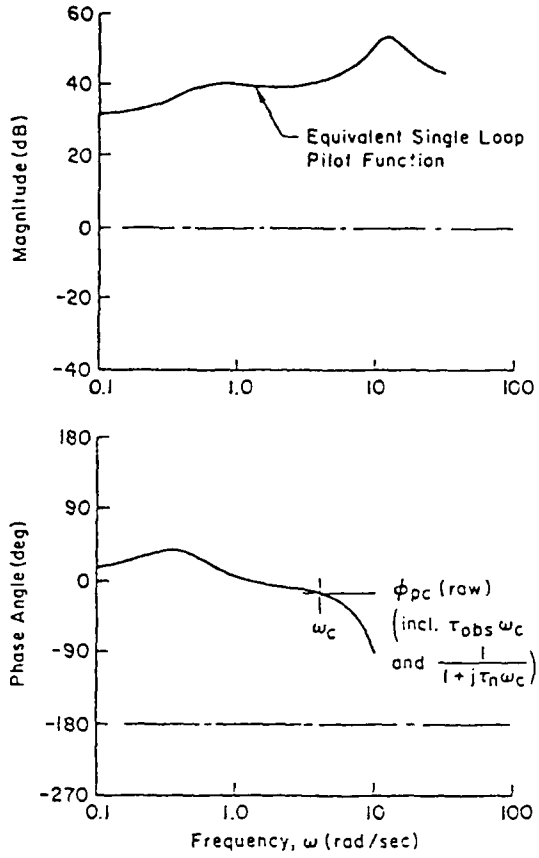

Figure A.2

 ☆U.S.Government Printing Office: 1989 — 748-056/24135